Title
Investigating the Role of Force and Stiffness in Controlling Cell Behavior

Author
Webster, Kevin Dwayne

Publication Date
2012

Peer reviewed|Thesis/dissertation

Investigating the Role of Force and Stiffness in Controlling Cell Behavior

by

Kevin Dwayne Eric-Jon Webster

A dissertation submitted in partial satisfaction of the

requirements for the degree of

Doctor of Philosophy

in

Biophysics

in the

Graduate Division

of the

University of California, Berkeley

Committee in charge:

Professor Daniel A. Fletcher, Chair
Professor Sanjay Kumar
Professor Jan Liphardt
Professor Matthew Welch

Fall 2012

Investigating the Role of Force and Stiffness in Controlling Cell Behavior

Abstract

Investigating the Role of Force and Stiffness in Controlling Cell Behavior

by

Kevin Dwayne Eric-Jon Webster

Doctor of Philosophy in Biophysics

University of California, Berkeley

Professor Daniel A. Fletcher, Chair

Forces and the mechanical properties surrounding eukaryotic cells have been increasingly shown to play crucial roles in modulating biological functions, from healthy tissue development to disease progression. This work focuses on three aspects of cellular responses to their mechanical microenvironment: stiffness sensing, force regulation, and the effect of cancer progression on tissue architecture and elasticity. To make quantitative measurements of cell properties, I developed a novel technology based on atomic force microscopy (AFM) that is capable of dynamically controlling microenvironmental stiffness, as well as measuring forces and displacements. I first observed that cells nearly instantly change their contraction in response to step changes in stiffness (Chapter 2). I then determined that this process requires a mechanical equilibrium that balances contraction of the viscoelastic cytoskeleton with deformation of the extracellular matrix. This seconds-timescale equilibration provides a lower bound to the rate of whole-cell scale stiffness sensing (Chapter 3).

Extracellular matrix stiffness has been identified as a key driver of tumorigenesis, but elucidating the link between tissue architecture and elasticity has remained experimentally difficult. Using AFM, I observed a near 2-fold stiffening of pre-malignant breast epithelial spherical structures, called acini, which are responsible for milk production, as well as are the initial site of many breast cancer cases. Further, the specific apparent microenvironmental stiffness for an epithelial cell within this acinar structure was calculated using 3D computational modeling, revealing a marked difference in compliance independent of extracellular matrix changes (Chapter 4).

A widely cited concept in cellular mechanosensing to explain the response of cells to changes in their mechanical microenvironment is “tensional homeostasis”, whereby adherent cells will actively respond to compression or extension by maintaining some previously established tension. However, no experiments have yet directly shown this behavior at the single cell level. Using a combination of protein patterning and AFM, I provide the first evidence of this homeostatic behavior. Notably, I found that cells do not maintain an absolute setpoint, but rather work to counteract force changes at a slow rate, beyond which force will freely change, a process I term *tensional buffering*. In addition, after rapid loading, cells will work to maintain their new level of tension, not returning to a previous setpoint (Chapter 5).

Ultimately, these advances further our understanding of the role of mechanics in both healthy and diseased cellular processes, laying the groundwork for tissue engineering approaches for growing healthy tissues or therapeutic targets for a new array of hard to treat diseases.

Table of Contents

Acknowledgements ..... **v**

Chapter 1. Introduction: Mechanical regulators of the cell – The role of tension and stiffness **1**

Force as a signal 2
Role of stiffness in cellular biology 2
Technologies for probing cell forces 3
Boundary conditions for stiffness sensing mechanism 4
Stiffness as a marker and driver in disease 5
Force balance: maintaining healthy cell function 5
Scope of dissertation 6
References 7

Chapter 2. An AFM-based stiffness clamp for dynamic control of rigidity **10**

ABSTRACT **11**
INTRODUCTION **12**
RESULTS **13**
Stiffness clamp concept 13
Stiffness clamp applied to an expanding hydrogel 14
Stiffness clamp applied to a contracting cell 14
DISCUSSION **15**
MATERIALS & METHODS **16**
Stiffness clamp algorithm 16
Atomic force microscope 17
Polyacrylamide hydrogels 18
Cell culture 18
Statistical analysis 18
ACKNOWLEDGEMENTS **18**
REFERENCES **19**
FIGURES **21**
Figure 1. Feedback control can change the apparent stiffness a cell experiences. 21
Figure 2. Conceptual design of the AFM stiffness clamp. 22
Figure 3. Response of expanding hydrogel to step changes in stiffness 23
Figure 4. Cell contraction rapidly responds to stiffness changes. 25
SUPPORTING MATERIAL **27**
Derivation 27
Range of apparent stiffnesses 28
SUPPORTING FIGURES **29**
Figure S1. Graph of the error function, Eq. (6), as a function of its parameters. 29
Figure S2. Extreme stiffnesses. 30

Chapter 3. Contractile equilibration of single cells to step changes in extracellular stiffness **31**

ABSTRACT **32**
INTRODUCTION **33**
MATERIALS AND METHODS **34**
Cell culture and sample preparation 34
Experimental setup 35

Stiffness cycling experiment 35
Measurement of response by ratio analysis 35
Measurement of response timescale by curve fitting 35
Statistical analysis 36
Osmotic swelling of polyacrylamide hydrogel 36
RESULTS 36
Cells spreading between an AFM cantilever and surface exhibit uniform contraction velocity and force rates for a given extracellular stiffness 36
Contracting cells adapt to step changes in extracellular stiffness on a timescale of seconds 37
Focal adhesion signaling does not affect the seconds-timescale response to a step change in extracellular stiffness 38
Partial inhibition of myosin lengthens the seconds-timescale response to a step change in extracellular stiffness 38
Stretch-activated ion channels are not involved in the seconds-timescale response to a step change in extracellular stiffness 39
A simple mechanical model predicts the seconds-timescale response to a step change in extracellular stiffness 39
Swelling hydrogels exhibit a similar seconds-timescale response to a step change in external stiffness 40
DISCUSSION 41
ACKNOWLEDGEMENTS 42
REFERENCES 43
FIGURES 46
Figure 1. Atomic force microscope based control of stiffness during single cell contraction 46
Figure 2. Contracting cells adapt to a step change in extracellular stiffness on a timescale of seconds 47
Figure 3. Inhibition experiments reveal a consistent response timescale dependent on cell mechanics rather than adhesion signaling. 48
Figure 4. Simple mechanical model describes contractile response upon a step change in stiffness. 49
Figure 5. Swelling hydrogel exhibits a seconds-timescale response to a step change in extracellular stiffness. 50
SUPPORTING MATERIAL 51
Conversion from stiffness to elasticity 51
Calculation of model parameters for a contracting cell 51
Table S1. Model Parameters calculated based on data. 52
Derivation of the response of the model to step changes in stiffness 53
References 55
SUPPORTING FIGURES 56
Figure S1. Contractile behavior of single cell under constant stiffness. 56
Figure S2. Same trend observed for force trace as for height trace upon a step change in stiffness. 57
Figure S3. Response timescale is independent of contractile force, cell height, force rate, and contraction velocity. 58
Figure S4. Contractile response of a cell to changes in stiffness in the presence of 30 μM blebbistatin. 59
Figure S5. Detailed explanation of mechanical model. 60
Chapter 4. Multicellular architecture of breast epithelia influences mechanics of the epithelial structure 61

ABSTRACT **62**
INTRODUCTION **63**
RESULTS **64**
Healthy and pre-malignant epithelial structures have different mechanical properties 64
Predicted mechanical property changes due to structural differences are consistent with measurements 65
Multicellular structure could affect perceived mechanical microenvironment independent of material properties 65
DISCUSSION **66**
SIMULATION DEVELOPMENT **66**
Development of simulation framework 66
Simulations of perceived stiffness 69
METHODS **70**
Cell culture 70
Immunofluorescence 71
Extraction from 3D culture 71
Surface preparation 71
Atomic force microscopy 71
Parameter fitting and statistics 72
Statistical tests 72
ACKNOWLEDGEMENTS **72**
REFERENCES **73**
FIGURES **76**
Figure 1. Using 3D culture and AFM to measure acinar mechanics. 76
Figure 2. Pre-malignant, filled acinus is stiffer than the healthy, hollow acinus. 77
Figure 3. Differences in multi-cellular architecture cause increased stiffness with malignancy. 78
Figure 4. Filled architecture increases stiffness of cellular microenvironment 79
SUPPORTING FIGURES **80**
Figure S1. Atomic force microscopy is used to apply defined loads. 80
Figure S2. After 1-week healthy and pre-malignant acini have the same architecture. 81
Figure S3. Three-dimensional model of acinus reveals internal stress propagation. 82
Figure S4. Creep response can be modeled by an SLS model 83

Chapter 5. Tensional homeostasis in single contractile cells occurs through a strain-rate dependent tensional buffer **84**
ABSTRACT **85**
INTRODUCTION **86**
MATERIAL & METHODS **86**
Cell culture and sample preparation 86
Experimental setup 87
Constraining spreading 87
Measuring contraction and spread area 87
Testing tensional homeostasis 87
Micro-rheology 88
Statistical analysis 88
RESULTS **88**
Steady-state tension is achieved when spreading is constrained 88
Cell spreading is necessary and precedes contraction in 3D 89
Steady-state tension is maintained in a rate-dependent manner 89

Tensional homeostasis through tensional buffering 90
Cellular elasticity measurements suggest rearrangement of cytoskeleton 90
DISCUSSION 91
Controls of cellular tension 91
Direct evidence for tensional homeostasis 91
Mechanism of tensional homeostasis 92
Conclusions 93
ACKNOWLEDGEMENTS 94
REFERENCES 95
FIGURES 97
Figure 1. Cell contraction between dual patterned surfaces. 97
Figure 2. Limiting cell spreading results in a steady-state force. 98
Figure 3. Cellular tension regulation is rate dependent. 99
Figure 4. Tensional buffering rather than tensional setpoint. 100
Figure 5. Cellular elasticity during contraction and dynamic loading 101
SUPPORTING FIGURES 102
Figure S1. Micropatterning promotes stabile 3D attachment 102
Figure S2. Viscoelastic response of cells to step strains. 103
Chapter 6. Concluding remarks: Thoughts on the future of cellular mechanobiology 104
Summary 105
Future challenges and opportunities 106

Acknowledgements

Over the past five and a half years, innumerable people have helped and supported me throughout my graduate career. Though I am certain I will not be able to recount everyone's contribution, I would like to take a moment to try and convey my gratitude.

First and foremost, I must acknowledge the incredible role my adviser, Dan Fletcher, had in my education. Dan is such a supportive leader, acting both as a role model and mentor, while also establishing a cooperative environment in the Lab. Reflecting Dan's various interests, the Fletcher Lab is composed of people from a diverse array of backgrounds. I have found it incredibly enjoyable and productive to work in such an environment, where I can get feedback from people working in so many different disciplinary fields.

Within the lab, I have worked most closely with two people. The first is Ailey Crow, who helped mentor me when I first joined the lab. Her exuberant energy and ability to effectively communicate complicated ideas were a joy to behold. A few years in to my graduate tenure, Win Pin Ng joined the lab and we have worked closely since. Win Pin's patience, persistence, and methodical approach have proved invaluable to the work we've done together. I am forever grateful for the collaborative and cooperative experience working with both Ailey and Win Pin.

Over the years I have also had the opportunity of working with the only other student in the lab from my year, Gautham Venugopalan. I have always enjoyed his comradery in the face of whatever challenges grad school might throw our way. I also would like to acknowledge the influence the first generation members of the Fletcher Lab had on my own experience. When I joined, already the lab was a fun place to work, thanks to the likes of Thomas Li, Jeanne Stachowiak, Mike Rosenbluth, Wendy Hansen, Sander Pronk, Ailey Crow, Viviana Risca, Sapun Parekh, Ovijit Chaudhuri, Dave Richmond, Ross Rounsevell, and Wilbur Lam. In the ensuing years, I have had the privilege of working with other great scientists and scientists-to-be that have come through the lab, including Eva Schmid, Eric Douglas, Lina Nilsson, Peter Bieling, Neil Switz, Mike D'Ambrosio, Alba Diz-Muñoz, Matt Good, Ben Ricca, Tai-De Li, Mike Vahey, Arunan Skandarajah, Matthew Bakalar, Clay Reber, Sara Berreto, Casper Clausen, Win Pin Ng, and Pamela Jreij. As a lab, our scientific endeavors have been incalculably aided by the work of Stephanie Eistetter and Ann Hyoungsook as staff members, and I certainly know my life has been made easier!

Beyond my lab, I'd also like to acknowledge my classmates within the Biophysics Graduate Group. When I first came to Berkeley, I moved into the unofficial Biophysics house and had a great time with my housemates, J.M. Mongeau, Elizabeth Xu, Vince Ramey, Viviana Risca, and Jacques Bothma. I also really appreciated the community present amongst the rest of the Class of 2007: David Adamson, Greg Alushin, Lia Ball, Alistair Boettiger, Michael Cianfrocco, Will Draper, Anna Labno, Elad Maor, Jean-Michel Mongeau, Carl Rogers, Elizabeth Xu, and Jaime Yassif.

Additionally, I would like to thank the faculty that have served in advisory roles to me in various capacities. In addition to Dan Fletcher, Professors Jan Liphardt and Jay Groves both

opened up their labs to me during rotations. I would also like to thank my qualifying exam committee, Sanjay Kumar, Jan Liphardt, Jay Groves, and David Schaffer. Finally, I sincerely appreciate the advice of the members of my dissertation committee, Dan Fletcher, Sanjay Kumar, Jan Liphardt, and Matt Welch, whose guidance during the course of my research was invaluable in completing this work.

Last but not least, I would like to thank the members of my family, who have always supported my ever-continuing pursuit of learning. My parents created an atmosphere where I always felt safe asking the questions: why and how? My siblings, all older than I, helped show me how to answer those questions. Finally, I am so lucky to thank my incredible wife, Hillary, whose gracious patience and support throughout the course of my PhD were indispensible to the completion of this dissertation.

While I know that I have not even come close to acknowledging all the people that have helped me during my entire graduate tenure, there is the matter of the *content* of my dissertation, so we should be moving along!

Chapter 1.

Introduction: Mechanical regulators of the cell – The role of tension and stiffness

Force as a signal

The role of mechanical processes in driving cellular functions has been a fruitful line of inquiry, with an emerging picture wherein mechanical conditions are serving similarly important functions as traditional biochemical signaling networks (Eyckmans et al. 2011). Adherent cells of all types have been shown to sense both the force and stiffness of their microenvironment. While certain specialized cell types have long been known to be force sensitive (e.g. cochlear outer hair cells within the ear (Brownell et al. 1985)), what has become increasingly apparent is the universality of force sensitivity within adherent mammalian cells (Janmey et al. 2009; Eyckmans et al. 2011; Schwarz and Gardel 2012). Understanding the specific nature of this sensitivity, what are its controls, timescales, and key molecular players has been the task of much of the mechanobiology field.

Role of stiffness in cellular biology

One of the most important parameters of the physical environment is the stiffness of the materials cells are attached to. The elasticity of tissues in the body varies from near 100 Pa for soft tissues such as the brain to 10-100 kPa for muscle tissue and up to MPa for cartilage (Georges and Janmey 2005). This property of a cell's microenvironment is influential in many biological processes such as embryogenesis (Jacot, Martin, and Hunt 2010), cell-cycle control (Klein et al. 2009), angiogenesis (Mammoto et al. 2009), motility (Lo et al. 2000) , tumorigenesis (Paszek et al. 2005), and stem cell differentiation (Engler et al. 2006). Elastic materials are characterized by a linear relationship between deformation or strain and applied force or stress ($F=k\Delta x$; $\sigma=E\varepsilon$). This relationship means that stiffer materials will require more force to deform the same amount as a soft material, or similarly, for a given force, the stiffer the material, the less it deforms.

Early experiments found that given a variety of substrate stiffnesses, cells tended to exert more force the stiffer their environment (Saez et al. 2007). Further, cells tended to migrate towards stiffer conditions when plated on elasticity gradients (Lo et al. 2000). One of the most widely cited and influential works investigating the effect of stiffness discovered that, given the same biochemical signals, substrate stiffness alone could determine stem cell differentiation lineage selection (Engler et al. 2006). This, along with numerous studies since, has ignited excitement in understanding the underlying mechanism that appears to be conserved across so many cell types, with the hope that this will enable new therapeutic avenues beyond pharmacological agents that disrupt biochemical signaling networks (Ladoux and Nicolas 2012; Schwarz and Gardel 2012; Eyckmans et al. 2011).

Technologies for probing cell forces

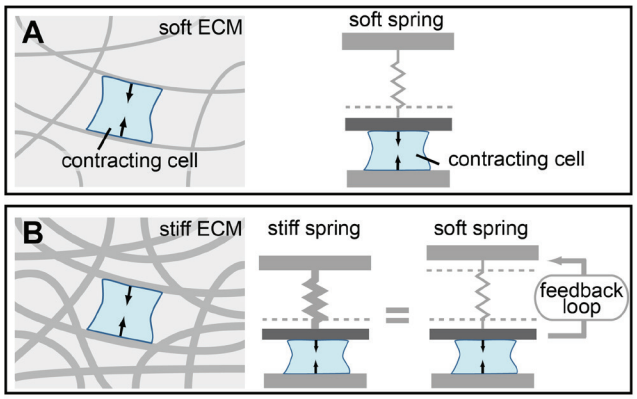

Figure 1. Cells pull on the surrounding extracellular matrix and sense a microenvironmental stiffness. Feedback control can change the apparent stiffness a cell experiences (Chapter 2).

Numerous assays have been developed to both measure and apply forces to cells, in order to ultimately better understand the molecular mechanism of cellular force and stiffness sensitivity. These include cells on, in or between soft gels (Pelham and Wang 1997; Hoffecker, Guo, and Wang 2011; Brown et al. 1998; Beningo, Dembo, and Wang 2004), cells spread over several small posts (Tan et al. 2003), cells horizontally spanning between micro-pillars (Kajzar et al. 2008), cells between parallel microplates (Mitrossilis et al. 2009; Mitrossilis et al. 2010) and cells adhered to coated beads restrained in an optical trap or magnetic field (Choquet, Felsenfeld, and Sheetz 1997). Of this wide array of techniques, traction force microscopy (TFM) is the most widely used, wherein cells are plated on an ECM-protein functionalized poly-acrylamide gel, which has small beads immobilized within the gel that are used to determine a strain field and ultimately a traction force map (Kraning-Rush et al. 2012). Work has continued on refining the capabilities of TFM and the technique has been extended to tracking beads in 3D with confocal microscopy in order to measure out-of-plane forces (Franck et al. 2011).

However, various limitations remain with this technique regarding both the ability to present the cell with a geometry that more closely mimics tissue, while also being able to dynamically and independently control the microenvironmental mechanics in order to observe the cellular response. While efforts have been made to address each of these limitations (geometry, (Beningo, Dembo, and Wang 2004); dynamic control (Frey and Wang 2009; Jiang et al. 2010)), combining geometry with dynamic, reversible control of stiffness requires the development of a novel experimental approach. Chapter 2 outlines the development of just such an apparatus (Figure 1), along with the unique observations that could only have been achieved using the new technology (Webster, Crow, and Fletcher 2011).

A common thread connecting all my work has been the use of atomic force microscopy (AFM) as a precise tool for both measuring and manipulating the mechanics of a cell and its mechanosensory machinery (Figure 2). Silicon or silicon nitride fabricated cantilevers can be manufactured to produce very thin and flexible beams, typically rectangular or triangular in shape. Using the principle of an optical lever system, a laser is reflected off of the back surface of the cantilever and is collected by a photodetector. In this way, sub-nanometer deflections of the cantilever are detectable. Additionally, for small strains, the cantilever behaves like a linear Hookean spring, allowing the conversion of displacement into force given the spring constant of the cantilever, $F = k_{cantilever}\Delta x_{cantilever}$. Adding the use of closed-loop piezo-electric positioning of the cantilever allows us to not only measure forces, but also to apply dynamic loads. I use this platform to change the microenviron-mental stiffness experienced by single contractile cells (Chapters 2-3), to measure the

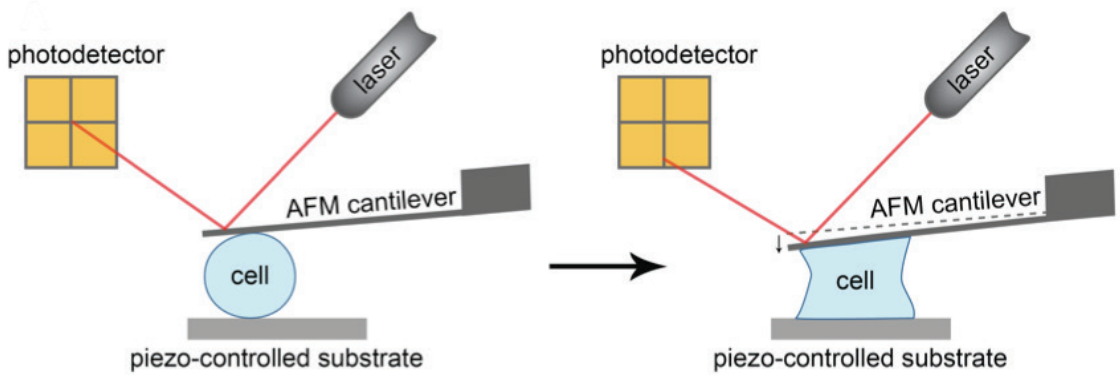

Figure 2. Contraction force microscopy. The precise control afforded by atomic force microscopy (AFM) enables unparalleled time, force, and spatial resolution to measure cellular contraction, rheology, and response to dynamic environments (Chapters 2-5).

mechanical properties of epithelial cells and the 3D structures they form (Chapter 4), and finally to apply dynamic loading to provide the first direct evidence for tensional homeostasis, a process whereby cells will maintain their tension when stretched or compressed (Chapter 5).

Boundary conditions for stiffness sensing mechanism

Given the lack of specific control of force, stiffness, and deformation using other techniques, one of the outstanding questions is the contribution of each of these three parameters in determining the cell's response. Two particular questions have remained unanswered by previous experiments within the literature. First, do cells respond directly to stiffness? Or instead do they sense the larger forces needed to displace a fixed amount on stiffer substrates? Or, alternately, do they instead respond to the increased deformations that result from a fixed force in soft environments? The experiments in Chapter 2 answer this first question, demonstrating that independent of absolute force or displacement, cellular contraction responds directly to stiffness itself.

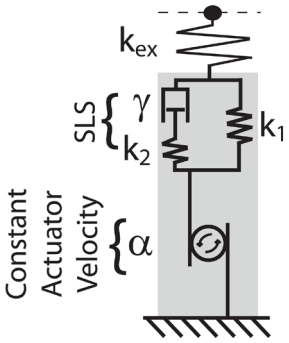

Figure 3. Simple mechanical model describes cell's contractile response upon a step change in stiffness (Chapter 3).

The second unanswered question is what is the timescale of cellular stiffness sensing? In Chapter 3, by applying step changes in stiffness over time, I demonstrate that the cell must integrate environmental stiffness properties with the cell's own viscoelastic cytoskeleton (Figure 3). This imposes a seconds-timescale buffering of environmental mechanical signals, which operates in a myosin-dependent manner (Crow, Webster et al. 2012). Used in conjunction with other technologies, we now have an even greater understanding of the boundary conditions of the cell's stiffness sensing machinery.

Stiffness as a marker and driver in disease

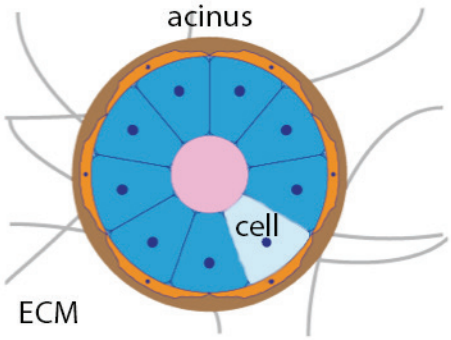

Figure 4. An acinus consists of mammary epithelial cells that grows in a dynamic environment surrounded by extracellular matrix, fluids, and other cells (Chapter 4).

Physicians for decades have used stiffness to identify diseased or damaged tissue, from identifying scar tissue to cancerous growths within breast tissue. More recently, however, beyond stiffness only helping us to identify disease states, stiffness has been implicated in driving and reinforcing the diseased condition (Paszek et al. 2005). This revelation has sparked renewed interest in understanding both how cells are sensitive to stiffness, as well as how changes in tissue mechanics progress during the development of disease.

One of the clearest examples of different tissue stiffness during disease is present in breast cancer. Invasive lobular carcinoma accounts for 10-15% of new invasive breast cancer cases (Lopez and Bassett 2009), afflicting approximately 30,000 women annually in the US. This form of cancer results from malignant epithelial cells lining the milk producing alveoli (or acini), which are found within lobule structures. Previous research has shown that, these epithelial cells are grown embedded within extracellular matrices (ECM) of different stiffnesses, stiffer matrices will promote the malignant phenotype (Paszek et al. 2005). However, these epithelial cells do not only sense the ECM stiffness. They in fact exist in spherical-like structures, where direct interactions with neighboring cells are an important mechanical signal defining their microenvironmental stiffness (Figure 4). In Chapter 4, I demonstrate that the changes in this multicellular architecture that accompany malignancy account for the acinur stiffening observed during cancer progression. This result suggests that it is no longer sufficient to think of only the stiffness of the ECM or cells themselves, but we must also account for how cells are geometrically arranged in multi-cellular structures in order to fully understand the mechanics of the epithelial microenvironment.

Force balance: maintaining healthy cell function

One of the most widely discussed concepts within the field of mechanobiology is the tensional homeostasis hypothesis (DuFort, Paszek, and Weaver 2011). The hypothesis states that cells will actively respond to loading from their environment to maintain a given level of tension. It is thought that this process is disrupted in disease and that this mis-regulation may in fact promote the disease state (Paszek et al. 2005). However, since first being introduced in 1998, only three studies have shown any evidence to support tensional homeostasis (Brown et al. 1998; Mizutani, Haga, and Kawabata 2004; Ezra et al. 2010). Unfortunately, the evidence to date only extrapolates a trend of millions of cells, or inaccurately uses cellular stiffness as a proxy for tension.

In Chapter 5, I provide the first direct evidence for tensional homeostasis. Using contraction force microscopy, I show that cells maintain their tension when undergoing substantial strain (>10%). Figure 5 shows this tensional homeostasis when a cell is stretched by 1 μm over a period of 10 minutes. Notably, unlike what has been previously suggested (Ezra et al. 2010), this tension regulation does not occur through a closed-loop feedback controller with a given force setpoint. Rather, it behaves like a tensional buffer that maintains, or buffers, tension for displacement rates within a certain range. Specifically, if the rate of loading is faster than what the cell can counteract (or buffer), tension will change in proportion to displacement. Once the loading stops (or the rate drops below the buffering threshold), the cell again maintains tension and will remain at the new force. Tensional buffering may enable the cell to modulate its response to loading where, during slow straining, the cell plastically deforms and absorbs the load, while for fast straining, the cell behaves more rigidly to stabilize the tissue and resist deformations.

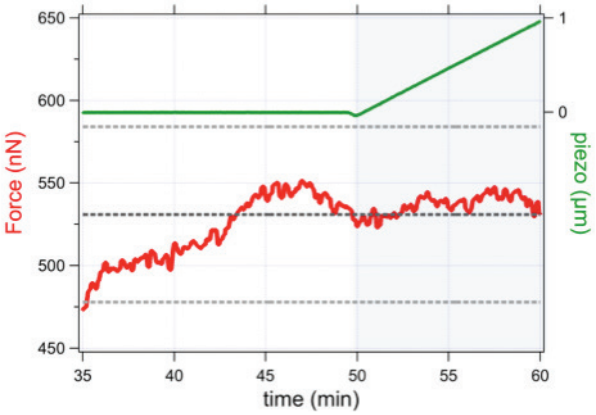

Figure 5. First direct evidence for tensional homeostasis in single cells. Cells maintain their tension for slow loading, but elastically resist fast loading (Chapter 5).

Scope of dissertation

This dissertation covers the majority of the research I have done throughout the course of my PhD. Beyond the chapters listed here, I have also collaborated on a published study investigating the mechanosensitive properties of platelets (Lam et al. 2011). Additionally, I have worked on an unpublished, ongoing study to understand the mechanical nature of transendothelial cell macroaperture tunnel formation, a process implicated in transendothelial migration as well as used by a class of bacterial toxins called tunnel-forming toxins (Maddugoda et al. 2011; Gonzalez-Rodriguez et al. 2012).

While there are many technologies that have been developed to investigate the processes of mechanobiology, I believe that contraction force microscopy is uniquely suited to combining both precise measurement *and* control of mechanics, with great temporal resolution, to enable a new understanding of the cell's relationship with its environment. Rather than thinking only of equilibrium behaviors, my research has highlighted the importance of the history dependence of a cell's mechanical environment over time. While this presents a substantial technical challenge to the field, this line of inquiry may yet help us make sense of the myriad of cellular mechanical responses, and ultimately to gain a deeper understanding of all the signals, both biochemical and mechanical, that guide cellular behaviors.

References

Beningo, Karen A., Micah Dembo, and Yu-li Wang. 2004. "Responses of Fibroblasts to Anchorage of Dorsal Extracellular Matrix Receptors." *Proceedings of the National Academy of Sciences* 101 (52) (December 28): 18024–18029. doi:10.1073/pnas.0405747102.

Brown, R. A., R. Prajapati, D. A. McGrouther, I. V. Yannas, and M. Eastwood. 1998. "Tensional Homeostasis in Dermal Fibroblasts: Mechanical Responses to Mechanical Loading in Three-dimensional Substrates." *Journal of Cellular Physiology* 175 (3): 323–332. doi:10.1002/(SICI)1097-4652(199806)175:3<323::AID-JCP10>3.0.CO;2-6.

Brownell, W., C. Bader, D Bertrand, and Y de Ribaupierre. 1985. "Evoked Mechanical Responses of Isolated Cochlear Outer Hair Cells." *Science* 227 (4683) (January 11): 194–196. doi:10.1126/science.3966153.

Choquet, Daniel, Dan P. Felsenfeld, and Michael P. Sheetz. 1997. "Extracellular Matrix Rigidity Causes Strengthening of Integrin–Cytoskeleton Linkages." *Cell* 88 (1) (January 10): 39–48. doi:10.1016/S0092-8674(00)81856-5.

Crow, Ailey, Kevin D. Webster, Evan Hohlfeld, Win Pin Ng, Phillip Geissler, and Daniel A. Fletcher. 2012. "Contractile Equilibration of Single Cells to Step Changes in Extracellular Stiffness." *Biophysical Journal* 102 (3) (February 8): 443–451. doi:10.1016/j.bpj.2011.11.4020.

DuFort, Christopher C., Matthew J. Paszek, and Valerie M. Weaver. 2011. "Balancing Forces: Architectural Control of Mechanotransduction." *Nature Reviews Molecular Cell Biology* 12 (5) (May 1): 308–319. doi:10.1038/nrm3112.

Engler, Adam J., Shamik Sen, H. Lee Sweeney, and Dennis E. Discher. 2006. "Matrix Elasticity Directs Stem Cell Lineage Specification." *Cell* 126 (4) (August 25): 677–689. doi:10.1016/j.cell.2006.06.044.

Eyckmans, Jeroen, Thomas Boudou, Xiang Yu, and Christopher S. Chen. 2011. "A Hitchhiker's Guide to Mechanobiology." *Developmental Cell* 21 (1) (July 19): 35–47. doi:10.1016/j.devcel.2011.06.015.

Ezra, Daniel G., James S. Ellis, Michèle Beaconsfield, Richard Collin, and Maryse Bailly. 2010. "Changes in Fibroblast Mechanostat Set Point and Mechanosensitivity: An Adaptive Response to Mechanical Stress in Floppy Eyelid Syndrome." *Investigative Ophthalmology & Visual Science* 51 (8) (August): 3853–3863. doi:10.1167/iovs.09-4724.

Franck, Christian, Stacey A. Maskarinec, David A. Tirrell, and Guruswami Ravichandran. 2011. "Three-Dimensional Traction Force Microscopy: A New Tool for Quantifying Cell-Matrix Interactions." *PLoS ONE* 6 (3) (March 29): e17833. doi:10.1371/journal.pone.0017833.

Frey, Margo T., and Yu-li Wang. 2009. "A Photo-modulatable Material for Probing Cellular Responses to Substrate Rigidity." *Soft Matter* 5 (9): 1918. doi:10.1039/b818104g.

Georges, Penelope C., and Paul A. Janmey. 2005. "Cell Type-specific Response to Growth on Soft Materials." *Journal of Applied Physiology* 98 (4) (April 1): 1547–1553. doi:10.1152/japplphysiol.01121.2004.

Gonzalez-Rodriguez, David, Madhavi P. Maddugoda, Caroline Stefani, Sebastien Janel, Frank Lafont, Damien Cuvelier, Emmanuel Lemichez, and Françoise Brochard-Wyart. 2012. "Cellular Dewetting: Opening of Macroapertures in Endothelial Cells." *Physical Review Letters* 108 (21) (May 25): 218105. doi:10.1103/PhysRevLett.108.218105.

Hoffecker, Ian T., Wei-hui Guo, and Yu-li Wang. 2011. "Assessing the Spatial Resolution of Cellular Rigidity Sensing Using a Micropatterned Hydrogel–photoresist Composite." *Lab on a Chip* 11 (20): 3538. doi:10.1039/c1lc20504h.

Jacot, Jeffrey G., Jody C. Martin, and Darlene L. Hunt. 2010. "Mechanobiology of Cardiomyocyte Development." *Journal of Biomechanics* 43 (1) (January 5): 93–98. doi:10.1016/j.jbiomech.2009.09.014.

Janmey, Paul A, Jessamine P Winer, Maria E Murray, and Qi Wen. 2009. "The Hard Life of Soft Cells." *Cell Motility and the Cytoskeleton* 66 (8) (August): 597–605. doi:10.1002/cm.20382.

Jiang, Frank X., Bernard Yurke, Rene S. Schloss, Bonnie L. Firestein, and Noshir A. Langrana. 2010. "The Relationship Between Fibroblast Growth and the Dynamic Stiffnesses of a DNA Crosslinked Hydrogel." *Biomaterials* 31 (6) (February): 1199–1212. doi:10.1016/j.biomaterials.2009.10.050.

Kajzar, A., C. M. Cesa, N. Kirchgeßner, B. Hoffmann, and R. Merkel. 2008. "Toward Physiological Conditions for Cell Analyses: Forces of Heart Muscle Cells Suspended Between Elastic Micropillars." *Biophysical Journal* 94 (5) (March 1): 1854–1866. doi:10.1529/biophysj.107.115766.

Klein, Eric A., Liqun Yin, Devashish Kothapalli, Paola Castagnino, Fitzroy J. Byfield, Tina Xu, Ilya Levental, Elizabeth Hawthorne, Paul A. Janmey, and Richard K. Assoian. 2009. "Cell-cycle Control by Physiological Matrix Elasticity and in Vivo Tissue Stiffening." *Current Biology* 19 (18) (September 29): 1511–1518. doi:10.1016/j.cub.2009.07.069.

Kraning-Rush, Casey M., Shawn P. Carey, Joseph P. Califano, and Cynthia A. Reinhart-King. 2012. "Chapter 6 - Quantifying Traction Stresses in Adherent Cells." In *Computational Methods in Cell Biology*, Volume 110:139–178. Academic Press.

Ladoux, Benoit, and Alice Nicolas. 2012. "Physically Based Principles of Cell Adhesion Mechanosensitivity in Tissues." *Reports on Progress in Physics* 75 (11) (November 1): 116601. doi:10.1088/0034-4885/75/11/116601.

Lam, Wilbur A., Ovijit Chaudhuri, Ailey Crow, Kevin D. Webster, Tai-De Li, Ashley Kita, James Huang, and Daniel A. Fletcher. 2011. "Mechanics and Contraction Dynamics of Single Platelets and Implications for Clot Stiffening." *Nat Mater* 10 (1) (January): 61–66. doi:10.1038/nmat2903.

Lo, C M, H B Wang, M Dembo, and Y L Wang. 2000. "Cell Movement Is Guided by the Rigidity of the Substrate." *Biophysical Journal* 79 (1) (July): 144–152. doi:10.1016/S0006-3495(00)76279-5.

Lopez, January K., and Lawrence W. Bassett. 2009. "Invasive Lobular Carcinoma of the Breast: Spectrum of Mammographic, US, and MR Imaging Findings1." *Radiographics* 29 (1) (January 1): 165–176. doi:10.1148/rg.291085100.

Maddugoda, Madhavi P., Caroline Stefani, David Gonzalez-Rodriguez, Juha Saarikangas, Stéphanie Torrino, Sebastien Janel, Patrick Munro, et al. 2011. "cAMP Signaling by Anthrax Edema Toxin Induces Transendothelial Cell Tunnels, Which Are Resealed by

MIM via Arp2/3-Driven Actin Polymerization." *Cell Host & Microbe* 10 (5) (November 17): 464–474. doi:10.1016/j.chom.2011.09.014.

Mammoto, Akiko, Kip M. Connor, Tadanori Mammoto, Chong Wing Yung, Dongeun Huh, Christopher M. Aderman, Gustavo Mostoslavsky, Lois E. H. Smith, and Donald E. Ingber. 2009. "A Mechanosensitive Transcriptional Mechanism That Controls Angiogenesis." *Nature* 457 (7233) (February 26): 1103–1108. doi:10.1038/nature07765.

Mitrossilis, D., J. Fouchard, A. Guiroy, N. Desprat, N. Rodriguez, B. Fabry, and A. Asnacios. 2009. "Single-cell Response to Stiffness Exhibits Muscle-like Behavior." *Proceedings of the National Academy of Sciences* 106 (43) (October): 18243–18248. doi:10.1073/pnas.0903994106.

Mitrossilis, D., Jonathan Fouchard, David Pereira, François Postic, Alain Richert, Michel Saint-Jean, and Atef Asnacios. 2010. "Real-time Single-cell Response to Stiffness." *Proceedings of the National Academy of Sciences* 107 (38): 16518 –16523. doi:10.1073/pnas.1007940107.

Mizutani, Takeomi, Hisashi Haga, and Kazushige Kawabata. 2004. "Cellular Stiffness Response to External Deformation: Tensional Homeostasis in a Single Fibroblast." *Cell Motility and the Cytoskeleton* 59 (4): 242–248. doi:10.1002/cm.20037.

Paszek, Matthew J., Nastaran Zahir, Kandice R. Johnson, Johnathon N. Lakins, Gabriela I. Rozenberg, Amit Gefen, Cynthia A. Reinhart-King, et al. 2005. "Tensional Homeostasis and the Malignant Phenotype." *Cancer Cell* 8 (3) (September): 241–254. doi:10.1016/j.ccr.2005.08.010.

Pelham, Robert J., and Yu-li Wang. 1997. "Cell Locomotion and Focal Adhesions Are Regulated by Substrate Flexibility." *Proceedings of the National Academy of Sciences of the United States of America* 94 (25) (December 9): 13661 –13665.

Saez, Alexandre, Marion Ghibaudo, Axel Buguin, Pascal Silberzan, and Benoît Ladoux. 2007. "Rigidity-driven Growth and Migration of Epithelial Cells on Microstructured Anisotropic Substrates." *Proceedings of the National Academy of Sciences* 104 (20) (May 15): 8281 –8286. doi:10.1073/pnas.0702259104.

Schwarz, Ulrich S., and Margaret L. Gardel. 2012. "United We Stand – Integrating the Actin Cytoskeleton and Cell–matrix Adhesions in Cellular Mechanotransduction." *Journal of Cell Science* 125 (13) (July 1): 3051–3060. doi:10.1242/jcs.093716.

Tan, John L., Joe Tien, Dana M. Pirone, Darren S. Gray, Kiran Bhadriraju, and Christopher S. Chen. 2003. "Cells Lying on a Bed of Microneedles: An Approach to Isolate Mechanical Force." *Proceedings of the National Academy of Sciences of the United States of America* 100 (4) (February 18): 1484 –1489. doi:10.1073/pnas.0235407100.

Webster, Kevin D, Ailey Crow, and Daniel A Fletcher. 2011. "An AFM-based Stiffness Clamp for Dynamic Control of Rigidity." *PloS One* 6 (3): e17807. doi:10.1371/journal.pone.0017807.

Chapter 2.

An AFM-based stiffness clamp for dynamic control of rigidity

*Reprinted with permission from the article "An AFM-based stiffness clamp for dynamic control of rigidity" by Kevin D. Webster, Ailey Crow, and Daniel A. Fletcher in PLoS ONE **6**(3), March 2011 (e17807).*

ABSTRACT

Atomic force microscopy (AFM) has become a powerful tool for measuring material properties in biology and imposing mechanical boundary conditions on samples from single molecules to cells and tissues. Constant force or constant height can be maintained in an AFM experiment through feedback control of cantilever deflection, known respectively as a 'force clamp' or 'position clamp'. However, stiffness, the third variable in the Hookean relation $F = kx$ that describes AFM cantilever deflection, has not been dynamically controllable in the same way. Here we present and demonstrate a 'stiffness clamp' that can vary the apparent stiffness of an AFM cantilever. This method, employable on any AFM system by modifying feedback control of the cantilever, allows rapid and reversible tuning of the stiffness exposed to the sample in a way that can decouple the role of stiffness from force and deformation. We demonstrated the AFM stiffness clamp on two different samples: a contracting fibroblast cell and an expanding polyacrylamide hydrogel. We found that the fibroblast, a cell type that secretes and organizes the extracellular matrix, exhibited a rapid, sub-second change in traction rate (dF/dt) and contraction velocity (dx/dt) in response to step changes in stiffness between 1-100 nN/μm. This response was independent of the absolute contractile force and cell height, demonstrating that cells can react directly to changes in stiffness alone. In contrast, the hydrogel used in our experiment maintained a constant expansion velocity (dx/dt) over this range of stiffness, while the traction rate (dF/dt) changed with stiffness, showing that passive materials can also behave differently in different stiffness environments. The AFM stiffness clamp presented here, which is applicable to mechanical measurements on both biological and non-biological samples, may be used to investigate cellular mechanotransduction under a wide range of controlled mechanical boundary conditions.

INTRODUCTION

Atomic force microscopy (AFM), initially developed as a topographical imaging modality, has become an important tool for investigating the mechanical properties and dynamic behavior of biological molecules, materials, cells, and tissues [1]. AFM-based techniques in cell and molecular biology leverage the high resolution of AFM in space, time, and force to study properties such as cell adhesion mechanics [2], polymer network dynamics [3], and protein folding [4]. Here we present the development of a method for dynamically varying AFM cantilever stiffness that takes advantage of precise AFM feedback control to create changes in the external rigidity felt by active samples. We use this method, which we call a 'stiffness clamp' by analogy to the existing 'force clamp' and 'position clamp', to investigate the cellular response to rigidity.

The rigidity of the cellular microenvironment has been shown to be an important input signal that influences a range of biological processes [5]. The resistance to deformation of tissues in vivo, characterized by an elastic modulus, varies from near 100 pascals for soft tissues such as the brain to tens of thousands of pascals for muscle tissue and up to millions of pascals for cartilage. This tissue rigidity, or stiffness, serves as an important in vivo cue in processes such as embryogenesis [6], cell proliferation [7], and angiogenesis [8]. Notably, numerous experiments have demonstrated the influence of microenvironmental rigidity in vitro on cellular morphology [9], motility [10], and differentiation [11]. While the importance of stiffness has been well-documented, the dynamics of rigidity sensing are poorly understood.

The predominant methods for studying the effects of microenvironmental rigidity on cellular behaviors involve culturing cells on deformable substrates (e.g. thin rubber films [12], polyacrylamide hydrogels [13], and microfabricated posts [14]). These studies, while instrumental in establishing the effect of substrate rigidity on cellular behaviors, are limited to a single static rigidity for each experiment. Similarly, the spring-like behavior of optical traps, AFMs, and microplates has also been used to expose single cells to different microenvironmental rigidities but these usually use only a single rigidity per experiment [15-17]. To expose a given cell to multiple rigidities, some studies have employed static rigidity gradients [18,19] or substrates of anisotropic rigidity [10]. Recent studies have demonstrated hydrogels with dynamic rigidities that utilize UV exposure [20] or DNA crosslinking [21] to change rigidity mid-experiment, though the stiffness changes are relatively slow, not reversible, and can only sample a narrow range of elastic moduli. Furthermore, none of these techniques distinguish between the cell's response to force, deformation, and stiffness. Recently, a custom-built parallel microplate system was used in combination with double-feedback to change the effective stiffness experienced by a single cell spread between the microplates [22]. While AFMs have the advantage of high resolution in space, time, and force, and cells can spread between a microfabricated cantilever and a surface [16,23], AFM systems are currently limited to a single stiffness per experiment given by the native cantilever stiffness.

We have developed an AFM feedback algorithm to reversibly and rapidly change the stiffness presented to the sample while accurately measuring force and deformation. We

apply this AFM stiffness clamp to study the dynamics of an expanding hydrogel and a single cell in response to step changes in stiffness.

RESULTS

Stiffness clamp concept

The mechanical interaction of contractile cells with their microenvironment, which is composed of polymeric extracellular matrix (ECM) proteins and other cells, can be modeled most simply as a cell pulling on a spring (FIG. 1A). Setting aside the nonlinear behavior of the ECM temporarily, a cell that deforms a Hookean spring experiences a resistance force given by the spring constant and the amount of deformation. The goal of the stiffness clamp is to tune the apparent stiffness a cell experiences by controlling how much force the cell must exert to change its height a given amount through feedback control of the spring deflection (FIG. 1B).

In theory, a wide range of apparent stiffnesses may be achieved using only a single spring together with feedback control (FIG. 2). If the spring base is moved away from the cell as it contracts, the spring will appear stiffer to the contracting cell than it actually is (FIG. 2A). If the spring base is moved upwards, away from the cell by the same amount that the cell deflects the spring downward, then the cell height, x_{cell}, will remain constant. Given this constraint, regardless of the force the cell exerts on the spring, the cell's height does not change, thereby exposing the cell to an infinitely stiff microenvironment:

$$k_{apparent} = \frac{\Delta F}{\Delta x_{cell}} = \frac{\Delta F}{0} \to \infty$$

By moving the spring base toward the cell as it contracts, the spring will appear softer than it actually is (FIG. 2B). If the feedback routine moves the spring base such that the spring does not change in length, the force exerted on the spring remains constant, and the stiffness of the microenvironment appears to be infinitely soft:

$$k_{apparent} = \frac{\Delta F}{\Delta x_{cell}} = \frac{0}{\Delta x_{cell}} \to 0$$

These two limits of constant height and constant force have been used elsewhere and are known as the position and force clamp, respectively [24]. Force and position clamps are based on a simple PID-feedback routine that uses the error between a given setpoint force or position and the current force or position to adjust the sample position. In contrast, stiffness is defined as the *change* in force over the *change* in displacement and therefore cannot be controlled using conventional feedback routines. The AFM stiffness clamp presented here is able to dynamically tune apparent stiffness *between* the extremes of infinitely soft and stiff.

Stiffness clamp applied to an expanding hydrogel

We tested the ability of the AFM stiffness clamp algorithm to produce a range of apparent stiffnesses with an expanding hydrogel, and we characterized the material's response to step changes in stiffness. Addition of phosphate buffered saline (PBS) to a dehydrated ~1 kPa polyacrylamide hydrogel caused it to gradually expand. As the gel expanded and increased in height, it pushed against the cantilever applying an increasing force (FIG. 3A&B). Without the stiffness clamp feedback loop, the spring constant of the cantilever defined how much force the gel applied to increase its height. When we changed the apparent stiffness of the cantilever using the stiffness clamp between 1-100 nN/μm, there was an immediate change in the force rate due to the modified feedback control of the cantilever position, while the gel expansion rate remained essentially constant (FIG. 3C). This behavior was observed for N = 5 gels.

With a single AFM cantilever with spring constant $k_{cantilever}$, we used the stiffness clamp to apply 11 different stiffnesses ranging from 0 to infinity as the gel expanded. By plotting the cantilever force versus the gel height we obtained a series of traces where the slopes define the achieved apparent stiffness (FIG. 3D). The apparent stiffness measured from the slope of the traces in FIG. 3D was less than 0.1% different from the desired value for a range of stiffnesses spanning two orders of magnitude from $1/16$ to 16 $k_{cantilever}$. The most extreme apparent stiffnesses (force clamp and position clamp) produced traces with Gaussian noise around a constant force and height with standard deviations of 15 pN and 0.34 nm, respectively. (See Supporting Material for further information.) Figure 3D demonstrates that we can accurately apply a wide range of apparent stiffnesses on an expanding hydrogel, all with a single cantilever, using the AFM stiffness clamp.

Stiffness clamp applied to a contracting cell

Fibroblast cells are used extensively as a model system to investigate the effect of substrate rigidity [5,9,13,14,18]. After demonstrating the range and precision of the stiffness clamp algorithm with a hydrogel, we used NIH 3T3 fibroblast cells to investigate how cellular rigidity sensing responds to a reversible step change in stiffness. Figure 4 shows the results of a typical experiment. Cells in suspension were flowed into a chamber and within minutes were brought into contact with both a fibronectin-coated glass surface and a fibronectin-coated tipless AFM cantilever ($k_{cantilever}$ = 18 nN/μm). After a small compressive force (4 nN) established contact, adhesions formed on both surfaces, and the cell contracted (FIG. 4A). Once contraction started we cycled between stiffnesses of $1/5$, 1, and 5 $k_{cantilever}$ (3.6, 18, 90 nN/μm) every 30 s. We chose a cycle period of 30 s to allow for exchange of cytoskeletal and focal adhesion components (timescale of seconds) but not full reorganization of adhesions or the cytoskeleton (timescale of minutes) [25]. A typical resulting traction force and cell height trace is shown in FIG. 4B.

We found that when the apparent stiffness changed to a larger value, the cell's traction rate dF/dt rapidly increased while the corresponding contraction velocity dx/dt decreased (FIG. 4D). Notably, this change in traction rate and contraction velocity happens nearly instantaneously (within 0.5 s) (FIG. 4B inset), indicating that cells can reversibly respond to a stiffness cue on a whole cell level on a timescale of seconds. The stiffness-dependent

traction rate and velocity were found to be reversible and consistent for a given cell, despite changes in absolute cell height and contractile force. Even though the absolute cell tension was greater later during contraction, the traction rate was dependent only on the instantaneously applied stiffness (and similarly for cell height and contraction velocity). Importantly, this indicates that the response of contraction rate is specifically due to a change in stiffness and not the cell tension or height. This behavior was observed for N=30 cells.

DISCUSSION

The AFM stiffness clamp provides a high-resolution method for varying apparent stiffness and evaluating cellular responses including contraction behavior. Using the AFM stiffness clamp, we show that cells rapidly change their traction rate and contraction velocity in response to step changes in apparent stiffness. Importantly, the stiffness clamp algorithm dynamically changes the apparent stiffness while the force and height are unchanged in the instant before and after the stiffness change. Therefore, any cellular response is a function of the step change in stiffness and not force or height. This decoupling of stiffness from force and height unambiguously shows that stiffness changes alone caused the change in contraction.

Our observation of stiffness dependent contraction of single cells is consistent with several previous studies. We recently used the high-resolution of AFM to characterize the contraction dynamics of single human platelet cells [16] and found that the force generation of platelets was dependent on microenvironmental stiffness, though each platelet was exposed to only a single stiffness. Other techniques, using systems limited to a single stiffness per experiment, have also observed a dependence of contraction on stiffness with a variety of cell types [10,15,19]. Our results with the AFM stiffness clamp are consistent with a recent study by Mitrossilis et al. that used a custom-built parallel microplate system to change the stiffness experienced by a single myoblast cell and found that traction rate was higher for larger stiffnesses and did not depend on absolute force [22].

It is worthwhile to note that the AFM stiffness clamp presented here only alters stiffness in one axis, though as demonstrated above, this appears to be sufficient to elicit a response from the contracting cell. Due to the fact that stiffness can only be measured by displacing a sample, the apparent stiffness can only be applied when cell height is actively changing, for example during fibroblast contraction, cardiomyocyte beating, neutrophil shape change in response to chemoattractants, and cell rounding during mitosis.

This AFM-based approach to dynamically tuning microenvironmental rigidity is broadly applicable to both biological and non-biological experimental situations. In essence, the algorithm we present can be applied to any system with a spring where there is precise knowledge of the force and a single means of adjusting the position of the spring base (as illustrated in FIG. 2). This stiffness clamp algorithm has the advantage of requiring only one actuator and therefore can be used with existing commercial AFMs. Furthermore, the algorithm can be adjusted to emulate nonlinear elastic properties, such as those of specific ECM networks.

In the case of single molecule experiments on mechanosensitive molecules, which typically employ an AFM or optical trap [26], the AFM stiffness clamp could be implemented to sample a wide range of apparent stiffness values. The stiffness clamp can also be integrated with cell rheology measurements and fluorescence microscopy to characterize the viscoelastic properties of the cell and protein localization under various apparent stiffnesses. At the multicellular scale, tissue stiffness has been shown to affect the cancerous phenotype of cell colonies [27], and the AFM stiffness clamp could be used to study the responses of tissues in microenvironments of changing stiffness. Importantly, our system allows for the use of apparent stiffness values outside of those that can be achieved by standard cantilever fabrication methods.

In this study, we have presented an AFM-based method for dynamically changing the apparent stiffness of the microenvironment surrounding a cell. We demonstrated the high temporal and spatial resolution of the AFM stiffness clamp using an expanding hydrogel and contracting cell, finding that the cell contraction rate reversibly changes nearly instantaneously with stiffness and does not depend on absolute force or cell height. Both cellular traction rate and contraction velocity were stiffness-dependent, whereas the expansion velocity of the hydrogel used in our experiments remained constant for stiffnesses ranging 1-100 nN/μm. The AFM stiffness clamp provides a powerful tool for investigating the role of mechanical boundary conditions on cellular behavior.

MATERIALS & METHODS

Stiffness clamp algorithm

The AFM stiffness clamp is implemented using a feedback algorithm based on the extension of a Hookean spring ($\Delta F = k_{spring}\,\Delta x_{spring}$), though this analysis can be extended to nonlinear springs. The microenvironmental stiffness a cell experiences is given by the amount of force it must apply to change its height, $\Delta F = k_{apparent}\,\Delta x_{cell}$. If the base of the spring can move by an amount Δx_{base}, the change in cell height is given by the difference between spring extension and movement of the spring base, $\Delta x_{cell} = \Delta x_{spring} - \Delta x_{base}$. The force resisting the change in cell height is provided solely by the extension of the spring. Therefore, equating the expressions for ΔF and solving for the movement of the spring base gives

$$\Delta x_{base} = \frac{k_{apparent} - k_{spring}}{k_{apparent}}\,\Delta x_{spring} \tag{1}$$

which defines how much the base must be moved to achieve the desired apparent stiffness, $k_{apparent}$, for a given deformation of the spring. Note that the position clamp can be obtained from Eq. (1) when $k_{apparent} = \infty$, in which case the base moves the same amount as the spring deforms, and the cell height remains constant. Similarly, the force clamp results when $k_{apparent} = 0$ and Δx_{base} cancels out the movement of the spring, such that $\Delta x_{spring} = 0$.

The AFM stiffness clamp feedback algorithm uses the desired apparent stiffness ($k_{apparent}$), the spring stiffness (k_{spring}), and Eq. (1), together with a measure of how much the cell

deforms the spring, to determine how far to move the base. Equation (1) is directly used in the feedback algorithm for $k_{apparent} > k_{spring}$, but for $k_{apparent} < k_{spring}$ Eq. (1) grows out of bounds as $k_{apparent}$ approaches zero. For $k_{apparent} < k_{spring}$, we alter Eq. (1) so that it iteratively converges to the same ratio $\Delta x_{base}/\Delta x_{spring}$ without growing out of bounds according to

$$\Delta x_{base,i} = \frac{k_{apparent} - k_{spring}}{k_{spring}} \left(\Delta x_{spring} - \Delta x_{base,i-1} \right) \quad (2)$$

where i is the index for each cycle of the iteration and $\Delta x_{base,i-1}$ is the amount the base was moved in the previous iteration (see Supporting Material for a detailed derivation).

Atomic force microscope

Atomic force microscope (AFM) experiments were conducted using a modified Veeco Bioscope I mounted on a Zeiss Axiovert 25 inverted microscope. The Bioscope I z-axis piezo in our system has a range of only 4 μm. Since a larger z range is more convenient for working with cells, the substrate was moved instead of the cantilever base with a feedback-controlled Mad City Labs piezo-actuator stage and controller with a range of 50 μm and a resolution of 0.1 nm. Cantilever deflection and substrate position was controlled with a National Instruments 16-bit, 250 kS/s PCI-6229 digital I/O card and a custom LabVIEW program to implement the stiffness clamp algorithm running at 100 Hz. The substrate was mounted on a heated stage and maintained at 37°C for cell experiments. Tipless silicon nitride MLCT (30-50 nN/μm, Veeco) and Arrow cantilevers (10-20 nN/μm, Nanoworld) were used for the gel and cell experiments, respectively. Calibration of the optical lever was conducted before each experiment by ramping a glass coverslip substrate up and down while in contact with the cantilever. The surface was ramped 450 nm and the average of 15 cycles was used to determine the volts to meters conversion factor. See supporting file 1 for a discussion on the effect of calibration errors on the apparent stiffness applied by the stiffness clamp. We then determined the cantilever spring constant before each experiment by recording the thermal fluctuations of the cantilever out of contact in air and fitting the first resonance peak of the power spectra with a Lorentzian function using the equipartition theorem [28]. This indicates that the resolution of the detection of the cantilever position was thermally limited.

To monitor drift in both the cell and gel experiments, we placed the cantilever in contact with the glass substrate in force clamp mode, immediately before each experiment. Experiments were not started until the system had equilibrated, such that a force clamp could be maintained with no significant change in stage position (generally 10-60 minutes). Drift over the course of the experiment was measured in two ways. First, the zero deflection point of the cantilever was compared before and after each experiment to measure any cantilever drift. Second, for cell experiments, the contact point between the surface and cantilever was measured before and after each experiment. These measurements confirmed that the drift over the course of the experiment was negligible compared to the active contraction of the cell and expansion of the gel. Drift accounted for <10% of the total deflection for all experiments used.

Polyacrylamide hydrogels

The ~1 kPa polyacrylamide hydrogel was dehydrated at 4°C overnight and was rehydrated immediately before the AFM experiment with a standard phosphate buffered saline (PBS) solution. The cantilever was brought into contact as the gel rehydrated and expanded.

Cell culture

NIH 3T3 fibroblast cells were cultured in DMEM (GIBCO) supplemented with 10% fetal bovine serum, 100 U/ml penicillin, and 100 µg/ml streptomycin. Cells were maintained in an incubator at 37°C with a humid, 5% CO_2 atmosphere. A trypsin solution was used to detach cells at which point trypsin neutralizer was added and cells were then centrifuged at 300 g for 5 minutes. The resulting supernatant was discarded and cells were resuspended in their culture medium (DMEM plus supplements). KOH cleaned glass substrates and cantilevers were immersed for 30 min in a 50 µg/ml fibronectin solution (F0895, Sigma). The fibronectin solution was then washed off and cells were added and the cantilever was brought on top of a cell as it settled on the substrate.

Statistical analysis

The inset of the FIG. 4B demonstrates the rapid change in traction rate upon a change in apparent stiffness. We found that this change occurred within 0.5 s. This response time was calculated by comparing two models with an F test with P values < 0.01. First, a 30 s window was applied centered on the timepoint when $k_{apparent}$ was changed. Then a simple linear regression was compared with a segmented linear regression where the timepoint of the intersection of the two segments must be determined from the data. This 30 s window was then moved earlier in time and the two models were again compared. The point at which the preferred model shifted to the simple linear regression is defined as the point when the traction rate has statistically changed.

ACKNOWLEDGEMENTS

We thank Sapun Parekh, Ovijit Chaudhuri, and the whole Fletcher Lab for helpful discussions and An-Chi Tsou and Win Pin Ng for providing the polyacrylamide hydrogels.

REFERENCES

1. Jena BP, Horber JH, Wilson L, Matsudaira PT (2002) Atomic Force Microscopy in Cell Biology, Volume 68. 1st ed. Academic Press.
2. Helenius J, Heisenberg C, Gaub HE, Muller DJ (2008) Single-cell force spectroscopy. J Cell Sci 121: 1785-1791. doi:10.1242/jcs.030999
3. Chaudhuri O, Parekh SH, Fletcher DA (2007) Reversible stress softening of actin networks. Nature 445: 295-298. doi:10.1038/nature05459
4. Puchner EM, Gaub HE (2009) Force and function: probing proteins with AFM-based force spectroscopy. Curr Opin Struc Biol 19: 605-614. doi:10.1016/j.sbi.2009.09.005
5. Janmey PA, Winer JP, Murray ME, Wen Q (2009) The hard life of soft cells. Cell Motil Cytoskel 66: 597-605. doi:10.1002/cm.20382
6. Jacot JG, Martin JC, Hunt DL (2010) Mechanobiology of cardiomyocyte development. J Biomech 43: 93-98. doi:10.1016/j.jbiomech.2009.09.014
7. Klein EA, Yin L, Kothapalli D, Castagnino P, Byfield FJ, et al. (2009) Cell-cycle control by physiological matrix elasticity and in vivo tissue stiffening. Curr Biol 19: 1511-1518. doi:10.1016/j.cub.2009.07.069
8. Mammoto A, Connor KM, Mammoto T, Yung CW, Huh D, et al. (2009) A mechanosensitive transcriptional mechanism that controls angiogenesis. Nature 457: 1103-1108. doi:10.1038/nature07765
9. Yeung T, Georges PC, Flanagan LA, Marg B, Ortiz M, et al. (2005) Effects of substrate stiffness on cell morphology, cytoskeletal structure, and adhesion. Cell Motil Cytoskel 60: 24–34.
10. Saez A, Ghibaudo M, Buguin A, Silberzan P, Ladoux B (2007) Rigidity-driven growth and migration of epithelial cells on microstructured anisotropic substrates. Proc Natl Acad Sci U S A 104: 8281 -8286. doi:10.1073/pnas.0702259104
11. Engler AJ, Sen S, Sweeney HL, Discher DE (2006) Matrix elasticity directs stem cell lineage specification. Cell 126: 677-689. doi:10.1016/j.cell.2006.06.044
12. Keese CR, Giaever I (1991) Substrate mechanics and cell spreading. Exp Cell Res 195: 528-532. doi:10.1016/0014-4827(91)90406-K
13. Pelham RJ, Wang Y (1997) Cell locomotion and focal adhesions are regulated by substrate flexibility. Proc Natl Acad Sci U S A 94: 13661 -13665.
14. Tan JL, Tien J, Pirone DM, Gray DS, Bhadriraju K, et al. (2003) Cells lying on a bed of microneedles: An approach to isolate mechanical force. Proc Natl Acad Sci U S A 100: 1484 -1489. doi:10.1073/pnas.0235407100
15. Mitrossilis D, Fouchard J, Guiroy A, Desprat N, Rodriguez N, et al. (2009) Single-cell response to stiffness exhibits muscle-like behavior. Proc Natl Acad Sci U S A 106: 18243-18248. doi:10.1073/pnas.0903994106
16. Lam WA, Chaudhuri O, Crow A, Webster KD, Li T, et al. (2011) Mechanics and contraction dynamics of single platelets and implications for clot stiffening. Nat Mater 10: 61-66. doi:10.1038/nmat2903
17. Mizuno D, Bacabac R, Tardin C, Head D, Schmidt CF (2009) High-resolution probing of cellular force transmission. Phys Rev Lett 102: 168102. doi:10.1103/PhysRevLett.102.168102

18. Lo CM, Wang HB, Dembo M, Wang YL (2000) Cell movement is guided by the rigidity of the substrate. Biophys J 79: 144-152. doi:10.1016/S0006-3495(00)76279-5
19. Alliouxguerin M, Icardarcizet D, Durieux C, Henon S, Gallet F, et al. (2009) Spatiotemporal analysis of cell response to a rigidity gradient: a quantitative study using multiple optical tweezers. Biophy J 96: 238-247. doi:10.1529/biophysj.108.134627
20. Frey MT, Wang Y (2009) A photo-modulatable material for probing cellular responses to substrate rigidity. Soft Matter 5: 1918. doi:10.1039/b818104g
21. Jiang FX, Yurke B, Schloss RS, Firestein BL, Langrana NA (2010) The relationship between fibroblast growth and the dynamic stiffnesses of a DNA crosslinked hydrogel. Biomaterials 31: 1199-1212. doi:10.1016/j.biomaterials.2009.10.050
22. Mitrossilis D, Fouchard J, Pereira D, Postic F, Richert A, et al. (2010) Real-time single-cell response to stiffness. Proc Natl Acad Sci U S A 107: 16518 -16523. doi:10.1073/pnas.1007940107
23. Chaudhuri O, Parekh SH, Lam WA, Fletcher DA (2009) Combined atomic force microscopy and side-view optical imaging for mechanical studies of cells. Nat Meth 6: 383-387. doi:10.1038/nmeth.1320
24. Sheetz MP, Wilson L, Matsudaira PT (1997) Laser tweezers in cell biology. San Diego: Academic Press.
25. Giannone G, Sheetz MP (2006) Substrate rigidity and force define form through tyrosine phosphatase and kinase pathways. Trends Cell Biol 16: 213-223. doi:10.1016/j.tcb.2006.02.005
26. Wen J, Manosas M, Li P, Smith S, Bustamante C, et al. (2007) Force unfolding kinetics of RNA using optical tweezers. I. Effects of experimental variables on measured results. Biophys J 92: 2996-3009. doi:10.1529/biophysj.106.094052
27. Paszek MJ, Zahir N, Johnson KR, Lakins JN, Rozenberg GI, et al. (2005) Tensional homeostasis and the malignant phenotype. Cancer Cell 8: 241-254. doi:10.1016/j.ccr.2005.08.010
28. Hutter JL, Bechhoefer J (1993) Calibration of atomic-force microscope tips. Rev Sci Instrum 64: 1868. doi:10.1063/1.1143970

FIGURES

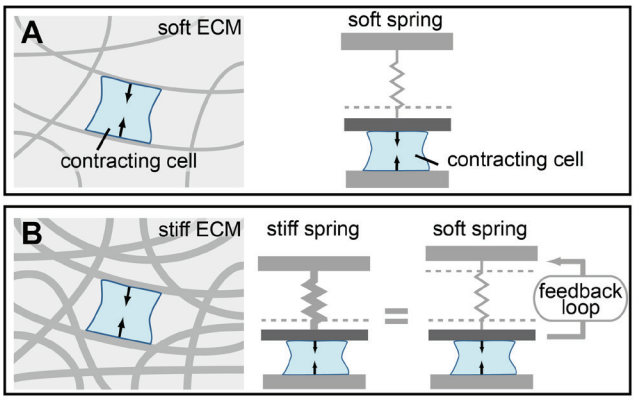

Figure 1. Feedback control can change the apparent stiffness a cell experiences.

(a) A contracting cell in a soft extracellular matrix (ECM) experiences little resistance to its contraction and can be modeled with a soft spring. (b) A contracting cell in a stiff ECM experiences a large resistance to its contraction and can be modeled with a stiff spring. Using the AFM stiffness clamp, a soft spring can be made to appear stiff (or vice-versa) by controlling the spring's extension as a function of the cell's contraction. This approach can be broadly applied to make springs appear stiffer or softer than their actual value.

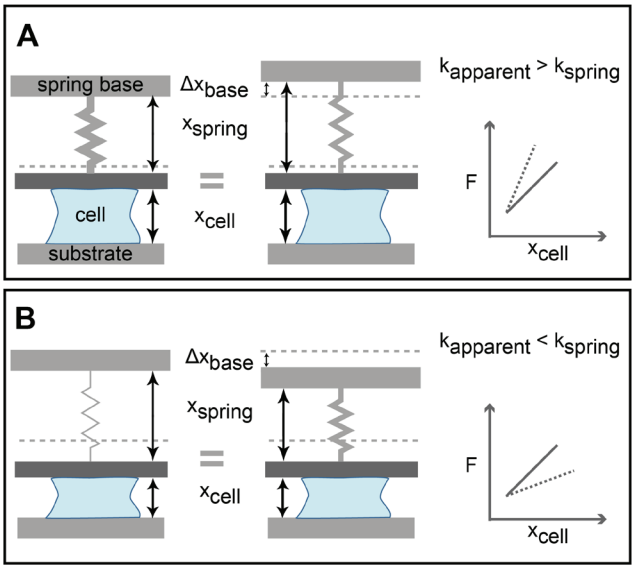

Figure 2. Conceptual design of the AFM stiffness clamp.

(a) A stiff spring can be simulated using a spring of a smaller stiffness. A cell applying a given force against a stiff spring achieves a smaller change in height than a softer spring. Moving the spring base up as the cell contracts makes a softer spring appear stiffer to the contracting cell. Plotting contractile traction force (F) versus cell height (x_{cell}) produces a trace whose steep slope is the apparent stiffness, $k_{apparent}$ (dotted line) and is greater than the native spring stiffness, k_{spring} (solid line). (b) A soft spring can be simulated using a spring of a greater stiffness. A cell applying a given force against a soft spring achieves a greater change in height than a stiffer spring. Moving the spring base down as the cell contracts makes a stiffer spring appear softer to the contracting cell. Plotting traction force (F) versus cell height (x_{cell}) produces a trace whose gradual slope is the apparent stiffness, $k_{apparent}$ (dotted line) and is less than the native spring stiffness, k_{spring} (solid line).

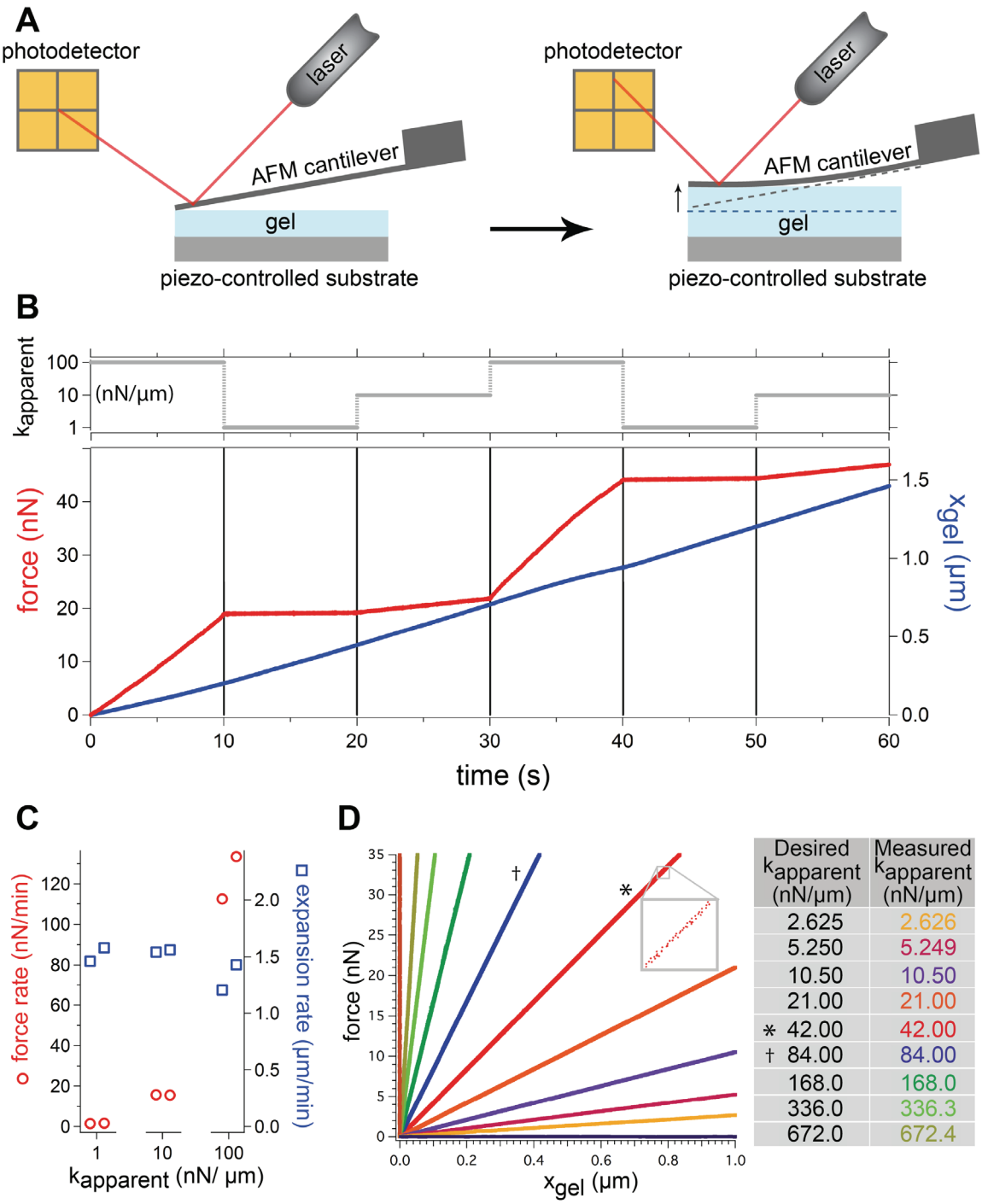

Figure 3. Response of expanding hydrogel to step changes in stiffness.

(a) The AFM stiffness clamp was applied to a rehydrated hydrogel that deflected an AFM cantilever as it expanded. Cantilever position is precisely measured using an optical lever system. Feedback was implemented by moving a piezo-controlled substrate. (b) A typical trace of how force and gel height (x_{gel}) changed over time as the cantilever deflected in response to the expansion of the hydrogel against apparent stiffnesses of 1, 10, and 100 nN/μm. Separate experiments conducted on 5 different gels all exhibited the same

stiffness-dependent behavior shown above. Note that the slope of the force trace clearly changes when the apparent stiffness changes, while the slope of the height trace remains basically constant over this range of stiffness. (c) Categorical plot of the force rate and velocity of gel expansion under three different apparent stiffnesses from the trace depicted in (b). The rates are determined from a linear regression fit where the 95% confidence interval for each slope is within ±0.25 nN/min and ±5 nm/min for the force and height, respectively. Force rate changes with stiffness while expansion rate does not over this range of stiffness. (d) Plot of force (F) versus gel height (x_{gel}) as the gel expanded under a wide range of apparent stiffnesses. Each trace represents a different apparent stiffness listed in the table and applied using the stiffness clamp algorithm. The traces were translated to begin at the origin for comparison. The horizontal and vertical traces represent desired stiffnesses approaching 0 and ∞, corresponding to a force and position clamp with standard deviations of 15 pN and 0.34 nm. Inset depicts the discrete but highly linear nature of the data. The * marks the trace without any feedback loop and whose slope is the spring constant of the cantilever, 42 nN/μm.

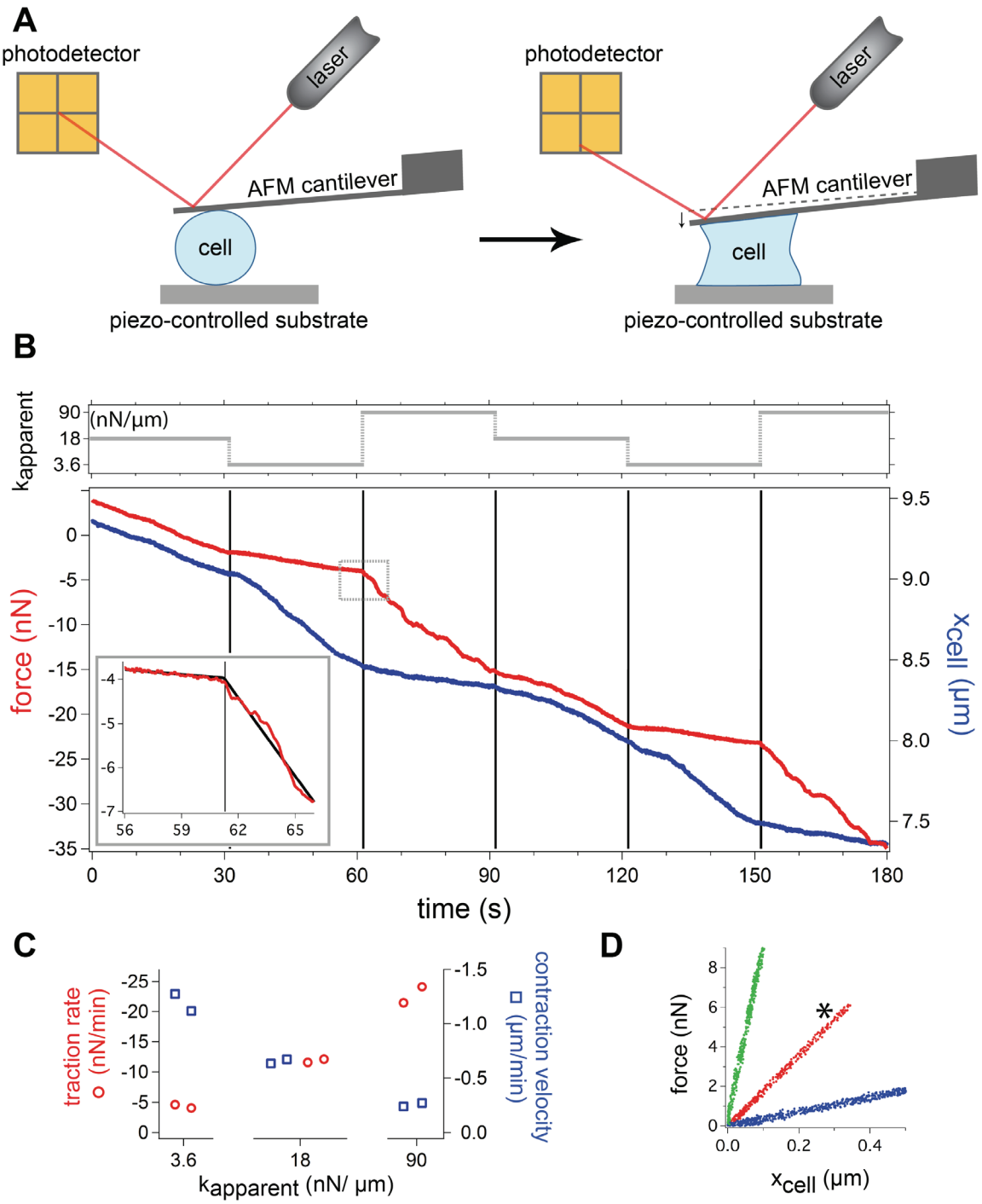

Figure 4. Cell contraction rapidly responds to stiffness changes.

(a) An AFM was used to expose a single fibroblast cell to dynamically changeable apparent stiffness values with the AFM stiffness clamp. The piezo-controlled substrate was moved in response to deflections of the cantilever, which were precisely measured with an optical lever system. (b) Force and cell height as the cell contracts under different apparent stiffnesses from a typical experiment. A total of 30 cells were tested, all exhibiting the same stiffness-dependent behavior shown above. Each interval is under an apparent stiffness of

3.6, 18, or 90 nN/μm as indicated at the top of the graph. The traction rate and contraction velocity rapidly change with a step change in stiffness. A segmented linear regression fit is plotted highlighting the change in traction rate (inset). Data displayed in (c) and (d) are compiled from this trace. (c) Traction rate increases with apparent stiffness while corresponding contraction velocity decreases. The rates are determined from a linear regression fit where the 95% confidence interval for each slope is within ±0.4 nN/min and ±20 nm/min for the force and height, respectively. (d) Plot of force versus cell height. The three linear, distinct traces each have slopes that indicate that the desired apparent stiffnesses were achieved. The * marks the trace without any feedback loop. Each interval was translated to begin at the origin for comparison.

SUPPORTING MATERIAL

Derivation

In the text the movement of the base to maintain the stiffness clamp is defined as:

$$\Delta x_{base} = \frac{k_{apparent} - k_{spring}}{k_{apparent}} \Delta x_{spring} \tag{1}$$

Noting that for $k_{apparent} << k_{spring}$ this equation becomes unstable for Δx_{base}, we use a modified iterative equation that achieves the same ratio of $\Delta x_{base}/\Delta x_{spring}$ as Eq. (1) but does not result in Δx_{base} growing out of bounds for $k_{apparent} \to 0$:

$$\Delta x_{base,i} = \frac{k_{apparent} - k_{spring}}{k_{spring}} \left(\Delta x_{spring} - \Delta x_{base,i-1}\right) \tag{2}$$

This equation converges to Eq. (1). Assume the deflection of the spring in each iteration is defined as:$\Delta x_{spring,i} = R + \varepsilon \Delta x_{base,i-1}$, where R is the distance the cell contracts in a single time step and ε is the absorption coefficient of the spring, defined as the ratio of the combined spring constant of the cell and spring in series and the spring's stiffness, where $\varepsilon = \frac{k_{cell}}{k_{spring}+k_{cell}}$. ε = 1 corresponds to the spring absorbing all the change in height and ε = 0 corresponds to the cell absorbing all the change in base height with no spring deflection.

Using the iterative model we derive an equation that relates how rapidly Eqs. (1) and (2) converge as a function of the relevant experimental parameters. We define the error as the ratio of the difference between Eqs. (2) and (1) over Eq. (1) as a function of *i*.

$$error(i) = \frac{\frac{\Delta x_{base,i}}{\Delta x_{spring,i}} - \frac{\Delta x_{base}}{\Delta x_{spring}}}{\frac{\Delta x_{base}}{\Delta x_{spring}}} \tag{3}$$

Using the iterative definitions, we derive Eqs. (4) and (5) for $i = 0, 1 \ldots \infty$.

$$\Delta x_{base,i} = R \left(\frac{k_{apparent}}{k_{spring}} - 1\right) \sum_{n=0}^{i-1} \left[\left(\frac{k_{apparent}}{k_{spring}} - 1\right)(\varepsilon - 1)\right]^n \tag{4}$$

$$\Delta x_{spring,i} = R + \varepsilon R \left(\frac{k_{apparent}}{k_{spring}} - 1\right) \sum_{n=0}^{i-2} \left[\left(\frac{k_{apparent}}{k_{spring}} - 1\right)(\varepsilon - 1)\right]^n \tag{5}$$

Substituting Eqs. (4) and (5) into Eq. (3) we find that R cancels out and we are left with a function for the error that, after substituting for a finite geometric series, tells us how rapidly Eq. (2) converges to Eq. (1) as a function of ε and the ratio $k_{spring}/k_{apparent}$.

$$error\left(\frac{k_{spring}}{k_{apparent}}, \varepsilon, i\right) = \frac{\left(\frac{k_{apparent}}{k_{spring}} - 1\right)(\varepsilon^{-1} - 1) - \frac{k_{spring}}{k_{apparent}} + 1}{\left[\left(\frac{k_{apparent}}{k_{spring}} - 1\right)(\varepsilon - 1)\right]^{(1-i)} \varepsilon^{-1} + \frac{k_{spring}}{k_{apparent}} - 1} \quad (6)$$

Figure S1 demonstrates how the error is affected by varying the experimental parameters. For the experiments described in the text, our ε was approximately 0.5. Even under the extreme conditions of low ε and high $k_{spring}/k_{apparent}$, Eq. (2) converges in just a few iterations. This error function, Eq. (6), can be used to select the required experimental parameters such as the spring constant or algorithm frequency for a desired experiment.

Range of apparent stiffnesses

The stiffness clamp was very accurately applied over a large range of stiffnesses on an expanding hydrogel (FIG. 3). The extreme clamped stiffnesses (4.2×10^{-9} and 4.2×10^{11} nN/μm) produced slopes in FIG. 3 of the text of essentially 0 and ∞, respectively. This is demonstrated by showing that the force and height respectively remain constant with only a small degree of Gaussian noise (FIG. S2).

SUPPORTING FIGURES

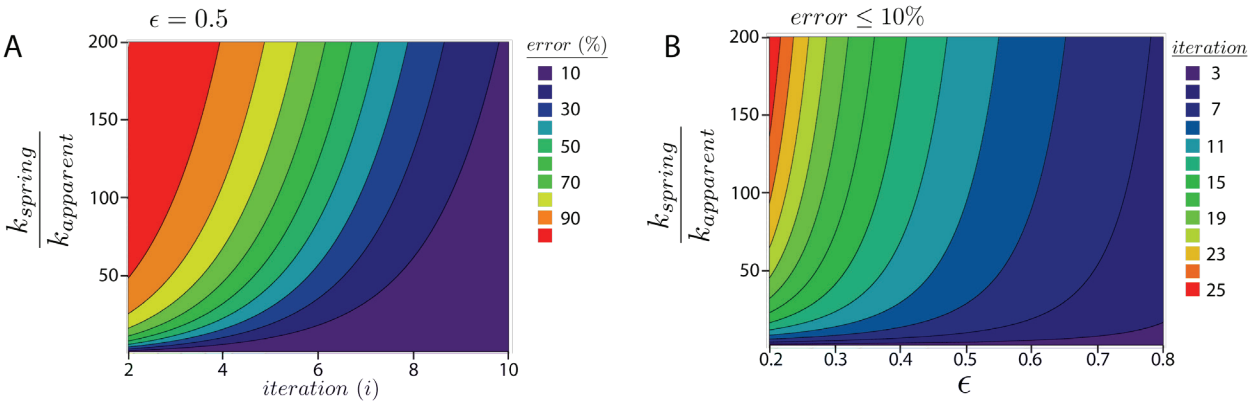

Figure S1. Graph of the error function, Eq. (6), as a function of its parameters.

(a) A contour plot of the error function for a constant ε = 0.5 (b) A contour plot of the error function depicting the required number of iterations for Eq. (2) to converge within 10% of Eq. (1).

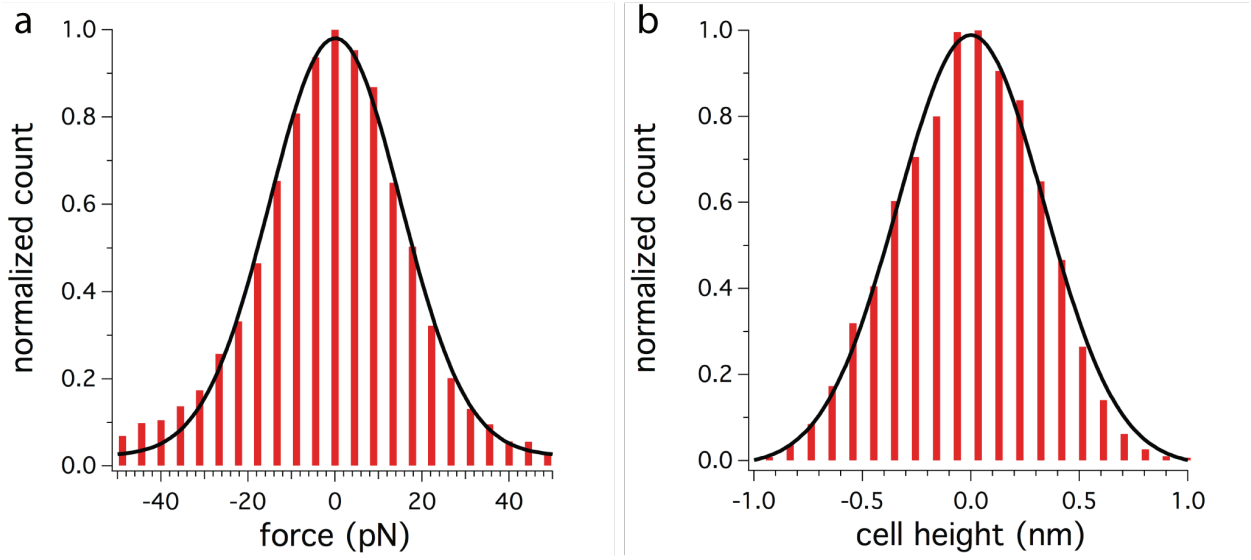

Figure S2. Extreme stiffnesses.

(a) Histogram of the variance in force under a stiffness clamp of 4.2×10^{-9} nN/μm. The histogram is fit with a Gaussian with a standard deviation of 15 pN. (b) Histogram of the variance in cell height under a stiffness clamp of 4.2×10^{11} nN/μm. The histogram is fit with a Gaussian with a standard deviation of 0.34 nm.

Chapter 3.

Contractile equilibration of single cells to step changes in extracellular stiffness

Reprinted with permission from the Biophysical Society from the article "Contractile equilibration of single cells to step changes in extracellular stiffness" by Ailey Crow, Kevin D. Webster*, Evan Hohlfeld, Win Pin Ng, Phillip Geissler, Daniel A. Fletcher in Biophysical Journal **102**(3), February 2012 (443-451).*

**Both authors contributed equally to this work.*

ABSTRACT

Extracellular stiffness has been shown to alter long timescale cell behaviors such as growth and differentiation, but the cellular response to changes in stiffness on short timescales is poorly understood. By studying the contractile response of cells to dynamic stiffness conditions using an atomic force microscope (AFM), we observe a seconds-timescale response to a step change in extracellular stiffness. Specifically, we observe acceleration in contraction velocity (μm/min) and force rate (nN/min) upon a step decrease in stiffness and deceleration upon a step increase in stiffness. Interestingly, this seconds-timescale response to a change in extracellular stiffness is not altered by inhibiting focal adhesion signaling or stretch-activated ion channels and is independent of cell height and contraction force. Rather, the response timescale is altered only by disrupting cytoskeletal mechanics and is well-described by a simple mechanical model of a constant velocity actuator pulling against an internal cellular viscoelastic network. Consistent with the predictions of this model, we find that an osmotically expanding hydrogel responds to step changes in extracellular stiffness in a similar manner to cells. We therefore propose that an initial event in stiffness sensing is establishment of a mechanical equilibrium that balances contraction of the viscoelastic cytoskeleton with deformation of the extracellular matrix.

INTRODUCTION

The stiffness of the extracellular microenvironment has been shown to affect a broad set of cellular behaviors including cell spreading (1), motility (2), proliferation, differentiation (3), and tumorigenesis (4, 5). Studies have implicated over 150 signaling and structural proteins involved in responding to mechanical cues such as stiffness and force (6, 7). Actomyosin contraction is known to play an important role in mechanosensing, as it is required for stiffness-directed stem cell differentiation (3), cytoskeletal coherence (8), and vinculin recruitment and reinforcement via FAK-mediated paxillin phosphorylation (9). Actomyosin stress fibers, which are linked to the extracellular matrix (ECM) via focal adhesions, pull not only against the ECM as the cell changes shape or moves but must compress the internal structure of the cell as well. While it is known that local changes in applied force can directly induce biochemical signaling over short timescales (10, 11), the response of cells to changes in extracellular stiffness is not well understood.

The cell is often represented in a state of tensional equilibrium in which contraction of stress fibers is balanced by resistance of the extracellular matrix to deformation (12-14). In this view, the cell is poised to rapidly respond to external changes in force, which in turn change the tension across mechanosensory proteins such as talin or p130cas, exposing phosphorylation sites or binding sites and initializing a cascade of signaling events (10, 15, 7). Recent studies of the cellular response to a step change in force demonstrate that signaling events such as Src activation and calcium spikes can occur on sub-second timescales (16, 17).

It remains unclear, however, whether changes in extracellular stiffness will immediately result in altered biochemical signaling or in movement that depend on biochemical signaling. Microenvironmental stiffness can be altered on longer timescales through ECM degradation by matrix metalloproteinases (MMPs) or ECM crosslinking by lysyl oxidase (LOX). Tissue stiffness can even change by an order of magnitude on the seconds timescale during muscle contraction (18). Fundamentally, changes in force boundary conditions and changes in stiffness boundary conditions should have different effects on mechanosensitive proteins. External force changes can directly stretch proteins and open binding sites, while external stiffness changes – which can be thought of as altering the force required for a given displacement – result in opening of binding sites only when stretched by internally-generated forces that act through the cell's cytoskeleton. This suggests that response timescales and mechanisms involved in force and stiffness sensing may be different.

Testing the adaptation of cells to rapid changes in stiffness requires a method that can alter only stiffness felt by the cell, independent of changes in cell height or tension. Several recent studies have presented platforms to vary the stiffness cues exposed to a single cell. Novel gels have been produced to enable changes in stiffness over the course of minutes to hours by photo-exposure (19), DNA cross-linking (20), polymer cross-linking dynamics (21), or pH changes (22). To create more rapid changes in stiffness (< 1 sec) that do not simultaneously alter cell force or displacement, feedback algorithms have been employed on microplate or atomic force microscope (AFM) systems to reversibly control stiffness signals exposed to a single-cell extended between two substrates in real-time (23, 24). We refer to this technique as an AFM stiffness clamp, as previously described (24). Employing a

stiffness clamp in this geometry moves beyond traditional 2D flexible substrate studies, in that the cell experiences a resistance to vertical contraction in addition to substrate rigidity, though this is by no means equivalent to a completely 3D configuration.

Here we use an AFM stiffness clamp to directly address the question of how single cells sense changes in extracellular stiffness. Previous work has demonstrated that contraction of single cells is stiffness dependent (23–26), but it remains unclear what role force-dependent signaling mechanisms play in the short timescale response to stiffness changes. Indeed, recent models suggest differing roles for players such as focal adhesions and acto-myosin contraction (12, 27, 28), and our work provides experimental data that can be used to evaluate the model predictions.

In this study, we impose a step change in stiffness on a contractile cell and observe an immediate (within the sub-second resolution of our system) change in both contraction velocity (μm/min) and force rate (nN/min), as previously reported (24). High-resolution measurements of the contractile response with AFM reveal a new and repeatable equilibration response in contraction on a timescale of seconds as the cell adapts to a new extracellular stiffness condition. Surprisingly, we found that this seconds-timescale response to changes in stiffness is not affected by disruption of focal adhesion signaling or stretch-activated channels. Rather, it is well described by a simple viscoelastic mechanical model that includes only cytoskeletal relaxation under a constant velocity contractile actuator. We confirm that the observed response is dependent only on mechanical properties in the absence of biochemical signaling by showing a similar response in expanding hydrogels. We therefore propose that the initial response of contractile cells to stiffness changes is mechanical equilibration of the cytoskeleton to the new boundary conditions, a process that is independent of focal adhesion signaling.

MATERIALS AND METHODS

Cell culture and sample preparation

NIH 3T3 fibroblasts were cultured in DMEM (Mediatech, Manassas, VA) supplemented with 10% fetal bovine serum (Lonza, Walkersville, MD), and 1% Penicillin/Streptomycin (Sigma, St Louis, MO). Prior to experiments, cells were trypsinized and resuspended in CO_2-independent media (Invitrogen, Carlsbad, CA) supplemented with 10% fetal bovine serum, and 1% Penicillin/Streptomycin. For inhibition experiments, cells were resuspended in CO_2-independent media containing the appropriate drug concentration and incubated for 30 minutes prior to experiments. Drugs used include pp2 (Calbiochem, Gibbstown, NJ), FAK inhibitor (Tocris, Ellisville, MO), gadolinium chloride (Sigma, St Louis, MO), cytochalasin D (Sigma, St Louis, MO), nocodazole (Sigma, St Louis, MO), and blebbistatin (Sigma, St, Louis, MO). Control experiments conducted in the presence of 0.33% DMSO, the maximum percentage required for any drug experiments, showed no distinct behavior from CO_2-independent media without DMSO or drug additions.

Experimental setup

Experiments were conducted with a modified Bioscope AFM (Veeco Metrology, Santa Barbara, CA) with a closed-loop piezoelectric platform stage (Mad City Labs, Madison, WI) and temperature control (Warner Instrument Corporation, Hamden, CT) atop an inverted microscope (Zeiss Axiovert 25, Carl Zeiss, Thornwood, NY) allowing brightfield imaging and alignment of the cantilever and cell (see Fig. 1b). Data acquisition and the stiffness clamp feedback algorithm are controlled by custom software (LabVIEW, National Instruments, Austin TX). For further details on the feedback algorithm please see (24). Tipless PNP cantilevers from Nanoworld (NeuChatel, Switzerland) were used in all experiments with spring constants ranging from 50-800 nN/mm as determined by fitting thermal fluctuations of each cantilever in air.

Stiffness cycling experiment

Prior to adding cells, the AFM cantilever and glass substrate were incubated with 50 μg/ml fibronectin (Sigma, St Louis, MO) in phosphate buffered saline (PBS) for at least 30 minutes and then rinsed. Concanavalin A (Sigma, St Louis, MO) and poly-L-Lysine (MW>300,000, Sigma, St Louis, MO) were also used as alternatives to fibronectin for experiments where indicated. All experiments were performed at 37°C with perfusion of media exchanging the chamber volume every hour to compensate for evaporation. The point of contact between the glass substrate and AFM cantilever was recorded as zero height and cell height was measured with respect to this point. Prepared cells in suspension were flowed into the system and within minutes of settling, a single cell was brought into contact with both the AFM cantilever and glass substrate with a 4 nN contact force. The cell was then allowed to adhere and contract a minimum of several nN before stiffness cycling began. Step changes in stiffness were imposed every 20 seconds. Multiple time intervals were tested to confirm that a steady state contraction velocity and tensile rate are reached within 20 seconds.

Measurement of response by ratio analysis

The nonlinearity of the contractile response to step changes in stiffness was established by measuring the slope of the traction force and cell height over the first quarter of the interval and the last quarter of the interval. A ratio of these slopes greater than 1 indicates acceleration, while a ratio less than 1 indicates deceleration. The p-value was determined using a binomial test with a null hypothesis of equal probability of acceleration or deceleration.

Measurement of response timescale by curve fitting

The response timescale was determined by fitting a linear-plus-exponential equation to each stiffness interval

$$f(t) = c_0 + c_1 t + c_2 e^{-t/\tau} \quad (1)$$

where c_0 is a constant offset, c_1 is the slope after equilibration, c_2 is the multiplier of the exponential term, and τ is the response timescale. For the accelerating intervals, c_1 and c_2

have opposite signs. This results in an extremum, $df(t_{extremum})/dt = 0$, where the exponential contribution exactly cancels out the linear contribution. When fitting step decreases in stiffness, this extremum point was constrained to be within 2 seconds of the beginning of the stiffness interval. For increases in stiffness, c_1 and c_2 have the same sign and t=0 is defined as the start of the interval. In order to compare response timescales, an F-test comparing the nested linear model to the linear-plus-exponential was used with only traces with $p<0.1$ used. This was done to exclude data whose noise precluded an accurate measurement of the response timescale.

Given the shorter response timescales for high stiffnesses, the F-value criterion yields fewer usable values at high stiffnesses for inhibition experiments where data is noisier. Therefore comparison of response timescales between inhibition experiments is based on low stiffnesses and analysis of the height trace.

The steady state contraction velocity is measured as the slope during the last 5 seconds of the interval where the velocity is constant (equivalent to c_1 from Eq. 1).

Statistical analysis

The significance of drug treatments and transformed cells on response timescales were investigated using a non-parametric rank sum test (Mann-Whitney U test) comparing each condition to the control. The underlying data is not normally distributed, and thus a non-parametric test was used. Levels of significance are reported for given conditions in the text. Box plot percentile values are calculated based on discrete stiffness intervals (n = number of intervals) across multiple cells (N = number of cells). Each stiffness interval was considered as independent because no greater correlation existed within a cell than between cells.

Osmotic swelling of polyacrylamide hydrogel

A polyacrylamide hydrogel with an elasticity of ~ 100 Pa was osmotically swelled by replacing the 10x PBS surrounding the gel with deionized water. As the gel swelled against the AFM cantilever, the stiffness clamp was applied, and the change in gel height and gel expansion force were measured in the same manner as for the contracting cells. Step changes in stiffness were imposed every 40 seconds to allow ample time for equilibration. Multiple time intervals were tested to confirm that a steady-state contraction velocity and force rate are reached within 40 seconds.

RESULTS

Cells spreading between an AFM cantilever and surface exhibit uniform contraction velocity and force rates for a given extracellular stiffness

We determined the whole-cell contractile response to extracellular stiffness using an AFM-based stiffness clamp. Briefly, a single fibroblast is simultaneously brought into contact with a fibronectin-coated tipless AFM cantilever and a fibronectin-coated glass substrate. As the cell adheres to the two surfaces and contracts, we record the cell-generated forces

and height changes with nanometer precision. Without feedback to control the cantilever deflection, cell contraction is resisted by a single extracellular stiffness in the vertical direction defined by the spring constant of the cantilever. Under these conditions, the contraction increases to a constant contraction velocity (μm/min) and force rate (nN/min) as the cell spreads onto both surfaces, consistent with previous studies (24, 26). A sample trace of this linear region under constant stiffness is shown in Fig. S1 in the Supporting Material with a subset shown in Fig. 2a.

Contracting cells adapt to step changes in extracellular stiffness on a timescale of seconds

To dynamically change the extracellular stiffness felt by the contracting cell, we employ a feedback algorithm for the AFM-based stiffness clamp, as previously described (24). Briefly, the stiffness clamp allows a rapid and reversible tuning of extracellular stiffness, independent of cell-generated force or contraction, by adjustment of the substrate position. For example, in the extreme case of infinite stiffness, $k_{ex} = \Delta F/\Delta X \rightarrow \infty$, no change in height is achieved ($\Delta X = 0$) regardless of the force applied by the cell. To achieve this, every incremental deflection of the cantilever is accompanied by an identical step of the substrate such that cell height remains constant. This feedback technique is referred to as a position clamp. By a similar argument, a force clamp ($\Delta F = 0$) yields an extracellular stiffness of 0. Any intermediate stiffness is obtained by appropriate adjustment of the substrate position based on cell-generated cantilever deflection.

We expose single contracting cells to a series of step changes in extracellular stiffness every 20 seconds during the linear region of contraction. Fig. 2b shows a typical cellular response to a series of step changes between 10 and 100 nN/μm, which are equivalent to cells contracting against an extracellular matrix with an elasticity of approximately 1 and 10 kPa, respectively, which is within the range of sensitivity previously reported for fibroblasts (2, 4, 29) (see Supporting Material for conversion calculation). Contraction velocity (and force rate) is stiffness-dependent, as shown in Fig. 2d, where a step change in stiffness results in a rapid change in both force rate and contraction velocity, as described previously (23, 24). However, examination of the high-resolution traces enabled by the AFM reveals a response period on a timescale of seconds immediately following a change in stiffness that has not been previously identified. Specifically, the cell accelerates to a constant rate upon a step decrease in stiffness and decelerates to a constant rate upon a step increase in stiffness. This response is even more pronounced when cycling between the extremes of $k_{ex} = 0$ (force clamp) and $k_{ex} = \infty$ (position clamp) every 20 seconds, as shown in Fig. 2c.

To quantify this response, we take the ratio of the slope during the last quarter of the stiffness interval to the slope during the first quarter of the stiffness interval. For an increase in stiffness (from 10 to 100 nN/μm or 0 to ∞) the ratio is <1 indicating a deceleration. For a decrease in stiffness, the ratio is >1 indicating an acceleration. These ratios, illustrated in Fig. 2g, are consistently distinct from 1 with $p<0.001$. The identical trend is observed in the force trace as in the height trace (see Fig. S2), indicating proper functioning of the stiffness clamp.

Notably, this response is consistent across the entire contractile regime of the cell. As demonstrated by normalizing and overlaying each stiffness interval for the entire contractile period (Fig. 2e,f), the shape of the response is preserved despite an increasing contractile force and decreasing cell height over the course of contraction. Indeed, the observed adaptation behavior is independent of force, cell height, force rate, and contraction velocity (see Fig. S3.) Based on the previously described cellular responses to changes in force (16, 17), we expect focal adhesion signaling to be involved in the consistently observed seconds-timescale response to changes in stiffness.

Focal adhesion signaling does not affect the seconds-timescale response to a step change in extracellular stiffness

Multiple studies have directly linked cellular stiffness sensing with focal adhesion activity. Specifically, the kinase activity of focal adhesion kinase (FAK) is regulated by mechanical stretching and likely plays a role in stiffness-sensitive adhesion turnover (7). Src family kinases are proposed to play an early role in the rigidity sensing cycle and are activated within 300 ms of mechanical perturbation via fibronectin linkages (7, 16). We therefore expect FAK and Src family kinases to be involved in the seconds-timescale contractile response to a step change in extracellular stiffness.

Focal adhesion activity was inhibited using either a FAK inhibitor or pp2, a Src family kinase inhibitor, and contraction experiments with step changes in extracellular stiffness between $k_{ex} = 0$ and $k_{ex} = \infty$ were performed as previously described. In the presence of 30 μM FAK inhibitor, the contraction velocity was significantly slower ($p<0.0001$) than the control; whereas 25 μM pp2 did not statistically significantly alter contraction velocity compared to the control (Fig. 3a). To quantify the response timescale under these drug conditions, we fit a linear-plus exponential curve (Eq. 1) to each interval of $k_{ex} = 0$ (Fig. 3b). The resulting response timescale in the presence of 30 μM FAK inhibitor and 25 μM pp2 was not statistically significantly different from the control response timescale, as shown in Fig. 3d. These results indicate that while focal adhesion signaling is known to be involved in long timescale stiffness-dependent behaviors, the seconds-timescale response to a step change in extracellular stiffness is independent of focal adhesion activity.

At high concentrations of either drug (50 μM), cells are able to adhere, as indicated by significant forces of de-adhesion required to detach the cell from either surface, but were unable to contract. The ability to adhere without contraction is consistent with the reported ability to form nascent adhesions in the absence of myosin II (30). Similarly, attachment by either poly-L-lysine or concanavalin A yields no contraction (data not shown), illustrating the need for integrin-mediated adhesion to generate contractile force in this system.

Partial inhibition of myosin lengthens the seconds-timescale response to a step change in extracellular stiffness

We next tested if disrupting the cytoskeleton of the cell using cytochalasin D, nocodazole, or blebbistatin would affect the response timescale. Intermediate concentrations of all three drugs decreased the steady state contraction velocity, as shown in Fig. 3a (500 nM

cytochalasin D, 30 μM nocodazole, and 30 μM blebbistatin). Interestingly, the response timescale was not significantly affected by disruption of the actin cytoskeleton with cytochalasin D or microtubules with nocodazole at concentrations that decreased the steady state contraction velocity, as shown in Fig. 3d. Only partial disruption of myosin ATPase activity with 30 μM blebbistatin showed a significant change in response timescale compared to control ($p<0.0001$). As expected, lower concentrations of all three drugs showed no significant difference in either steady state contraction velocity or response timescale. Higher concentrations of the drugs completely disrupted contraction (1 μM cytochalasin D and 50 μM blebbistatin, data not shown), thereby indicating the requirement of an intact cytoskeleton and active myosin for the buildup of traction forces.

Stretch-activated ion channels are not involved in the seconds-timescale response to a step change in extracellular stiffness

Stretch-activated ion channels are another proposed sensor of extracellular mechanics, and calcium signaling is expected to operate within the seconds timescale observed here (31–33). We therefore explored whether the response timescale was dependent on the activity of stretch-sensitive ion channels. Gadolinium chloride has been used previously to inhibit stretch-activated ion channels resulting in decreased traction forces and migration (32). In our experiments, blocking of stretch-activated ion channels with a high dose of gadolinium chloride slightly decreased the steady state contraction velocity during the force clamp ($p=0.0025$ compared to control), but it did not affect the response timescale compared to the control, as shown in Fig. 3. This result indicates that stretch-activated ion channels do not play a significant role in the seconds-timescale stiffness response observed here.

A simple mechanical model predicts the seconds-timescale response to a step change in extracellular stiffness

The repeatability of the seconds-timescale response at different contractile forces over the course of contraction of a single cell and from cell to cell, combined with the robustness of the response timescale against inhibition of focal adhesion signaling and stretch-activated ion channel activity, suggests that the response might be mechanical in nature rather than a biochemically controlled event. We therefore sought a simple mechanical model to describe the observed behavior. Because cell contraction changes immediately with a change in stiffness, independent of the tensile force, we hypothesized that the passive viscoelasticity of the whole cell was influencing the coupling of the extracellular stiffness to an underlying contractile process that is independent of force and stiffness.

A simple mechanical model that has a transient response to both step increases and decreases in stiffness is the standard linear solid viscoelastic model, which is a spring in parallel with a spring and dashpot in series, as shown in Fig. 4a. We found that a constant velocity actuator representing a simple spring with a reference length changing at a fixed rate captures the measured response of the cell to step changes in stiffness, suggesting that active biochemical changes in the contractile response, such as force-dependent changes in myosin contraction velocities, are dwarfed by passive whole-cell viscoelasticity on the seconds-timescale. The viscoelastic network couples the internal contraction of the actuator to the extracellular stiffness resisting contraction. The actuator is independent of

the current state of the transducer and also independent of the instantaneously applied extracellular stiffness.

As shown in Fig. 4b, the model predicts the observed deceleration upon a step increase in stiffness and acceleration upon a step decrease in stiffness. Derivation of the response of the model to step changes in stiffness is described in the Supporting Material. The model predicts the response timescale τ_{kex} for any step change to extracellular stiffness k_{ex}:

$$\tau_{k_{ex}} = \gamma\left(\frac{1}{k_1 + k_{ex}} + \frac{1}{k_2}\right) \tag{2}$$

where γ is the damping parameter, and k_1 and k_2 are the stiffness values of the two internal springs as labeled in Fig. 4a. The extreme cases of the force clamp ($k_{ex} = 0$) and position clamp ($k_{ex} = \infty$) follow:

$$\tau_{k_{ex}=0} = \gamma\left(\frac{1}{k_1} + \frac{1}{k_2}\right) \tag{3}$$

$$\tau_{k_{ex}=\infty} = \frac{\gamma}{k_2} \tag{4}$$

The model makes two important predictions. First, the model predicts a lack of hysteresis. In other words, the response timescale is only dependent on the current k_{ex} and not on the previous extracellular stiffness, assuming consecutive stiffness intervals that are greater than the response timescale. Second, the model predicts a shorter response timescale at higher stiffness and longer response timescale at lower stiffness, as indicated in Fig. 4b. We tested and confirmed both of these predictions experimentally. As shown in Fig. 4c, the response timescale at 100 nN/μm is the same regardless of whether the previous stiffness was 10 nN/ μm or ∞, confirming the prediction of no hysteresis. Next we measured the response timescale for a range of extracellular stiffness values and observed statistically significantly different values at $k_{ex} = 0$ versus $k_{ex} = \infty$ as shown in Fig. 4d, again confirming the model prediction.

Swelling hydrogels exhibit a similar seconds-timescale response to a step change in external stiffness

Our simple mechanical model suggests that the observed response to step changes in extracellular stiffness should occur for any system with an independent actuator and standard linear solid viscoelastic material properties. We tested whether this was true using a polyacrylamide hydrogel, which exhibits seconds-timescale viscoelastic behavior (34) and can be driven to expand by changes in osmotic pressure. The hydrogel was subjected to a change in osmotic pressure and exposed to the same stiffness cycling between $k_{ex} = 0$ and $k_{ex} = \infty$, but for 40 second intervals to accommodate longer response times. As shown in Fig. 5, we indeed observe the same acceleration upon a step decrease in stiffness and deceleration upon a step increase in stiffness with response timescales longer than those observed for cells, but still dependent on the current external stiffness. This supports that the mechanical equilibration of the viscoelastic properties of the cell are

sufficient to describe the observed short-timescale adaptation to a step change in extracellular stiffness.

DISCUSSION

Our measurements of cellular contraction upon a step change in extracellular stiffness reveal a seconds-timescale response that shows the importance of cytoskeletal mechanics for models of stiffness sensing. Using an AFM stiffness clamp to control the extracellular stiffness exposed to contractile fibroblasts, we consistently observe acceleration to a constant contraction velocity and force rate upon a step decrease in stiffness and deceleration upon a step increase in stiffness. Experiments with drugs that disrupt adhesion signaling and the cytoskeleton suggest that the response timescale depends only on the extracellular stiffness and intracellular mechanical properties. In our experiments the adaptation of cells to changes in stiffness is well-described by a simple mechanical model of an internal cellular actuator pulling at a constant velocity against both the extracellular stiffness and intracellular mechanics (Fig. 4). Indeed, when we expose an actively swelling gel to the same conditions as the cell, we observe comparable behavior (Fig. 5), reinforcing the idea that the stiffness adaptation results from the viscoelastic properties of the cell.

The simple mechanical model can be used to extract viscoelastic and contractile properties from the experimental data. The actuator velocity, α, is simply the steady state contractile velocity at $k_{ex} = 0$, as described in the supplemental section. We find a median actuator velocity of α = 13 nm/s (25^{th}, 75^{th} percentile: 8.3, 20 nm/s), which is consistent with reported velocities of retrograde actin flow in the presence of focal adhesions of 10-20 nm/s (35). As expected, disruption of either the actin network with cytochalasin D or myosin ATPase activity with blebbistatin decreases a as shown in Fig. 3a. Furthermore by fitting the model predictions to the control data, we found the viscoelastic components of the actomyosin network to be k_1 = 36, k_2 = 53 nN/μm, and γ = 140 nN*s/μm (corresponding to approximately E_1 = 3.6, E_2 = 5.3 kPa, and γ = 14 kPa*s, see Supporting Material for calculation of model parameters and elasticity conversion). These values are consistent with previously published values of E = 0.5-20 kPa (29, 36) and γ = 1-100 kPa*s (36, 37). Interestingly, a study by Humphrey et al. showed that actomyosin networks of a similar ratio of actin to myosin as in vivo environments relieve macroscopic stress over an average relaxation time of ~8 seconds – remarkably similar to the response timescale observed here (38). Consistent with this, we expect that the physiological basis of the viscoelastic component of our model is dominated by the actomyosin network, which may include contributions from the cortex and stress fibers.

Close examination of the viscoelastic parameters in Table S1 reveals a robustness of the response timescale such that changes in elastic (k_1, k_2) and viscous (γ) components have opposing effects on the response timescale. For example, both 500 nM cytochalasin D and 30 μM blebbistatin cause a significant decrease in all viscoelastic parameters compared to control. As seen in Eq. 2, the elastic and viscous components have opposing effects on the response timescale. Therefore, in the case of cytochalasin D, the decrease in the viscous component counteracts the decrease in the elastic components resulting in a response timescale consistent with the control. However the decrease in the viscous component is

smaller for blebbistatin, resulting in a response timescale distinct from the control. These competing effects point to the complexity of the role of intracellular mechanics such that changes in distinct mechanical components may not translate to the whole-cell scale.

The model we propose does not require incorporation of force-dependent motor activity to explain the response timescale. This is distinct from previous models that combine the force-velocity relationship with binding and unbinding kinetics of adhesions to predict stiffness-dependent motility and stress fiber development (12, 39). It has also been proposed that actomyosin contraction itself may be stiffness-dependent either due to catch bond behavior (7, 40) or load-dependent resistance from internal friction due to cross-linkers (26). While the inverse force-velocity relationship has been well-characterized for skeletal myosin and on the whole-cell scale for muscle cells where load is directly and efficiently applied to myosin networks (26, 41, 42), the effect of force on less organized acto-myosin networks in non-muscle cells remains unclear. Recent studies of non-muscle myosins IIa and IIb suggest that load dependent kinetics are complex (43, 44) and are likely further complicated by dynamic re-organization of actin in non-muscle cells. Only a constant velocity actuator is required in our simple mechanical model, potentially due to activity in a regime of minimal force sensitivity or the re-organization of actin structures that results in approximately constant myosin activity. A simple mechanical model has been proposed recently by Marcq et al. where "adaptation to substrate rigidity results from an interplay between passive elasticity and active contractility" (28). That recent model, however, incorporates a different specific force-velocity relationship and does not address the short timescale equilibration that we report here.

This study finds that viscoelastic equilibration of the cytoskeleton is central to stiffness-dependent contraction over short timescales. We observe a seconds-timescale response to a step change in extracellular stiffness, independent of focal adhesion signaling and dependent only on actomyosin mechanics. In the simple mechanical model we propose, extracellular stiffness is coupled through the viscoelastic cytoskeleton such that stretching of mechanosensory proteins and subsequent intracellular signaling result from a combination of extracellular stiffness and cytoskeletal mechanics that equilibrate after several seconds. Examination of longer timescale responses to stiffness changes will be required to characterize signal transduction from cytoskeletal relaxation and focal adhesion signaling to changes in gene expression.

ACKNOWLEDGEMENTS

The authors thank Dr. Ross Rounsevell, Dr. Lina Nilsson, Dr. Ben Ricca, Gautham Venugopalan and other members of the Fletcher Lab for helpful discussions, and Luke Cassereau for donation of polyacrylamide material.

REFERENCES

1. Peyton, S.R., and A.J. Putnam. 2005. Extracellular matrix rigidity governs smooth muscle cell motility in a biphasic fashion. J Cell Physiol. 204: 198-209.
2. Lo, C.M., H.B. Wang, M. Dembo, and Y.L. Wang. 2000. Cell movement is guided by the rigidity of the substrate. Biophys J. 79: 144-52.
3. Engler, A.J., S. Sen, H.L. Sweeney, and D.E. Discher. 2006. Matrix elasticity directs stem cell lineage specification. Cell. 126: 677-89.
4. Wang, H.B., M. Dembo, and Y.L. Wang. 2000. Substrate flexibility regulates growth and apoptosis of normal but not transformed cells. Am J Physiol, Cell Physiol. 279: C1345-50.
5. Munevar, S., Y. Wang, and M. Dembo. 2001. Traction force microscopy of migrating normal and H-ras transformed 3T3 fibroblasts. Biophys J. 80: 1744-57.
6. Geiger, B., J.P. Spatz, and A.D. Bershadsky. 2009. Environmental sensing through focal adhesions. Nat Rev Mol Cell Biol. 10: 21-33.
7. Moore, S.W., P. Roca-Cusachs, and M.P. Sheetz. 2010. Stretchy proteins on stretchy substrates: the important elements of integrin-mediated rigidity sensing. Dev Cell. 19: 194-206.
8. Cai, Y., O. Rossier, N.C. Gauthier, N. Biais, M.-A. Fardin, et al. 2010. Cytoskeletal coherence requires myosin-IIA contractility. J Cell Sci. 123: 413-23.
9. Pasapera, A.M., I.C. Schneider, E. Rericha, D.D. Schlaepfer, and C.M. Waterman. 2010. Myosin II activity regulates vinculin recruitment to focal adhesions through FAK-mediated paxillin phosphorylation. The Journal of Cell Biology. 188: 877-890.
10. Sawada, Y., M. Tamada, B.J. Dubin-Thaler, O. Cherniavskaya, R. Sakai, et al. 2006. Force sensing by mechanical extension of the Src family kinase substrate p130Cas. Cell. 127: 1015-26.
11. Wang, Y., E.L. Botvinick, Y. Zhao, M.W. Berns, S. Usami, et al. 2005. Visualizing the mechanical activation of Src. Nature. 434: 1040-5.
12. Schwarz, U.S., T. Erdmann, and I.B. Bischofs. 2006. Focal adhesions as mechanosensors: the two-spring model. BioSystems. 83: 225-32.
13. Chen, C.S. 2008. Mechanotransduction - a field pulling together? J Cell Sci. 121: 3285-92.
14. Paszek, M.J., N. Zahir, K.R. Johnson, J.N. Lakins, G.I. Rozenberg, et al. 2005. Tensional homeostasis and the malignant phenotype. Cancer Cell. 8: 241-54.
15. del Rio, A., R. Perez-Jimenez, R. Liu, P. Roca-Cusachs, J.M. Fernandez, et al. 2009. Stretching single talin rod molecules activates vinculin binding. Science. 323: 638-41.
16. Na, S., O. Collin, F. Chowdhury, B. Tay, M. Ouyang, et al. 2008. Rapid signal transduction in living cells is a unique feature of mechanotransduction. Proc Natl Acad Sci USA. 105: 6626-31.
17. Hayakawa, K., H. Tatsumi, and M. Sokabe. 2008. Actin stress fibers transmit and focus force to activate mechanosensitive channels. J Cell Sci. 121: 496-503.
18. Shinohara, M., K. Sabra, J. Gennisson, M. Fink, and M. Tanter. 2010. Real-time visualization of muscle stiffness distribution with ultrasound shear wave imaging during muscle contraction. Muscle & Nerve. 42: 438-441.
19. Frey, M.T., and Y.-L. Wang. 2009. A photo-modulatable material for probing cellular responses to substrate rigidity. Soft Matter. 5: 1918-1924.

20. Jiang, F.X., B. Yurke, R.S. Schloss, B.L. Firestein, and N.A. Langrana. 2010. The relationship between fibroblast growth and the dynamic stiffnesses of a DNA crosslinked hydrogel. Biomaterials. 31: 1199-212.
21. Young, J.L., and A.J. Engler. 2011. Hydrogels with time-dependent material properties enhance cardiomyocyte differentiation in vitro. Biomaterials. 32: 1002-9.
22. Yoshikawa, H.Y., F.F. Rossetti, S. Kaufmann, T. Kaindl, J. Madsen, et al. 2011. Quantitative Evaluation of Mechanosensing of Cells on Dynamically Tunable Hydrogels. Journal of the American Chemical Society. 133: 1367-1374.
23. Mitrossilis, D., J. Fouchard, D. Pereira, F. Postic, A. Richert, et al. 2010. Real-time single-cell response to stiffness. Proc Natl Acad Sci USA. 107: 16518-23.
24. Webster, K.D., A. Crow, and D.A. Fletcher. 2011. An AFM-Based Stiffness Clamp for Dynamic Control of Rigidity. PLoS ONE. 6: e17807.
25. Lam, W.A., O. Chaudhuri, A. Crow, K.D. Webster, T.-D. Li, et al. 2011. Mechanics and contraction dynamics of single platelets and implications for clot stiffening. Nat Mater. 10: 61-6.
26. Mitrossilis, D., J. Fouchard, A. Guiroy, N. Desprat, N. Rodriguez, et al. 2009. Single-cell response to stiffness exhibits muscle-like behavior. Proc Natl Acad Sci USA. 106: 18243-8.
27. Fouchard, J., D. Mitrossilis, and A. Asnacios. 2011. Acto-myosin based response to stiffness and rigidity sensing. Cell Adhesion & Migration. 5: 16-19.
28. Marcq, P., N. Yoshinaga, and J. Prost. 2011. Rigidity Sensing Explained by Active Matter Theory. Biophysical Journal. 101: L33-L35.
29. Solon, J., I. Levental, K. Sengupta, P.C. Georges, and P.A. Janmey. 2007. Fibroblast adaptation and stiffness matching to soft elastic substrates. Biophys J. 93: 4453-61.
30. Choi, C.K., M. Vicente-Manzanares, J. Zareno, L.A. Whitmore, A. Mogilner, et al. 2008. Actin and alpha-actinin orchestrate the assembly and maturation of nascent adhesions in a myosin II motor-independent manner. Nat Cell Biol. 10: 1039-50.
31. Beningo, K.A., M. Dembo, and Y.-L. Wang. 2004. Responses of fibroblasts to anchorage of dorsal extracellular matrix receptors. Proc Natl Acad Sci USA. 101: 18024-9.
32. Munevar, S., Y.-L. Wang, and M. Dembo. 2004. Regulation of mechanical interactions between fibroblasts and the substratum by stretch-activated Ca2+ entry. J Cell Sci. 117: 85-92.
33. Matthews, B.D., C.K. Thodeti, J.D. Tytell, A. Mammoto, D.R. Overby, et al. 2010. Ultra-rapid activation of TRPV4 ion channels by mechanical forces applied to cell surface beta1 integrins. Integr Biol (Camb). 2: 435-42.
34. Constantinides, G., Z.I. Kalcioglu, M. McFarland, J.F. Smith, and K.J. Van Vliet. 2008. Probing mechanical properties of fully hydrated gels and biological tissues. J Biomech. 41: 3285-3289.
35. Aratyn-Schaus, Y., P.W. Oakes, and M.L. Gardel. 2011. Dynamic and Structural Signatures of Lamellar Actomyosin Force Generation. Mol Biol Cell. .
36. Thoumine, O., and A. Ott. 1997. Time scale dependent viscoelastic and contractile regimes in fibroblasts probed by microplate manipulation. J Cell Sci. 110 (Pt 17): 2109-16.
37. Bausch, A.R., F. Ziemann, A.A. Boulbitch, K. Jacobson, and E. Sackmann. 1998. Local measurements of viscoelastic parameters of adherent cell surfaces by magnetic bead microrheometry. Biophys J. 75: 2038-49.

38. Humphrey, D., C. Duggan, D. Saha, D. Smith, and J. Käs. 2002. Active fluidization of polymer networks through molecular motors. Nature. 416: 413-6.
39. Walcott, S., and S.X. Sun. 2010. A mechanical model of actin stress fiber formation and substrate elasticity sensing in adherent cells. Proc Natl Acad Sci USA. .
40. Guo, B., and W.H. Guilford. 2006. Mechanics of actomyosin bonds in different nucleotide states are tuned to muscle contraction. Proc Natl Acad Sci USA. 103: 9844-9.
41. Hill, A. 1938. The heat of shortening and the dynamic constants of muscle. Proc R Soc London Ser B. 126: 136-195.
42. Piazzesi, G., M. Reconditi, M. Linari, L. Lucii, P. Bianco, et al. 2007. Skeletal muscle performance determined by modulation of number of myosin motors rather than motor force or stroke size. Cell. 131: 784-95.
43. Kovács, M., K. Thirumurugan, P.J. Knight, and J.R. Sellers. 2007. Load-dependent mechanism of nonmuscle myosin 2. Proc Natl Acad Sci USA. 104: 9994-9.
44. Norstrom, M.F., P.A. Smithback, and R.S. Rock. 2010. Unconventional processive mechanics of non-muscle myosin IIB. J Biol Chem. 285: 26326-34.

FIGURES

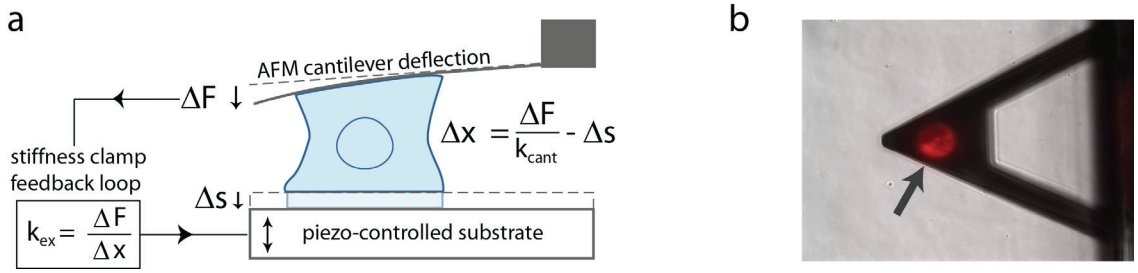

Figure 1. Atomic force microscope based control of stiffness during single cell contraction.

(*a*) Setup of single cell contraction experiments. Cell-generated forces and cell height are measured by deflection of the AFM cantilever (of stiffness k_{cant}) while extracellular stiffness, k_{ex}, is controlled in real time using the stiffness clamp feedback algorithm (24). (*b*) Top-down view of cell adhered to AFM cantilever and substrate. The cell membrane is fluorescently labeled for visual clarity (arrow).

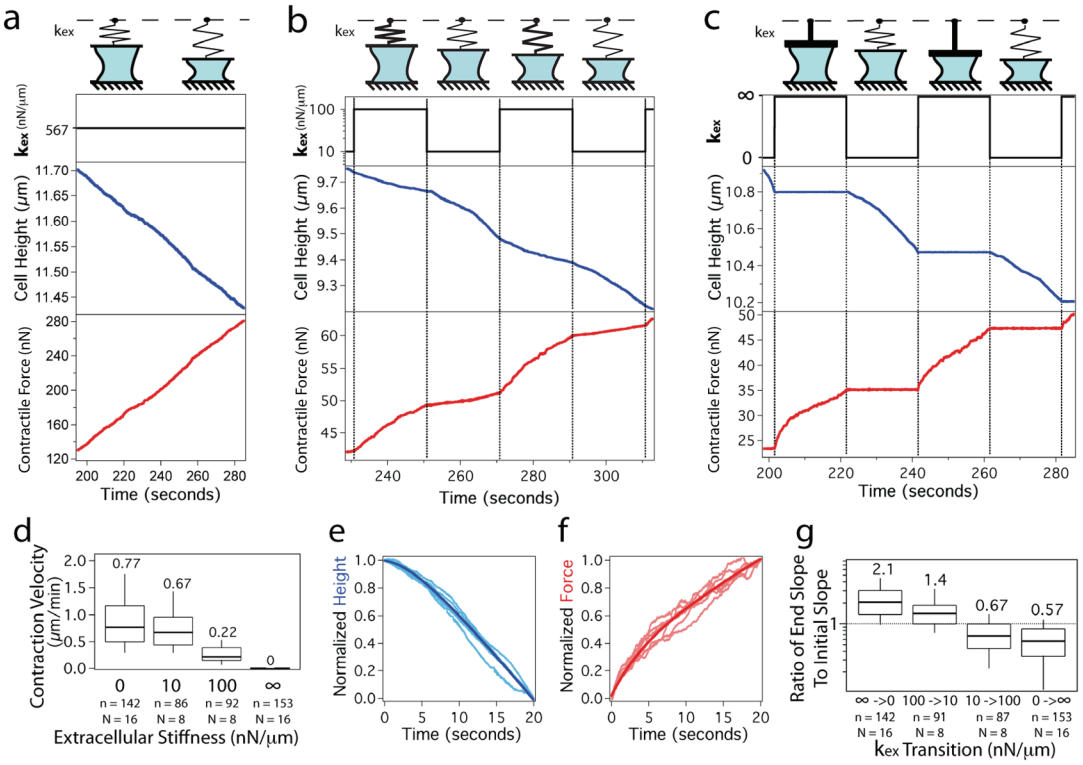

Figure 2. Contracting cells adapt to a step change in extracellular stiffness on a timescale of seconds.

(*a*) Typical trace of cell height and contractile force of a single cell contracting under a constant extracellular stiffness as illustrated by the top row cartoons. Once contact with both surfaces is established, the cell contracts at a constant rate for several minutes before slowing. (Full trace shown in Fig. S1.) (*b*) Step changes in extracellular stiffness between 10 and 100 nN/μm every 20 seconds yield changes in both contraction velocity and the rate at which force changes in time. (*c*) Extreme step changes in stiffness between k_{ex} =0 and k_{ex} = ∞ clearly reveal a response period following the step change. (*d*) Steady-state contraction velocity depends directly on extracellular stiffness. (*e*) The response timescale is consistent across the entire contractile period of the cell as shown by the normalization and overlay of all k_{ex} = 0 intervals from a single trace. The dark line is the average over all the intervals. (*f*) Normalization and overlay of all k_{ex} = ∞ intervals from a single trace. (*g*) The ratio of the slope over the last quarter of the interval to the slope over the first quarter of the interval is calculated for each 20-second stiffness interval for the height traces. n represents number of stiffness transitions, N represents number of cells, and box plot presents median, 25th and 75th percentile and 10 and 90th percentile outliers. The median value is indicated above each box for clarity.

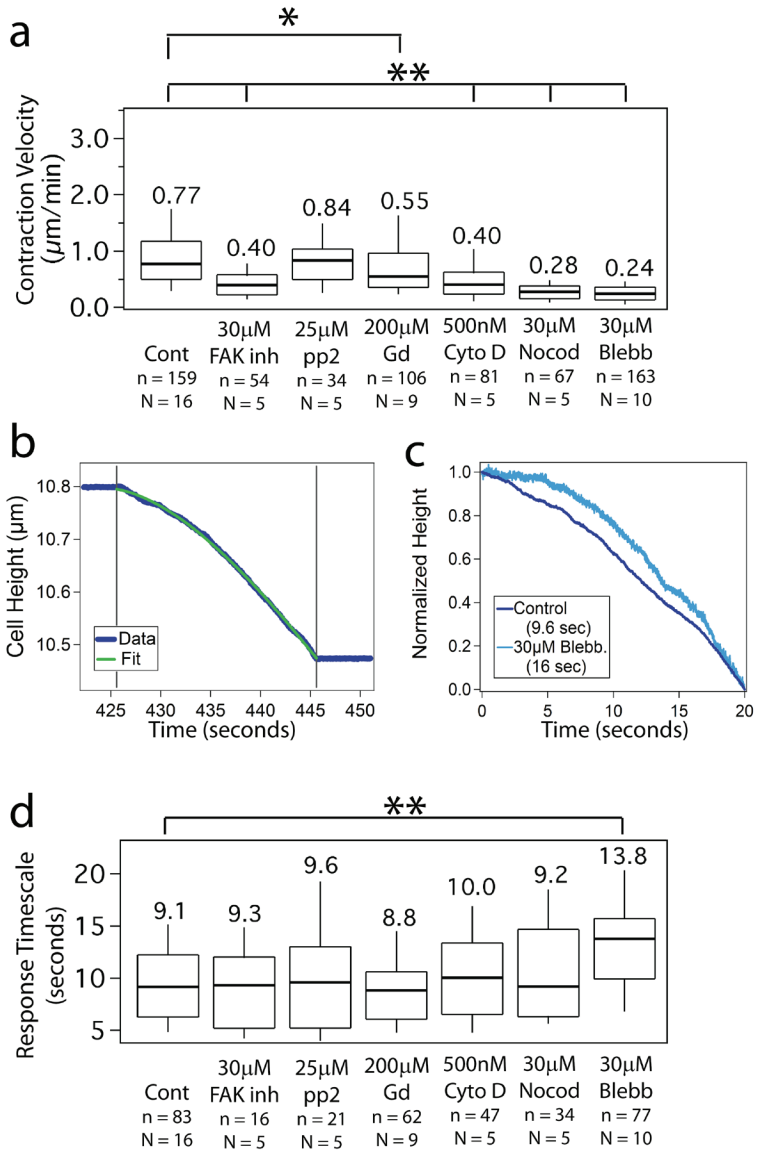

Figure 3. Inhibition experiments reveal a consistent response timescale dependent on cell mechanics rather than adhesion signaling.

(*a*) Steady state contraction velocity for the control, FAK inhibitor, Src family kinase inhibitor pp2, gadolinium chloride, cytochalasin D, nocodazole, and blebbistatin. All conditions are statistically significantly slower than the control except pp2. (*b*) Linear plus exponential fit to typical height trace. (*c*) Demonstration of distinct adaptation timescales. Normalized traces from k_{ex} = 0 under control and 30 μM blebbistatin conditions are overlaid for comparison. See Fig. S4 for multiple cycles of stiffness changes in the presence of blebbistatin. (*d*) Response timescale from k_{ex} = 0 intervals remains unchanged under all conditions except 30 μM blebbistatin. For all box plots, n represents number of transitions or intervals and N represents number of cells. Median values are shown below each box plot while the plot presents median, 25th and 75th percentile and 10 and 90th percentile outliers. * indicates $p<0.01$ and ** indicates $p<0.0001$.

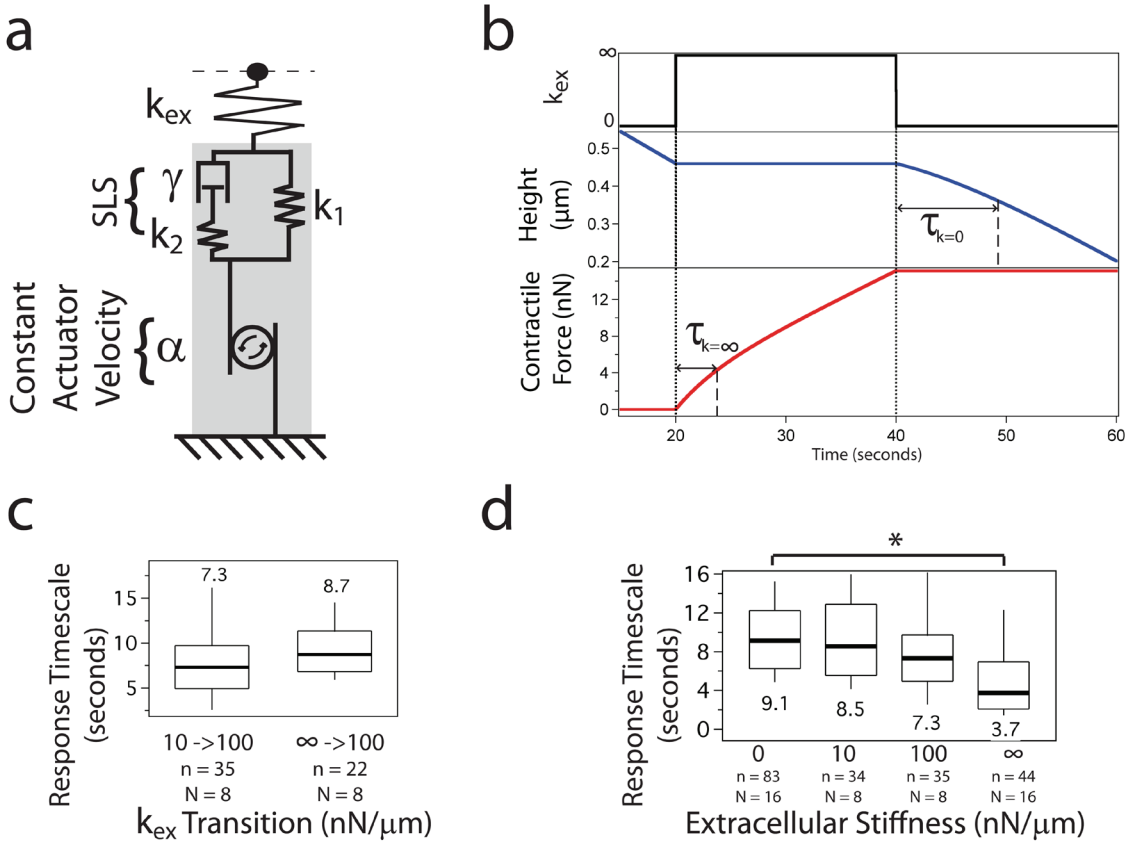

Figure 4. Simple mechanical model describes contractile response upon a step change in stiffness.

(*a*) Cartoon illustrating an independent actuator moving at a constant velocity α in series with the standard linear solid (SLS) element consisting of a spring k_1 in parallel with a dashpot γ and spring k_2 in series. As extracellular stiffness conditions change, different elements of the SLS absorb the sudden change in stiffness as illustrated in Fig. S5. (*b*) Predictions of the model successfully simulate the observed response timescale for a step increase and step decrease in stiffness, for both the height and force behavior. Response timescale, τ, is indicated for both the $k_{ex} = 0$ and $k_{ex} = \infty$ cases. (*c*) Experimental validation of the model prediction that response timescale is independent of the previous stiffness. (*d*) Experimental validation of the model prediction that response timescale is longer for lower stiffness and shorter for higher stiffness. The differences between the groups was confirmed with a Kruskal-Wallis one-way analysis of variance (ANOVA) across all four groups, with * indicating $p<0.0001$.

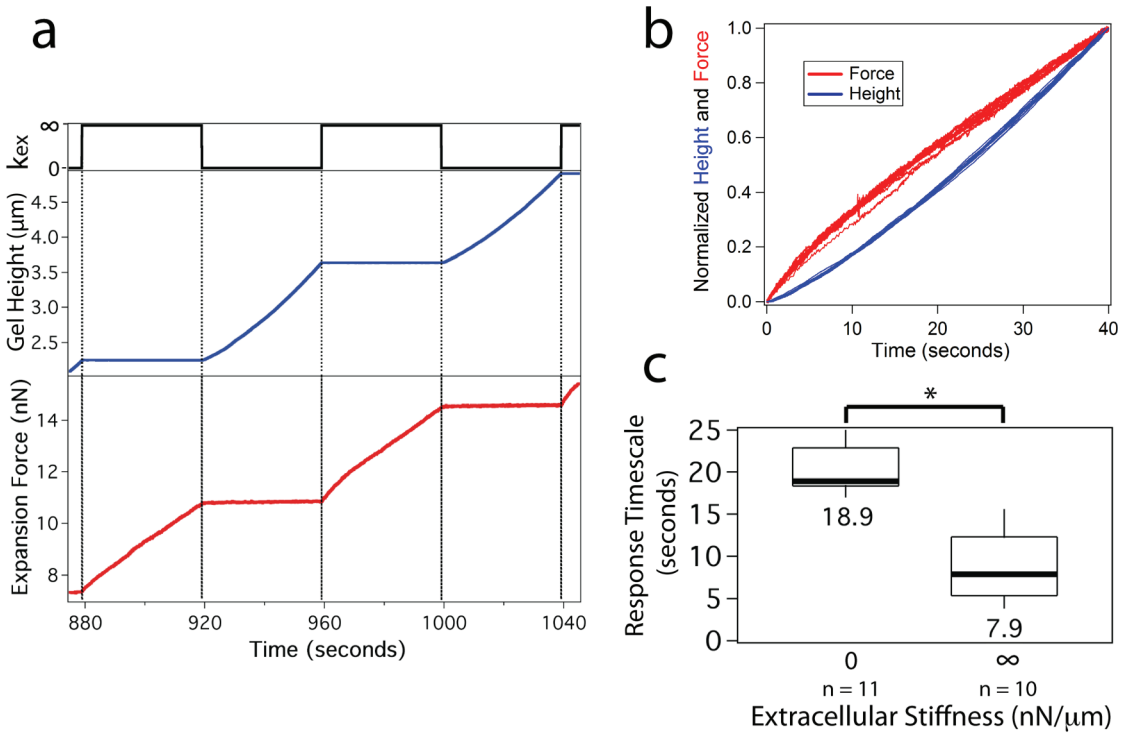

Figure 5. Swelling hydrogel exhibits a seconds-timescale response to a step change in extracellular stiffness.

(*a*) Step changes in stiffness between $k_{ex} = 0$ and $k_{ex} = \infty$ applied to an expanding hydrogel every 40 seconds yield changes in both expansion velocity and force rate. (*b*) Force and height traces for each stiffness interval are normalized and overlaid, revealing a deceleration for a step increase in stiffness (force trace) and an acceleration for a step decrease in stiffness (height trace). Force and height traces are displayed on the same plot to emphasize curvature. (*c*) Gel response timescale for extreme extracellular stiffness values. * indicates $p<0.001$. n represents number of stiffness transitions and box plot presents median, 25th and 75th percentile and 10 and 90th percentile outliers.

SUPPORTING MATERIAL

Conversion from stiffness to elasticity

We use a simple conversion that assumes cell height is on the order of 10 μm and contact area on the order of 100 μm^2. Young's modulus can then be calculated according to

$$E = \frac{kH_{cell}}{A_{contact}} = 0.1k$$

where k is in nN/μm and E is in kPa.

Calculation of model parameters for a contracting cell

The model predictions may be retroactively applied to the data to get median and percentile values for the independent actuator rate, α, and viscoelastic parameters as follows:

$$\alpha = \left(\frac{dX}{dt}\right)_{k_{ex}=0, t\gg\tau}$$

$$k_1 = \frac{\left(\frac{dF}{dt}\right)_{k_{ex}=\infty, t\gg\tau}}{\left(\frac{dX}{dt}\right)_{k_{ex}=0, t\gg\tau}}$$

$$k_2 = k_1\left(\frac{\tau_{k_{ex}=0}}{\tau_{k_{ex}=\infty}} - 1\right)$$

$$\gamma = k_1\tau_{k_{ex}=\infty}$$

where τ is the response timescale. Calculations based on the median, 25th and 75th percentile values reported yield the following presented as median (25th percentile, 75th percentile):

Table S1. Model Parameters calculated based on data.

	α (nm/s)	k_1 (nN/μm)	k_2 (nN/μm)	γ(nN*s/μm)
Control	-13 (-8.3, -20)	36 (35, 37)	53 (27, 75)	140 (78, 240)
30 μM Blebbistatin	-4.8 (-3.5, -6.7)	16 (12, 23)	25 (14, 34)	89 (82, 90)
500 nM Cyto D	-6.7 (-3.8, -10)	15 (7.0, 23)	12 (3.1, 46)	64 (51, 83)
10 nM Jasplakinolide	-15 (-9.3, -24)	26 (16, 27	40 (11, 62)	89 (48, 98)
30 μM Nocodazole	-4.7 (-2.5, -6.3)	93 (73, 97)	140 (48, 190)	340 (210, 600)
25 μM pp2	-14 (-8.2, -17)	40 (34, 58)	85 (61, 110)	140 (92, 150)
30 μM FAK inhibitor	-6.7 (-3.7, -9.5)	42 (11, 53)	52 (12, 67)	170 (60, 180)
200 μM Gadolinium	-9.2 (-5.9, -16)	51 (43, 55)	110 (38, 120)	170 (92, 240)

The calculated viscoelastic parameters reveal interesting inhibition-based trends that are not visible by simply studying the response timescale. Specifically, both elastic and viscous parameters decrease for blebbistatin and cytochalasin D treated cells while elastic and viscous parameters increase for nocodazole-treated cells. These changes in mechanical properties are not observed in the response timescale because elastic and viscous properties have opposing effects:

$$\tau_{k_{ex}=0} = \gamma\left(\frac{1}{k_1}+\frac{1}{k_2}\right)$$

Therefore corresponding increases or decreases in both parameters may cancel resulting in a response timescale consistent with the control. The decrease in elastic components in the cases of blebbistatin and cytochalasin D and the increase in elastic components in the case of nocodazole are consistent with previously published results (1). To further examine the role of actin structures, we stabilized the actin cytoskeleton with Jasplakinolide. This had a similar effect to cytochalasin D in that 10 nM Jasplakinolide had no effect on the response timescale compared to the control, but 50 nM was adequate to stop contraction altogether. Calculation of viscoelastic parameters in the presence of 10nM Jasplakinolide reveals a slight decrease in all values to yield a response timescale indistinguishable from the control, as shown in Table S1. In the case of blebbistatin, the decrease in the viscous component is not as great and therefore does not fully cancel the decrease in elastic component, resulting in a response timescale distinct from control.

Inhibition of FAK, Src family kinases, or stretch-activated ion channels did not yield any major difference in k_1 or γ components compared to the control in our system. We note that the internal spring parameter k_2 shows the greatest inhibition-induced changes compared to the control in all cases, including focal adhesion signaling. We therefore expect we may see a difference in response timescale for extreme step increases in stiffness:

$$\tau_{k_{ex}=\infty} = \frac{\gamma}{k_2}$$

While we do anecdotally observe the expected trends, we are unable to show statistical significance with the limited number of force trace intervals that pass our F-test criterion. We therefore leave investigation of this intriguing phenomenon to a subsequent study.

Derivation of the response of the model to step changes in stiffness

The equations for the model are:

$$f(t) = k_1(x_1 - \alpha t) + f_2$$
$$f_2 = k_2 x_2 = \gamma \dot{x}_3$$
$$x_1 = x_2 + x_3$$

where $f(t)$ is the tensile force applied at the cell-cantilever interface, α is the velocity at which the reference length of the spring x_1 is changing (i.e., this is the actuator), and x_2 and x_3 describe the state of the internal spring and dashpot, respectively.

In the experiment, the effective stiffness jumps at the set of times $\left\{t_j\right\}_{j=1}^{j=N}$. This can be described within the model by setting

$$f\left(t\right) = f\left(t_j\right) - k_{ex}\left(t_j\right)\left(x_1 - x_1\left(t_j\right)\right)$$

for $t \in \left[t_j, t_{j+1}\right)$ where $k_{ex}\left(t\right)$ is the applied stiffness at time *t*. When the intervals between jumps in stiffness are very long, $t \gg \tau$, we can analyze the model by considering its behavior for a single jump. First we define: $t' = t - t_j$ and

$$x_1'\left(t'\right) = x_1\left(t' + t_j\right) - x_1\left(t_j\right)$$
$$x_2'\left(t'\right) = x_2\left(t' + t_j\right)$$
$$x_3'\left(t'\right) = x_3\left(t' + t_j\right) - x_1\left(t_j\right)$$

so that the equations take the form

$$f\left(t_j\right)-k_{ex}\left(t_j\right)x_1'=k_1\left(x_1'-\alpha t'\right)+k_1\left(x_1\left(t_j\right)-\alpha t_j\right)+f_2$$
$$f_2=k_2x_2'=\gamma\dot{x}_3'$$
$$x_1'=x_2'+x_3'$$

This can be rearranged to

$$f'=k_1'\left(x_1'-\alpha' t'\right)+f_2$$
$$f_2=k_2x_2'=\gamma\dot{x}_3'$$
$$x_1'=x_2'+x_3'$$

with

$$k_1'=k_1+k_{ex}\left(t_j\right)$$
$$\alpha'=\frac{k_1}{k_1'}\alpha$$
$$f'=f\left(t_j\right)-k_1\left(x_1\left(t_j\right)-\alpha t_j\right)$$

The solution of this model is

$$x_3'\left(t'\right)=x_3'\left(0\right)\exp\left(-\frac{t'}{\tau}\right)+\frac{f'}{k_1'}\left(1-\exp\left(-\frac{t'}{\tau}\right)\right)+\alpha'\left(t'-\tau\left(1-\exp\left(-\frac{t'}{\tau}\right)\right)\right)$$
$$x_1'\left(t'\right)=\frac{f'}{k_1'}-\left(\frac{f'}{k_1'}-x_3'\left(0\right)\right)\left(\frac{k_2}{k_2+k_1'}\right)\exp\left(-\frac{t'}{\tau}\right)+\alpha'\left(t'-\tau\left(1-\exp\left(-\frac{t'}{\tau}\right)\right)+\frac{\gamma}{k_2}\left(1-\exp\left(-\frac{t'}{\tau}\right)\right)\right)$$
$$\tau=\gamma\left(\frac{1}{k_1'}+\frac{1}{k_2}\right)$$

and for long stiffness intervals we find

$$x_3'\left(t'\right)\approx\alpha' t'+\frac{f'}{k_1'}-\alpha'\tau$$
$$x_1'\left(t'\right)\approx\alpha' t'-\alpha'\tau+\frac{\gamma\alpha'}{k_2}+\frac{f'}{k_1'}$$

Using these asymptotic relations we can deduce the values of $x_3'\left(0\right)$ and f' immediately following a change in stiffness at $t=t_{j+1}$, let us call these $x_3''\left(0\right)$ and f''. Assuming $t'\gg\tau$ so that we can use the asymptotic formulas, with the recurrence formula for $f\left(t\right)$ and the formula for τ we find $f''=\gamma\alpha'$. We can also easily find that $x_3''\left(0\right)=-\frac{\gamma}{k_2}\alpha'$. These formulas

can be used to give the final complete solution for changes in stiffness with long time intervals as

$$x_1(t) - x_1\left(t_{j+1}\right) = \alpha \frac{k_1}{k_1 + k_{ex}\left(t_{j+1}\right)}\left(t - t_{j+1}\right)$$

$$+\alpha \frac{k_1 \gamma}{k_1 + k_{ex}\left(t_{j+1}\right)}\left(\frac{1}{k_1 + k_{ex}\left(t_j\right)} - \frac{k_1}{k_1 + k_{ex}\left(t_{j+1}\right)}\right)\left(1 - \exp\left(-\frac{t - t_{j+1}}{\tau_{j+1}}\right)\right)$$

where

$$\tau_{j+1} = \gamma\left(\frac{1}{k_1 + k_{ex}\left(t_{j+1}\right)} + \frac{1}{k_2}\right)$$

The increment to the measured force during the interval $\left[t_{j+1}, t_{j+2}\right)$ can be derived from this relation by multiplying by $k_{ex}\left(t_{j+1}\right)$, and in the case of a displacement clamp, taking the limit $k_{ex}\left(t_{j+1}\right) \to \infty$.

References

1. Sen, S., and S. Kumar. 2009. Cell-Matrix De-Adhesion Dynamics Reflect Contractile Mechanics. Cellular and molecular bioengineering. 2: 218-230.

SUPPORTING FIGURES

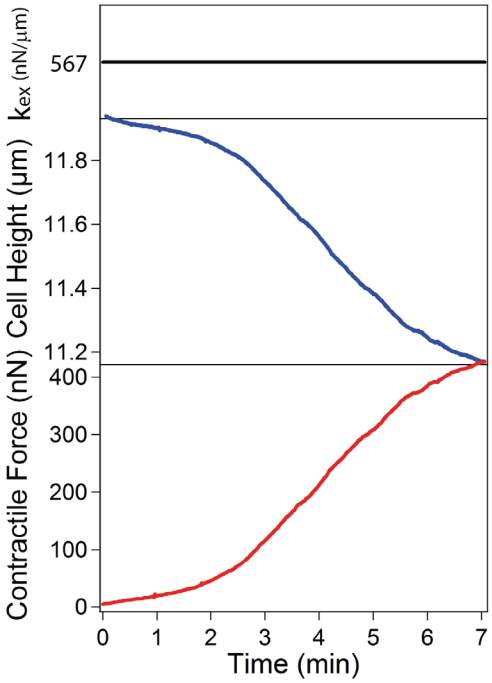

Figure S1. Contractile behavior of single cell under constant stiffness.

Under a constant extracellular stiffness, k_{ex}, here presented as the stiffness of the cantilever, the cell originally accelerates (decreasing cell height and increasing contractile force) to a constant contraction velocity and traction rate. This linear regime is maintained over several minutes before slowing. We consistently observe this linear contractile regime whereas behavior upon slowing is variable ranging from a temporary tensional equilibrium at constant force to the cell releasing one surface resulting in a decrease in contractile force and lengthening of the cell. Note a stable steady-state force/height is never permanently reached in our setup due to the motile nature of fibroblasts. All stiffness response data were collected from the middle linear regime of contraction.

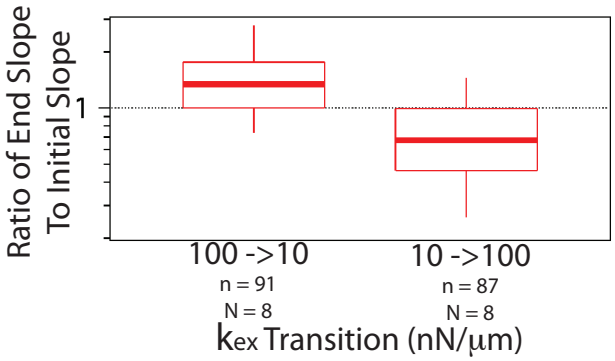

Figure S2. Same trend observed for force trace as for height trace upon a step change in stiffness.

The ratio of the slope over the last quarter of the interval to the slope over the first quarter of the interval is calculated for each 20-second stiffness interval for the force trace. At a given stiffness, the force and height traces are directly related by the extracellular stiffness. Therefore by definition of the system we observe the same trend as seen for the height trace in Figure 2g. n represents number of stiffness transitions, N represents number of cells, and box plot presents median, 25th and 75th percentile and 10 and 90th percentile outliers.

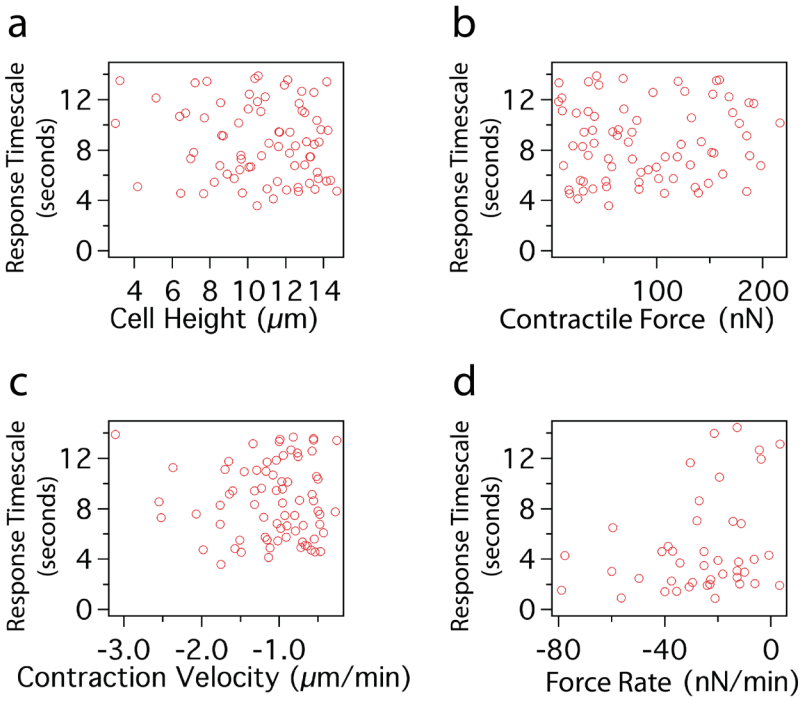

Figure S3. Response timescale is independent of contractile force, cell height, force rate, and contraction velocity.

Response time was not statistically significantly correlated with (a) cell height, (b) contractile force, (c) contraction velocity, (d) or force rate, as determined by Spearman's rank correlation analysis ($p>0.2$).

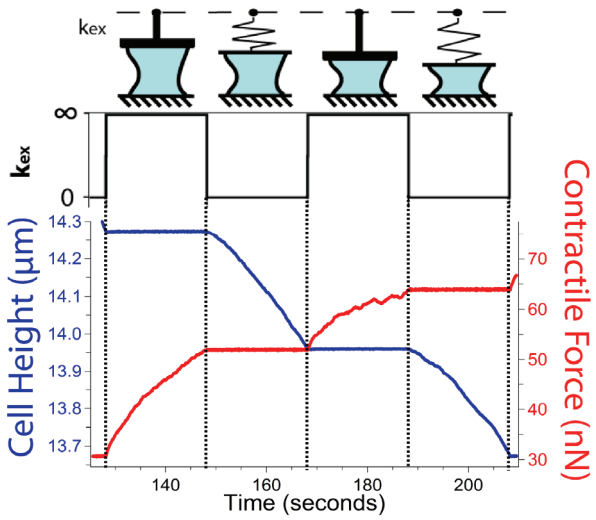

Figure S4. Contractile response of a cell to changes in stiffness in the presence of 30 µM blebbistatin.

At an intermediate dose of blebbistatin, acto-myosin contraction is slowed, but the seconds timescale acceleration upon a reduction in stiffness and deceleration upon an increase in stiffness are present. However, the median response timescale is 52% longer with 30 µM blebbistatin than for the control.

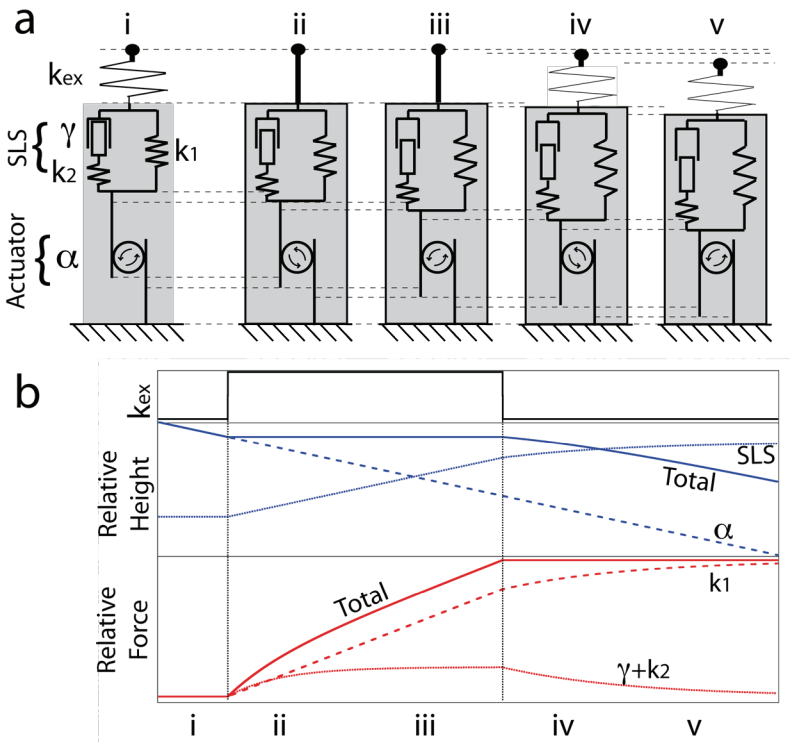

Figure S5. Detailed explanation of mechanical model.

(a) Cartoon illustrating the independent actuator moving at rate α in series with the standard linear solid (SLS) element consisting of a spring k_2 and dashpot γ in parallel with a spring k_1. As extracellular stiffness conditions change, different elements of the SLS absorb the sudden change in stiffness as illustrated. (b) Predictions of the model perfectly simulate the observed response for a step increase and step decrease in stiffness, for both the height and force behavior, as shown by the solid lines labeled "Total" (indicating whole-cell behavior). The activity of individual elements is indicated by dashed lines. For the height trace, the change in height of the actuator is constant as indicated by the linearity of the trace marked α. The standard linear solid element (SLS), however, equilibrates to the step change in extracellular stiffness. For the force channel, the individual activity of the two sides of the SLS model are shown: the lone spring k_1 and the spring and dashpot in series: k_2+γ. The sum of these two curves yields the total force exerted by the whole-cell. The roman numerals indicate corresponding time points in (a) and (b).

Chapter 4.

Multicellular architecture of breast epithelia influences mechanics of the epithelial structure

This study was conducted in collaboration with Gautham Venugopalan, David B. Camarillo, Chris H. Rycroft, Clay D. Reber, James A. Sethian, Valerie M. Weaver, Hana El-Samad, and Daniel A. Fletcher.

ABSTRACT

During breast carcinoma progression, epithelial cells often grow into the lumen and form a filled structure. Breast cancers are often stiffer than healthy tissue, and breast epithelial cells grow into abnormal, filled structures in response to matrix stiffness. Cell-matrix interactions have been an area of extensive study, and a growing body of work indicates that cell-matrix 'mechanosensing' is an important player in many cellular processes. Recent evidence suggests that epithelial cells also mechanosense through their cell-cell junctions, but it remains unclear how this interaction changes as a result of changes to multicellular structure during cancer progression. In this study, we investigated the role of multicellular structure on mechanical properties of the epithelial subunit. We extracted multicellular breast epithelial structures from laminin-rich extracellular matrix and performed creep compression tests on the structures. We found that hollow (MCF10A) structures were significantly more compliant than filled (MCF10AT) ones. This difference was found to be dependent on acinar structure, as neither single cells nor multicellular structures tested before lumen formation exhibited these differences. To further investigate the role of multicellular structure, we developed a multiphase simulation framework using the level set method to track displacements. Our model suggested a 3-fold increase in stiffness due to the lumen filling with cells, consistent with the 1.6-fold increase observed in experiment. We then used this model to simulate a single contracting cell in different multicellular structures. Using the forces and displacements from this single cell contraction simulation, we predicted the "perceived stiffness" of a single contracting cell as the lumen fills with cells. Based on this model, lumen filling could contribute approximately a 15% increase in the "perceived stiffness" of a single contracting cell independent of any changes to matrix mechanics.

INTRODUCTION

Physical forces drive many multicellular processes such as morphogenesis [1] and tumor growth [2]. Forces either originate from cells themselves, or can be applied externally to the tissue. Forces transmit through a tissue to single cells via direct attachment to other cells [3], adhesion to the extracellular matrix (ECM) [4], or the shearing force of fluid flow [5]. One important determinant of this force transmission is the mechanics of the cellular microenvironment. Previous studies extensively characterized the structure-mechanics relationship in ECMs (for example [6]) and showed that changes to ECM mechanical properties affect active cellular processes such as contraction [7], stem-cell differentiation [8], and growth signaling [9]. In mammary epithelial cells, milk production requires the appropriate ECM stiffness [10]. At the multicellular level, disruptions to ECM mechanics scale up to disrupt normal mammary epithelial tissue structure and growth [11] and contribute to malignancy [12].

In addition to the ECM, epithelial cells reside in a multicellular configuration where they are tightly attached to several other cells (Figure 1A). These connections are essential for proper development [13, 14] and function [15] of the tissue. Multicellular structure often changes during mammary ductal carcinoma progression as the lumen fills with cells (e.g., ductal carcinoma in situ [16]), but it remains unclear how these structural changes are associated with changes in multicellular mechanics or cell-cell forces. Epithelial cells have been shown to mechanosense through their cell-cell contacts [17], and increases in cell-ECM forces have been correlated to increases in cell-cell forces using traction force microscopy [3]. Taken together, these data suggest that nanonewton scale forces play essential roles in cancer and development, but we do not know whether multicellular architectural changes like lumen filling contribute to changes in cellular mechanosensing.

Single cell experiments suggest a mechanical difference between non-malignant and malignant mammary epithelial cells spread on a glass surface [18], but we do not yet fully understand the roles of multicellularity and biologically-relevant ECM on cell and tissue mechanics. Multicellular atomic force microscope (AFM) experiments characterized the elasticity of healthy mouse mammary organoids on a laminin-rich ECM gel [10]. Recently micropipette aspiration has been used to apply step forces to multicellular structures and study their time-dependent response. Xenopus laevis embryonic tissue behaves in a linear viscoelastic fashion [19] while murine sarcoma model tissues behave like a string of Kelvin-Voigt elements [20]. However, an investigation of how multicellular mechanics differs in phenotypically normal (hollow lumen) and pre-malignant (filled lumen) epithelia has not been performed.

To investigate differences in the mechanics of phenotypically normal and pre-malignant structures, we carried out *in situ* experiments using MCF10A (non-malignant) and MCF10AT (pre-malignant) mammary epithelial cells. We cultured MCF10A and MCF10AT cells long-term embedded within a laminin-rich ECM, extracted multicellular structures, and performed creep compression tests using an AFM (Figure 1B). The filled structures formed by MCF10AT cells were less compliant (stiffer) than hollow structures formed by MCF10A cells. To study how changes in multicellular structure influence bulk multicellular elasticity, we developed a three-dimensional mechanical simulation of an acinus and

calibrated it using our experimental creep data. Our simulation predicts that lumen filling would lead to decreased compliance consistent with the experimental results. Further simulations of single cell contraction within a hollow or filled structure predict approximately a 15% increase in perceived stiffness of single cells in a filled structure, suggesting an architectural reinforcement of the stiffening, possibly amplifying the tumorigenic mechanical signaling.

RESULTS

Healthy and pre-malignant epithelial structures have different mechanical properties

We measured the mechanics of healthy and pre-malignant epithelial structures using the MCF10A and MCF10AT model system. MCF10A cells are a human-derived breast epithelial cell line [21]. When embedded in laminin-rich ECM, MCF10A single cells grow into large, structures with lumens after a period of 2-3 weeks (Figure 2A, [22]). In contrast, c-Ha-Ras transformed MCF10AT cells [23] do not form lumens (Figure 2B, [24]). The MCF10A cell line has been used to demonstrate mechanical sensitivity of breast epithelial cells in the context of acinar morphogenesis [11] and growth factor sensitivity [9].

Because mechanosensitive breast epithelial cells form filled lumen structures in response to both genetic mutations [24] and increased matrix stiffness [11], we hypothesized that healthy and pre-malignant structures could have different mechanical properties, which might provide a mechanical reinforcement of pre-malignancy. Given recent evidence that cell-cell junctions are mechanosensitive [17], the mechanics of the whole multicellular structure could play an important role in tumor formation. We developed an extraction protocol that allowed us to extract cells from a laminin-rich ECM without protease digestion, allowing us to extract cells and colonies without cleaving structurally important proteins such as integrins and cadherins (Figure 1B). Using a parallel plate geometry, we applied step loads on the order of 10-50 nN to isolated colonies, and used force-feedback control to maintain a given load while recording colony deformation (Figure S1B). Both MCF10A and MCF10AT colonies exhibited large initial displacements followed by continuous creep (Figure 2C). However, their responses were markedly different from each other. Pre-malignant MCF10AT colonies, given the same environmental conditions and time to grow, were significantly stiffer than phenotypically normal MCF10A colonies (two-sided t-test, $p=5.5x10^{-5}$).

The difference in compliance between MCF10A and pre-malignant MCF10AT colonies could primarily be due to three different factors (Figure 2D): (1) single cell mechanics, (2) cell-cell connection strength, or (3) changes in multicellular structure. To test single cells, we embedded MCF10A and MCF10AT cells in laminin-rich ECM as before, but extracted them after 12 hours for creep compression tests. MCF10AT single cells were not noticeably stiffer than MCF10A single cells (one-sided t-test, $p=0.329$), suggesting that the increased stiffness observed for pre-malignant colonies does not result from stiffer cells (Figure 3A). To test cell-cell connectivity, we extracted MCF10A and MCF10AT colonies after 6-8 days of growth. As suggested by previous literature [22], 6-8 day-old MCF10A colonies did not yet

have lumens (i.e. colonies were filled structures, Figure S2). When healthy and pre-malignant colonies had the same multicellular structure, MCF10AT were once again not distinguishably stiffer than MCF10A colonies (Figure 3B, p=0.963). Changes in cell-cell connectivity would be present at the 6-8 day time point, suggesting that neither single cell mechanics nor cell connectivity accounted for the increased stiffness observed in "mature" pre-malignant colonies. Notably, both of the 6-8 day "filled" colonies (Figure 3B) exhibited similar creep response to "mature" MCF10AT colonies (Figure 2C). This suggested that lumen formation significantly decreased the stiffness of the colony.

Predicted mechanical property changes due to structural differences are consistent with measurements

As creep response of MCF10A and MCF10AT were only different upon lumen formation, we developed a computational model to investigate how differences in multicellular structure could affect the mechanical properties of the colonies. Constitutive modeling of cells has been previously considered by a number of authors. Some of the most detailed models made use of a biphasic approach, in which the cell cytosol was modeled as having both a solid phase and a fluid phase that interact [25, 26, 27, 28]. Similar approaches have also been extensively used to model collagen networks [25, 29]. However, because our measurements were on the multicellular scale and probed relatively small strains, we adopted a simpler modeling approach, whereby the acinus was modeled using the level set method [30] as an incompressible linear viscoelastic solid immersed in an incompressible fluid (see Simulation Development).

Within this simulation framework, there is a clear correspondence between the simulation parameters and the experimental measurements. Using a system identification method, we fit a standard linear solid (SLS) model to our single-cell experimental data and converted these results into simulation parameters (see Simulation Development). To investigate the effects of multicellular structure alone, we created hollow and filled models using identical material properties, with structure being the only difference between the two. Our model predicted approximately a 3-fold increase in compliance for a hollow structure (Figure 3C). This is on the same scale as the 1.6-fold increase observed in experiments (Figure 2C), suggesting that multicellular structure could be an important determinant of the mechanical properties of breast epithelial cell subunits.

Multicellular structure could affect perceived mechanical microenvironment independent of material properties

If multicellular structure affects the mechanical response of epithelial subunits, individual cells could mechanically sense these differences in structure. Epithelial cells have been shown to mechanosense through cadherin junctions [17], and disrupting these cadherin junctions causes formation of a disorganized, filled structure [13]. Here, we consider a simple case corresponding to when a cell undergoes a very small isotropic contraction, due to a small amount of fluid flow across the cell boundary. Considering the cell as a small control volume within the multicellular structure, we can apply small changes to this control volume as a simple model of cellular contraction. Using our multiphase simulation, we can model contraction and predict the force-displacement response of the surrounding

structure. With this prediction, we can calculate a "perceived stiffness" for the cell based only on the surrounding cells (see Simulation Development). We simulated single cells on the edges of both hollow and filled structures (Figure 4 A-B), and predict approximately a 15% increase in "perceived stiffness" due to lumen filling alone.

DISCUSSION

We investigated changes to mechanical properties of a breast epithelial structure during lumen filling. Our data indicate that the filling of the lumen leads to about a 1.6-fold decrease in short-timescale creep compliance (i.e. increased stiffness). We observed this difference despite single MCF10A and MCF10AT cells having very similar mechanical properties, and multicellular structures pre-lumen formation not being detectably different from each other. From these data, we concluded that the arrangement of cells in the epithelial subunit could affect the mechanical properties of the structure itself.

Our results highlight a key role for tissue structure in the mechanosensing at the single cell level. Considering that a two-fold increase in matrix stiffness leads to lumen filling [11], a 15% increase in perceived stiffness due to multicellular structure alone could be a potentially significant step towards loss of structure and function in the mammary gland. In humans, many – but not all – filled-lumen structures progress to form malignant tumors [16]. As increased matrix stiffness drives the malignant phenotype through a contraction-mediated process [11], a 15% increase in perceived stiffness could further destabilize the equilibrium of a multicellular structure. Increased perceived stiffness could lead to a loss of contact inhibition [9] and eventually promote tumor progression [12] and invasion into the surrounding environment [31].

In order for this type of mechanical difference to be biologically significant, individual cells would have to be capable of mechanosensing through cadherins or other cell-cell junctions. A growing body of evidence suggests that cells can sense mechanical forces through cadherins. For example, vinculin localizes to E-cadherin when cells are pulled with cadherin-coated beads [17], similar to behavior observed with integrins [32]. Interestingly, cadherins also play an important role in morphogenesis and tumor growth. Blocking E-cadherin function in non-malignant breast epithelial cells leads to disorganized, non-polarized structures [13]. This has been previously shown to affect mechanical phenomena such as coherent rotation in breast epithelia [1]. The molecular mechanisms behind cadherin-based mechanosensing are still under investigation, and the techniques described here provide additional tools to study this process.

SIMULATION DEVELOPMENT

Development of simulation framework

The simulations are carried out within a cube, using a right-handed coordinate system in which the z-axis points upwards (Figure S3A). The cube is filled with a background fluid that is modeled using the Navier-Stokes equations

$$\rho\frac{\partial \mathbf{u}}{\partial t} + \rho(\mathbf{u}\cdot\nabla)\mathbf{u} = -\nabla p + \nu\nabla^2\mathbf{u}$$

with the incompressibility constraint

$$\nabla\cdot\mathbf{u} = 0 \qquad [1]$$

where ***u*** is the fluid velocity, ρ is the density of the fluid, p is the fluid pressure, and ν is the fluid viscosity. For the small length scales considered, the term $(\mathbf{u}\bullet\nabla)\mathbf{u}$ corresponding to the fluid inertia is negligible. This system of equations is simulated using the finite-difference method on a fixed rectangular grid, with the incompressibility constraint imposed via a finite-element projection step [33, 34].

The acinus is modeled using the level set method [30], which is well-suited for tracking deforming boundaries on a fixed rectangular grid. Within the acinus, the velocity follows the equation

$$\rho\frac{\partial \mathbf{u}}{\partial t} + \rho(\mathbf{u}\cdot\nabla)\mathbf{u} = -\nabla p + \nu\nabla^2\mathbf{u} + \nabla\cdot\sigma + \nabla\cdot\varsigma.$$

where σ is an elastic stress tensor, and ς is a viscoelastic stress tensor. Here, we assume that the density and viscosity of the acinus is the same as the fluid. Since we are interested in quasi-static behavior, the viscosity will not play a significant role, and since gravity in negligible at the small scales considered, the relative difference in density will have only a limited effect.

Since the material is incompressible, there is no notion of a bulk modulus due to volumetric deformations, and σ and ς are therefore traceless. For small strains, the two tensors can be updated using the equations

$$\frac{\mathcal{D}\sigma}{\mathcal{D}t} = 2\mu_0\mathbf{D}, \qquad \frac{\mathcal{D}\varsigma}{\mathcal{D}t} = 2\mu_1\mathbf{D} - 2\lambda\varsigma \qquad [2]$$

where the derivative D incorporates advection and tensor spin components, and $D = (\nabla u + (\nabla u)^T)/2$ is the rate-of-deformation tensor. Here μ_0 and μ_1 are the elastic and viscoelastic shear moduli respectively, and λ is a viscoelastic damping parameter. Equation 2 has a very similar form to the SLS model, and is a natural three-dimensional extension, with the parameters μ_0, μ_1, and λ being analogous to k_0, k_1, and η from a SLS 1-dimensional linear viscoelastic model.

To inform the simulation with properties based on our measurements, we used a system identification method to fit our creep data to the SLS model. This model (Figure S4A) consists of a spring (k_1) in parallel with a spring-dashpot (k_0, η). As a check, the parameters obtained from this model (Figure S4B-D) are qualitatively consistent with the data presented in Figures 2 and 3. While other models may also fit our data, we use the SLS model here simply to inform our simulation with a set of reasonable mechanical parameters.

To carry out the compression of an acinus, a horizontal plate is introduced into the simulation that is free to move in the vertical direction, onto which a constant downward force of F_p is applied. As it comes into contact with the acinus, it exerts a force on the acinus causing it to deform, until it reaches equilibrium. Figures S3C and S3D show typical snapshots of the simulation for a sphere to model the MCF10AT geometry, and a spherical shell to model the MCF10A geometry. In Figure S3D, four small tubes are placed in the acinus, since the acini in experiments are assumed not to be watertight, and allowing fluid to flow out of the lumen can affect the mechanical response. However, simulations using a watertight central cavity were also carried out.

Using the simulation to quantify the effects of geometry is simplified by the fact that the mechanical model is linear, and that the time scale for the acinus to reach quasistatic equilibrium, t_E, is much smaller than the viscoelastic relaxation time scale τ. Since the model is linear, if the elastic modulus is scaled by a factor α, then the force response for a given, fixed displacement will be scaled by α also. Over an intermediate time t_1, where $t_E \ll t_E \ll \tau$, the effective elastic modulus is given by $\mu_0 + \mu_1$, whereas over a much longer time t_2 where $\tau \ll t_2$, the effective elastic modulus is given by μ_0. The force response at t_2 will therefore be equal the force response at t_1 but scaled by a factor of $\mu_0/(\mu_0 + \mu_1)$. Because of this, it is possible to focus on simulations using elasticity only, setting $\mu_1 = \lambda = 0$. By carrying out severalsimulations with different displacements, a constant G representing a geometrical scaling factor can be obtained, so that $K_0 = G\mu_0$. By the above argument, it must also be true that $(K_0 + K_1) = G(\mu_0 + \mu_1)$ and thus $K_1 = G\mu_1$.

The simulations are carried out in dimensionless units that are differentiated from their physical counterparts by writing them with a tilde. To connect the simulations to experiments, a mass scale M, length scale L, and time scale T must be introduced, after which any simulation quantity can be related to a physical value by multiplying by the appropriate scales. The simulation cube has side length 3, the acinus has radius 1.1, and the fluid has unit density $\tilde{\rho} = 1$. In the MCF10A simulations, the shell has thickness 0.4, which was chosen based on the confocal microscope images in Figure 2. To model a 55 μm diameter acinus, a length scale of L=25 is chosen, and by assuming the density is close to that of pure water, so that $\rho = 10^3$, then the mass scale must be

$$M = 10^3 \times L^3 = 1.56 \times 10^{-11}.$$

For each acinus geometry, simulations over a range of plate forces were carried out, using $\tilde{\mu} = 1$ and $\mu_1 = \lambda = 0$. For each simulation, the change in height of the acinus once it has reached equilibrium is recorded. By carrying out a linear fit of the height changes with respect to the plate force, a spring constant $\widetilde{K}_0$ can be calculated. To estimate the shear modulus of the acinus, the value of $\widetilde{K}_0 = 0.0193$ for the solid sphere is compared to the value $K_0 = 0.018$ from experiment. Since

$$\widetilde{K}_0 = \frac{K_0 T^2}{M}$$

it follows that the time scale is

$$T = \sqrt{\frac{M\tilde{K}_0}{K_0}} = 3.35\times10^{-5}.$$

Hence the shear modulus is

$$\mu = \frac{\tilde{\mu}M}{LT^2} = 557.$$

For an incompressible material where the Poisson ratio is 0.5, the Young's modulus is $E = 3\mu = 1670$. With the physical scales now calibrated, the simulation data of plate force against height change can now be plotted in physical units as in Figure 3C. This figure gives a value of K_0 for the MCF10A acinus as 0.0055. The three-fold difference is roughly similar to the differences in the 1.6-fold difference in experimental measures for K_0, and thus it is consistent that the differences could be explained by geometry.

Figures S3A and S3B show plots of pressure in a vertical cross-section through the hollow and filled acini. As would be expected, regions of higher pressure are visible at the locations where the plate and bottom surface make contact. However, in the hollow simulation, a region of negative pressure is also visible, as the interior part of the shell is stretched during the deformation.

Simulations of perceived stiffness

Suppose first that a single cell is centered at the origin in three-dimensional material that is incompressible with Young's modulus, *E*, which initially has no stress within it. A spherical region *S* centered on the origin with radius *R* can be introduced, where *R* is chosen to be large enough to enclose the cell. Suppose that the cell's volume decreases by a very small amount *V*. If the radial symmetry is assumed, then it can be analytically derived (Supplemental Information) that the components of the stress tensor $\boldsymbol{\sigma}$ can be expressed in spherical coordinates (r, θ, ϕ) as

$$\sigma_{rr} = \frac{EV}{3\pi r^3}, \qquad \sigma_{\theta\theta} = \sigma_{\phi\phi} = -\frac{EV}{6\pi r^3},$$
$$\sigma_{r\theta} = \sigma_{r\phi} = \sigma_{\theta\phi} = 0. \qquad \textbf{[3]}$$

The total force exerted on the spherical region can therefore be calculated by integrating the radial coordinate of the stress tensor over the surface of sphere ϕS to obtain

$$F = \int_{\phi S} \mathbf{n}\cdot\boldsymbol{\sigma}\cdot\mathbf{n}\, dS = 4\pi R^2 \frac{EV}{3\pi R^3} = \frac{4EV}{3R}.$$

It therefore follows that force exerted on the cell will be proportional to the shear modulus of the material. This provides a method in which cells can probe their local environment: if a cell contracts by a volume V and experiences a total radial force F, then the perceived shear modulus of the nearby material is given by

$$E = \frac{3RF}{4V}. \qquad \textbf{[4]}$$

Using the simulations, we can now address how the effective shear modulus will vary depending on where a cell is situated within a given geometry. To carry this out, we modify the incompressibility condition of Equation 1 to include a small volume removal, with the form

$$\tilde{\nabla} \cdot \tilde{\mathbf{u}} = \tilde{c}(1 - \cos 2\pi\tilde{t})(\tilde{q} - |\tilde{\mathbf{x}} - \tilde{\mathbf{x}}_c|)$$

for $\tilde{t} < 1$ and $\left|\tilde{X} - X_c\right| < \tilde{q}$. Values of the simulation constants of $\tilde{q} = 0.5$, $\tilde{c} = 0.15$, and $R = \widetilde{0.25}$ were used, corresponding to a removal of 307μm² in physical units.

Three simulations carried out for a contraction in the center of a sphere, at the edge of a sphere, and at the edge of a spherical shell. For each one, the effective stiffness that a cell would perceive, using Equation 4, is shown in Figure 4C. In the center of the sphere, the effective stiffness closely matches the real stiffness of the material, as would be expected for a cell in an infinite medium. However, the stiffness is significantly lessened for the other two simulations, particularly for the spherical shell. While the precise reductions in perceived stiffness are dependent on the parameters used, a marked drop in perceived stiffness and a difference depending on the geometrical configuration of the cells appear to be general features. Using the parameters described here yields a 15% drop in stiffness due to lumen formation alone.

Figures 4A and 4B show plots of the magnitude of the deviatoric stress tensor, computed as $|\sigma - 1(\mathrm{tr}\,\sigma)|$, for a contraction at the edge of sphere and spherical shell respectively. This quantity provides a useful scalar measure of shear stress, and for this case is more instructive than examining pressure, given that the analytic solution in Equation 3 predicts zero pressure. As expected, the shear stresses decay rapidly as a function of distance from the contraction region. Shear stresses are slightly higher for the spherical shell, since it provides less resistance to deformation.

METHODS

Cell culture

Mammary epithelial cells (MCF10A, Ha-Ras MCF10AT) were stably transfected with a lentiviral tet-off promoter to express Histone-H2B labeled with eGFP ([35], Addgene plasmid 21210). Following a previously established protocol [22], cells were cultured in DMEM/F12 (UCSF Cell Culture Facility) supplemented with 5% horse serum (Invitrogen), 20 ng/mL EGF (Peprotech), 0.5 μg/mL hydrocortisone (Sigma), 100 ng/mL cholera toxin (Sigma), 10 μg/mL insulin (Sigma) and 1x penicillin/streptomycin (Invitrogen). Cells were passaged using 0.05% tripsin-EDTA (UCSF).

Cells were then fully embedded in laminin-rich, growth-factor reduced extracellular matrix (Matrigel™, BD Biosciences) at a concentration of approximately 100 cells/mL using previously described methods [22, 36]. Cells embedded in gels were fed with DMEM/F12 supplemented with 2% horse serum, 5 ng/mL EGF, 0.5 μg/mL hydrocortisone, 100 ng/mL cholera toxin, 10 μg/mL insulin and 1x penicillin/streptomycin. For single cell experiments,

cells were extracted from the lrECM gels after 12 hours. For multicellular experiments, structures were extracted either between days 6-8 or days 15-21. Measurements were not noticeably different as a function of number of days in culture.

Immunofluorescence

Embedded structures fixed as previously described [36]. Structures were pipetted directly onto a glass slide and fixed with 4% paraformaldehyde in phosphate-buffered saline (PBS). Samples were washed with PBS, permeabilized with 1% Triton-X 100, and blocked with 3% BSA in PBS. Samples were stained with anti-α_6-integrin (1:500). Images were taken on a Yokogawa spinning disk confocal microscope on a Zeiss Axio Observer Z1 using a thermoelectrically cooled Cascade II EMCCD and a 20x 0.4NA objective.

Extraction from 3D culture

Single cells and colonies were extracted from the lrECM gels for AFM study with an adapted version of previously described colony-extraction method [36]. The lrECM gels were quickly washed with PBS and then mechanically detached from the culture well. To dissolve the matrix, embedded gels were soaked in a cold PBS-EDTA mixture (0.5 M EDTA pH8.0 from Invitrogen diluted to 5.5μM final concentration in PBS) for 10 minutes before being placed in a 1.5∼mL tube with excess PBS-EDTA for an additional 25 minutes. The resulting mixture was gently centrifuged at 100-200g (single cells 3-5 minutes/colonies ∼10s) and the supernatant was aspirated away. Cells/colonies were resuspended in CO2-independent media (Invitrogen) with 10% fetal bovine serum and 1x penicillin-streptomycin and plated on a poly-L-lysine-coated (MW>300,000, P5899 Sigma-Aldrich) cover slip for AFM experiments. Poly-L-lysine coatings were used to allow samples to electrostatically attach without activating cell adhesion machinery on the surface.

Surface preparation

Custom chambers for AFM experiments were made by UV-gluing custom laser-cut acrylic walls (3mm tall) to a pre-cleaned (KOH base bath) cover slip. Chambers were coated with poly-L-lysine immediately before the experiments by incubating for 20 minutes with a 0.1 mg/mL solution of poly-L-lysine in PBS. Chambers were washed ten times with deionized water and dried with a nitrogen stream before plating samples.

Atomic force microscopy

AFM experiments were performed on a modified Veeco Bioscope I mounted on a Zeiss Axiovert 25 inverted microscope [7] and a Veeco Catalyst mounted on a Zeiss Axio Observer Z1. Tipless silicon nitride MLCT (30-50 nN/μm, Veeco) cantilevers were used for multicellular experiments, and tipless Arrow cantilevers (10-20 nN/μm, Nanoworld) were used for single cell experiments. Force steps were applied to the samples using a closed-loop piezoelectric, and sample deformation were measured over time. Data analysis was performed on the force reduction step, after a series initial compression and relaxation steps that ensured good contact between the samples and both the cantilever and substrate. Experiments were performed at 37C and completed within 2 hours of plating on

poly-L-lysine. There was no discernible change in measured mechanical properties over the course of the experiment. Each sample was also imaged in brightfield and eGFP epifluorescence (nuclei), and its position on the coverslip was recorded to prevent duplicate testing of the same sample.

Parameter fitting and statistics

Quantification of the compliance of acini and single cells was performed using techniques from system identification. A three-parameter SLS model, as shown in Figure S4A, is a simple linear viscoelastic system that can capture the observed instantaneous response followed by an exponential decay. We selected an eight-second interval, beginning with the force step, to fit the data to a Kelvin body parameterized by k0, k1, and η.

The parameter fitting was accomplished by first downsampling with a moving average at 5~Hz to filter out high-frequency noise. Next, Matlab's `idgrey' was used to solve for the state-space parameters of the first-order ODE for a SLS body, given an initial guess. To ensure a valid solution, the output SLS body was then simulated with the measured force input. The simulated SLS body and actual measured displacements were compared visually to ensure a reasonable fit to the data. SLS fits that were very far from the measured response were discarded, usually due to noise in the measurement.

Statistical tests

Creep compliances were compared at 8s time points using t-tests as described in the results section with $p<0.05$ as the significance threshold.

ACKNOWLEDGEMENTS

We would like to thank Matt Paszek and Luke Cassereau for providing GFP-H2B labeled cells. Thanks to the members of the Sethian, Weaver, Fletcher and Bissell Labs for helpful comments and feedback on the manuscript.

REFERENCES

1. Tanner, K., Mori, H., Mroue, R., Bruni-Cardoso, A., & Bissell, M. J. (2012) Coherent angular motion in the establishment of multicellular architecture of glandular tissues. *Proceedings of the National Academy of Sciences* 109, 1973-1978.
2. Cheng, G., Tse, J., Jain, R. K., & Munn, L. L. (2009) Micro-Environmental Mechanical Stress Controls Tumor Spheroid Size and Morphology by Suppressing Proliferation and Inducing Apoptosis in Cancer Cells. *PLoS ONE* 4, e4632.
3. Maruthamuthu, V., Sabass, B., Schwarz, U. S., & Gardel, M. L. (2011) Cell-ECM traction force modulates endogenous tension at cell--cell contacts. *Proceedings of the National Academy of Sciences* 108, 4708-4713.
4. Munevar, S., Wang, Y., & Dembo, M. (2001) Traction force microscopy of migrating normal and H-ras transformed 3T3 fibroblasts. *Biophysical Journal* 80, 1744-1757.
5. Dewey Jr, C., Bussolari, S., Gimbrone Jr, M., & Davies, P. (1981) The dynamic response of vascular endothelial cells to fluid shear stress. *Journal of biomechanical engineering* 103.
6. Vader, D., Kabla, A., Weitz, D., & Mahadevan, L. (2009) Strain-Induced Alignment in Collagen Gels. *PLoS ONE* 4, e5902.
7. Crow, A., Webster, K., Hohlfeld, E., Ng, W., Geissler, P., & Fletcher, D. (2012) Contractile Equilibration of Single Cells to Step Changes in Extracellular Stiffness. *Biophysical journal* 102, 443-451.
8. Engler, A. J., Sen, S., Sweeney, H. L., & Discher, D. E. (2006) Matrix elasticity directs stem cell lineage specification. *Cell* 126, 677-689.
9. Kim, J. H. & Asthagiri, A. R. (2011) Matrix stiffening sensitizes epithelial cells to EGF and enables the loss of contact inhibition of proliferation. *Journal of cell science* 124, 1280-1287.
10. Alcaraz, J., Xu, R., Mori, H., Nelson, C. M., Mroue, R., Spencer, V. A., Brownfield, D., Radisky, D. C., Bustamante, C., & Bissell, M. J. (2008) Laminin and biomimetic extracellular elasticity enhance functional differentiation in mammary epithelia.. *EMBO J* 27, 2829-2838.
11. Paszek, M. J., Zahir, N., Johnson, K. R., Lakins, J. N., Rozenberg, G. I., Gefen, A., Reinhart-King, C. A., Margulies, S. S., Dembo, M., Boettiger, D., Hammer, D. A., & Weaver, V. M. (2005) Tensional homeostasis and the malignant phenotype.. *Cancer Cell* 8, 241-254.
12. Levental, K. R., Yu, H., Kass, L., Lakins, J. N., Egeblad, M., Erler, J. T., Fong, S. F. T., Csiszar, K., Giaccia, A., & Weninger, W. (2009) Matrix crosslinking forces tumor progression by enhancing integrin signaling. *Cell* 139, 891-906.
13. Fournier, M. V., Fata, J. E., Martin, K. J., Yaswen, P., & Bissell, M. J. (2009) Interaction of E-cadherin and PTEN regulates morphogenesis and growth arrest in human mammary epithelial cells. *Cancer Res* 69, 4545-52.
14. Watabe, M., Nagafuchi, A., Tsukita, S., & Takeichi, M. (1994) Induction of polarized cell-cell association and retardation of growth by activation of the E-cadherin-catenin adhesion system in a dispersed carcinoma line. *J Cell Biol* 127, 247-56.
15. Boussadia, O., Kutsch, S., Hierholzer, A., Delmas, V., & Kemler, R. (2002) E-cadherin is a survival factor for the lactating mouse mammary gland. *Mechanisms of development* 115, 53-62.
16. Virnig, B. A., Tuttle, T. M., Shamliyan, T., & Kane, R. L. (2010) Ductal Carcinoma In Situ of the Breast: A Systematic Review of Incidence, Treatment, and Outcomes. *Journal of*

the National Cancer Institute 102, 170-178.
17. le Duc, Q., Shi, Q., Blonk, I., Sonnenberg, A., Wang, N., Leckband, D., & de Rooij, J. (2010) Vinculin potentiates E-cadherin mechanosensing and is recruited to actin-anchored sites within adherens junctions in a myosin II--dependent manner. *The Journal of cell biology* 189, 1107-1115.
18. Li, Q., Lee, G., Ong, C., & Lim, C. (2008) AFM indentation study of breast cancer cells. *Biochemical and biophysical research communications* 374, 609-613.
19. von Dassow, M., Strother, J. A., & Davidson, L. A. (2010) Surprisingly simple mechanical behavior of a complex embryonic tissue. *PloS one* 5, e15359.
20. Guevorkian, K., Gonzalez-Rodriguez, D., Carlier, C., Dufour, S., & Brochard-Wyart, F. (2011) Mechanosensitive shivering of model tissues under controlled aspiration. *Proceedings of the National Academy of Sciences* 108, 13387-13392.
21. Soule, H. D., Maloney, T. M., Wolman, S. R., Peterson, W. D., Brenz, R., McGrath, C. M., Russo, J., Pauley, R. J., Jones, R. F., & Brooks, S. (1990) Isolation and characterization of a spontaneously immortalized human breast epithelial cell line, MCF-10. *Cancer research* 50, 6075-6086.
22. Debnath, J., Muthuswamy, S. K., & Brugge, J. S. (2003) Morphogenesis and oncogenesis of MCF-10A mammary epithelial acini grown in three-dimensional basement membrane cultures. *Methods* 30, 256-268.
23. Basolo, F., Elliott, J., Tait, L., Chen, X. Q., Maloney, T., Russo, I. H., Pauley, R., Momiki, S., Caamano, J., & Klein-Szanto, A. J. P. (2006) Transformation of Human Breast Epithelial Cells by c-Ha-ras Oncogene. *Molecular carcinogenesis* 4, 25-35.
24. Dawson, P. J., Wolman, S. R., Tait, L., Heppner, G. H., & Miller, F. R. (1996) MCF10AT: a model for the evolution of cancer from proliferative breast disease. *The American journal of pathology* 148, 313.
25. Barocas, V. H., Moon, A. G., & Tranquillo, R. T. (1995) The fibroblast-populated collagen microsphere assay of cell traction force--Part 2: Measurement of the cell traction parameter. *Journal of biomechanical engineering* 117, 161.
26. Dembo, M. & Harlow, F. (1986) Cell motion, contractile networks, and the physics of interpenetrating reactive flow. *Biophysical journal* 50, 109-121.
27. Herant, M., Marganski, W. A., & Dembo, M. (2003) The mechanics of neutrophils: synthetic modeling of three experiments. *Biophysical journal* 84, 3389-3413.
28. Herant, M. & Dembo, M. (2010) Form and function in cell motility: from fibroblasts to keratocytes. *Biophysical journal* 98, 1408.
29. Moon, A. G. & Tranquillo, R. T. (2004) Fibroblast-populated collagen microsphere assay of cell traction force: Part 1. Continuum model. *AIChE journal* 39, 163-177.
30. Sethian, J. A. (1999) Level set methods and fast marching methods: evolving interfaces in computational geometry, fluid mechanics, computer vision, and materials science. Cambridge University Press.
31. Provenzano, P., Eliceiri, K., Campbell, J., Inman, D., White, J., & Keely, P. (2006) Collagen reorganization at the tumor-stromal interface facilitates local invasion. *BMC Medicine* 4, 38.
32. Plopper, G. & Ingber, D. E. (1993) Rapid induction and isolation of focal adhesion complexes. *Biochemical and biophysical research communications* 193, 571-578.
33. Chorin, A. J. (1968) Numerical solution of the Navier-Stokes equations. *Math. Comp* 22, 745-762.

34. Almgren, A. S., Bell, J. B., & Szymczak, W. G. (1996) A numerical method for the incompressible Navier-Stokes equations based on an approximate projection. *SIAM Journal on Scientific Computing* 17, 358-369.
35. Kita-Matsuo, H., Barcova, M., Prigozhina, N., Salomonis, N., Wei, K., Jacot, J. G., Nelson, B., Spiering, S., Haverslag, R., & Kim, C. (2009) Lentiviral vectors and protocols for creation of stable hESC lines for fluorescent tracking and drug resistance selection of cardiomyocytes. *PLoS One* 4, e5046.
36. Lee, G. Y., Kenny, P. A., Lee, E. H., & Bissell, M. J. (2007) Three-dimensional culture models of normal and malignant breast epithelial cells. *Nat Methods* 4, 359-65.

FIGURES

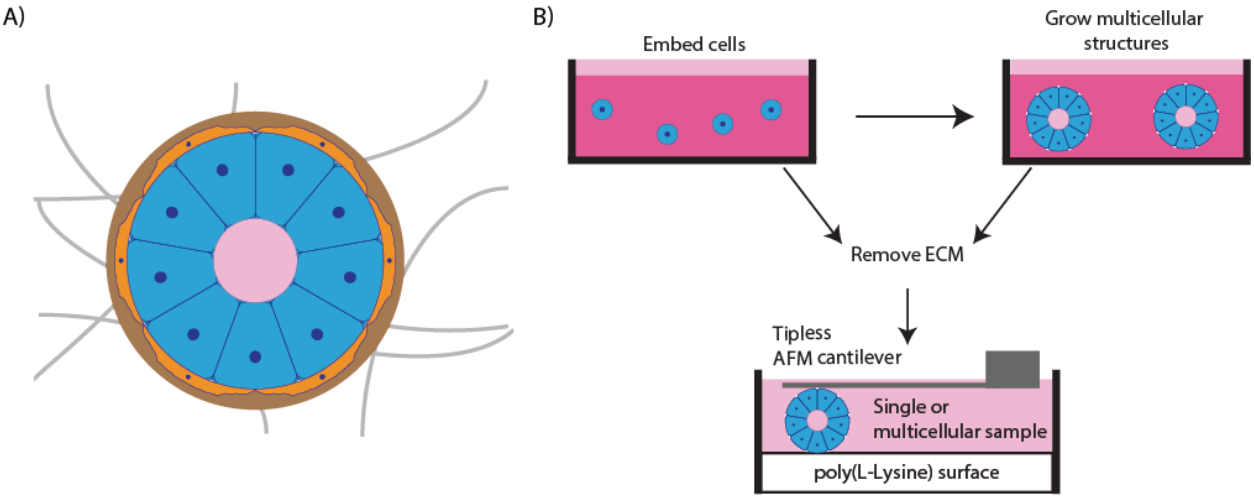

Figure 1. Using 3D culture and AFM to measure acinar mechanics.

(A) A mammary epithelial cell grows in a dynamic environment surrounded by extra-cellular matrix, fluids, and other cells. (B) Mammary epithelial cells grown in laminin-rich extracellular matrix can be extracted and mechanically probed at single and multicellular states using identical trypsin-free extraction methods.

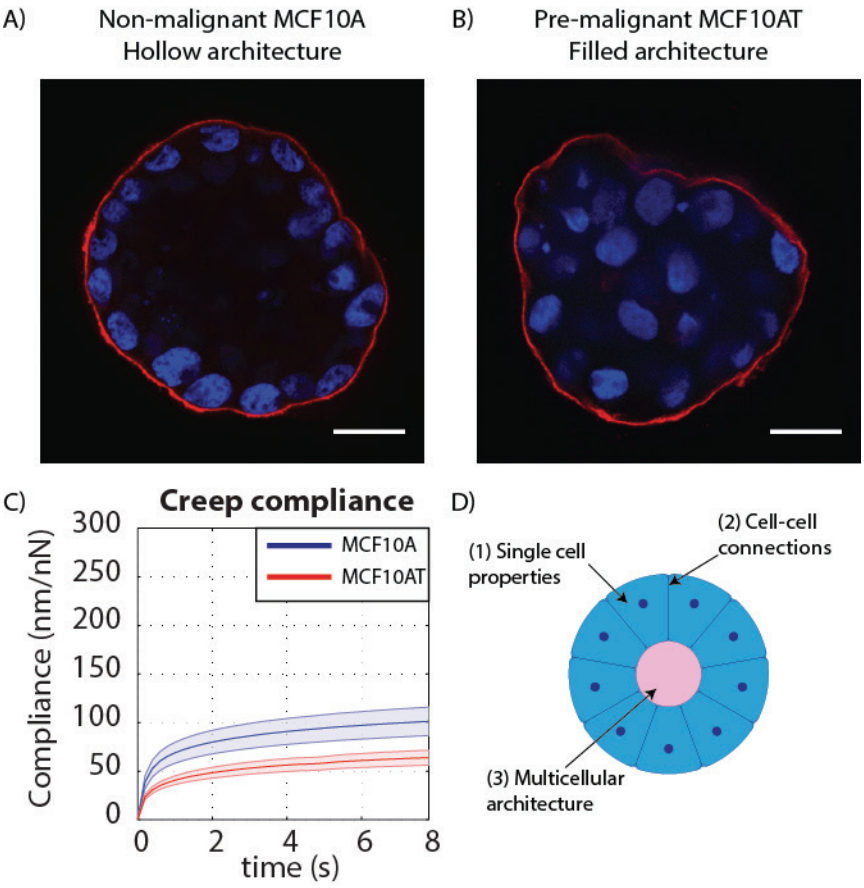

Figure 2. Pre-malignant, filled acinus is stiffer than the healthy, hollow acinus.

Confocal immunofluorescence images of (A) non-malignant MCF10A (hollow lumen) and (B) pre-malignant MCF10AT (filled lumen) colonies. Scale bars 25μm. (C) Creep compliance (mean +/- 95% CI) of hollow and filled breast epithelial colonies. (N=32 and 31 colonies for A and T) (D) Differences in mechanical response could be due to (1) different properties of single cells (2) changes in connectivity or (3) changes in multicellular architecture.

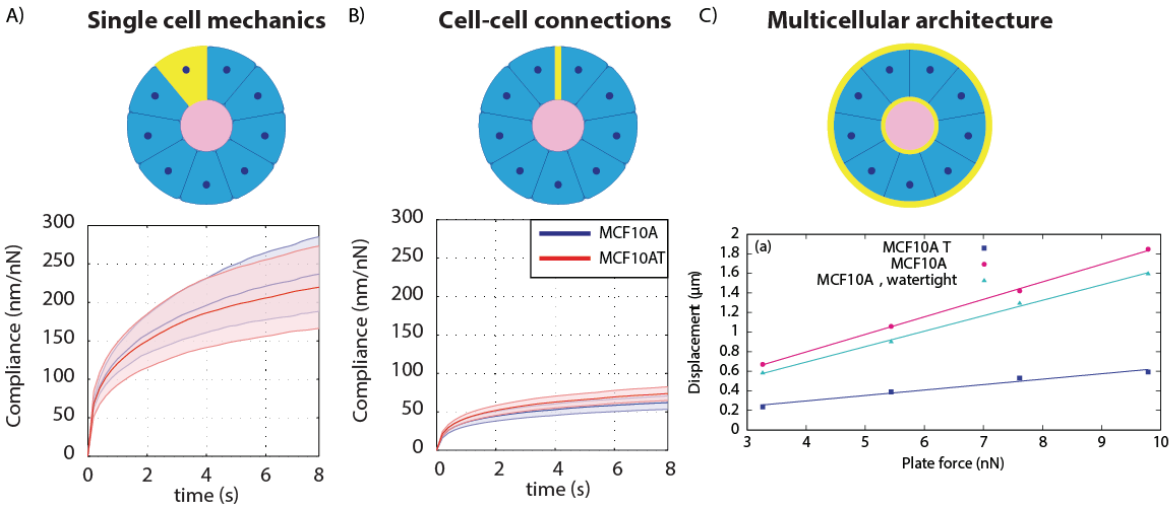

Figure 3. Differences in multi-cellular architecture cause increased stiffness with malignancy.

Creep compliance (mean +/- 95% CI) of MCF10A and MCF10AT cells at (A) single cell state (N=14 and 15 cells for A and T) and (B) 6-8 day state before lumen formation (N=34 and 33 colonies for A and T). (C) Simulation of hollow and filled structures predicts decreased compliance (increased stiffness) of the structure associated with multicellular architecture.

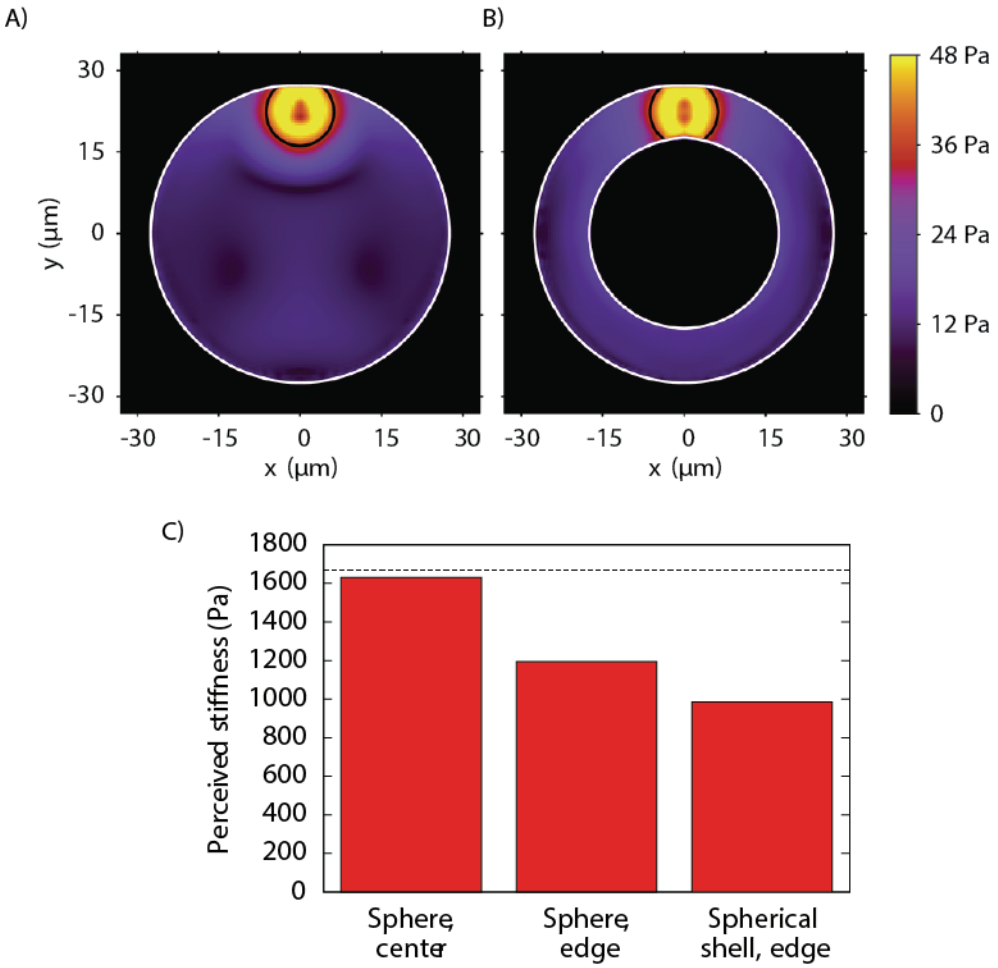

Figure 4. Filled architecture increases stiffness of cellular microenvironment.

Cross-section through 3D simulations of single cell contraction in (A) filled and (B) hollow structures. (C) Perceived stiffness for a single cell in a hollow structure is approximately 15% lower than a filled structure.

SUPPORTING FIGURES

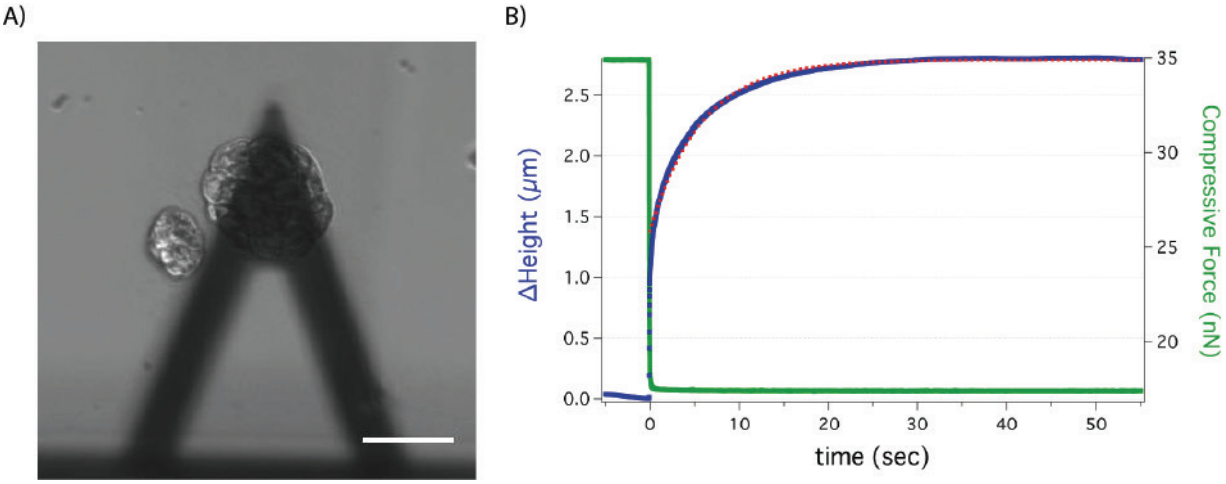

Figure S1. Atomic force microscopy is used to apply defined loads.

(A) Example image of an MCF10A acinus under a tipless atomic force microscope cantilever. Scale bar 50μm. (B) Representative creep response of an MCF10A acinus.

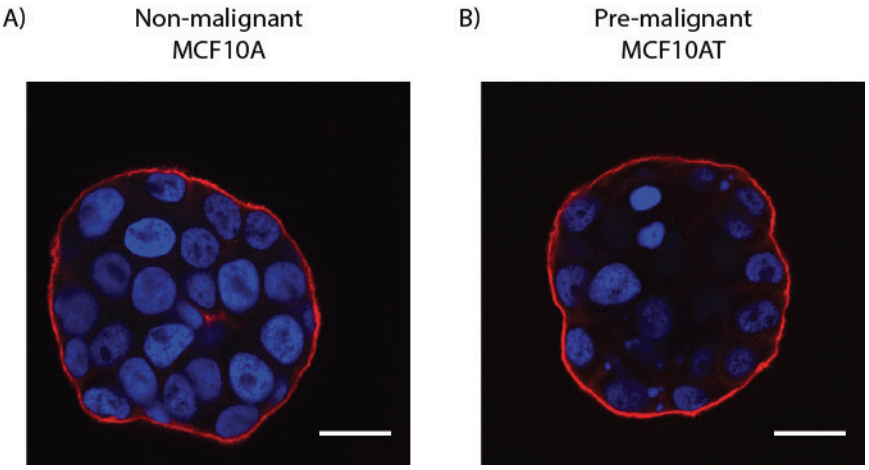

Figure S2. After 1-week healthy and pre-malignant acini have the same architecture.

Confocal immunofluorescence images of 8 day colonies of (A) MCF10A and (B) MCF10AT. 6-8 day time points were selected for testing because this was before lumens formed. Scale bars 25μm.

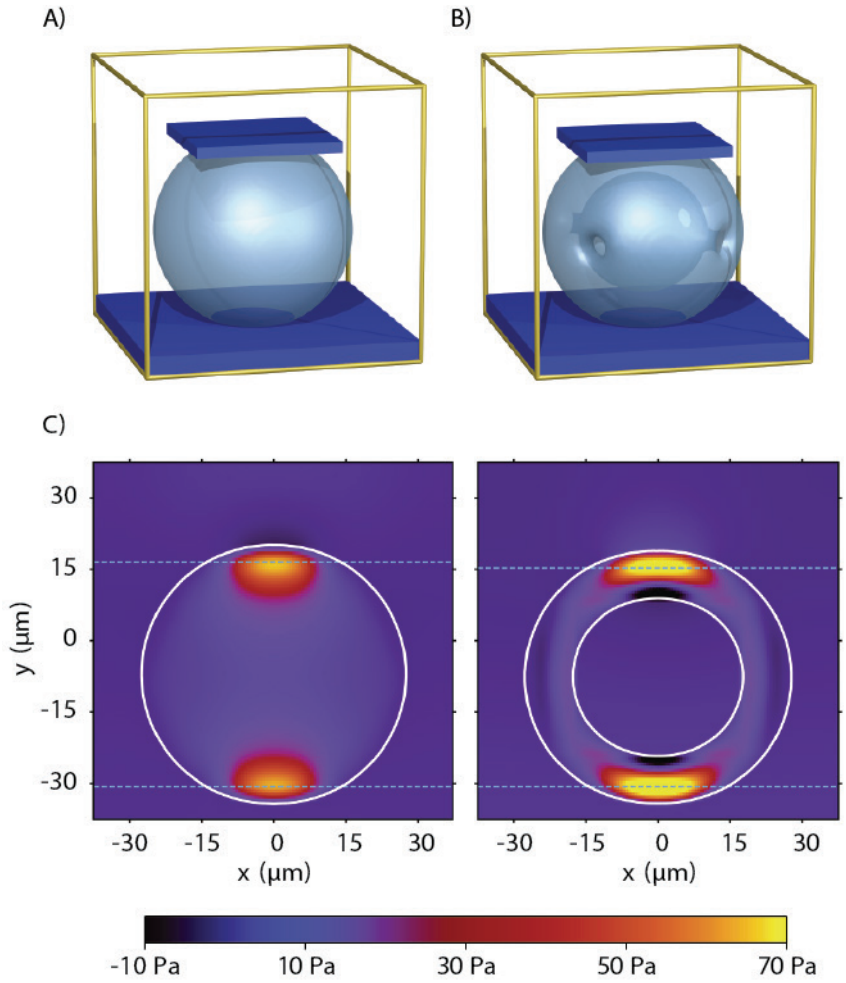

Figure S3. Three-dimensional model of acinus reveals internal stress propagation.

(A-B) Visualization of the 3D plate compression simulation environment used in this study.
(C) Cross-section through 3D simulation of plate for hollow and filled structures.

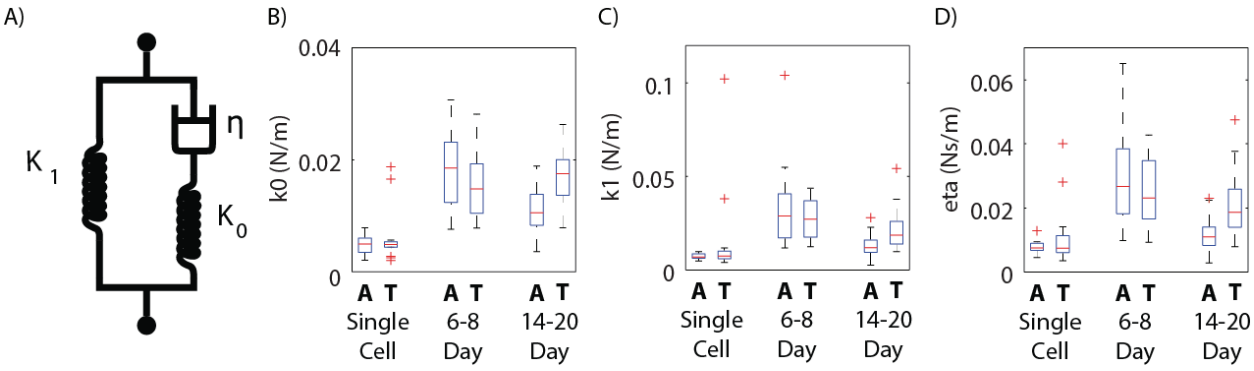

Figure S4. Creep response can be modeled by an SLS model.

(A) Standard Linear Solid model and (B-D) relevant parameters measured by fitting creep curves using system identification techniques. Fit parameters were used to extract mechanical properties for the model.

Chapter 5.

Tensional homeostasis in single contractile cells occurs through a strain-rate dependent tensional buffer

This study was conducted in collaboration with Win Pin Ng and Daniel A. Fletcher.

ABSTRACT

Adherent cells generate forces through acto-myosin contraction and sense the mechanical properties of their environment. In the context of tissues, these cells have been described as existing in tensional homeostasis with their surroundings, implying an internal regulation of tension at the cellular level. However, changes in spread area of the cell and alterations in extracellular matrix organization and mechanical properties complicate interpretation of experiments that implicate tensional homeostasis. Here we directly test this tension regulation by mechanically perturbing fibroblast cell tension and observing the contractile response. As a cell spreads and contracts, sandwiched between two parallel fibronectin-patterned surfaces, it exerts a tensile load across the height of the cell. We use a flexible, tipless atomic force microscope (AFM) cantilever as the top surface to measure and to modulate forces and displacements of the contracting cell. Cell spreading is confined on both surfaces to defined regions using micropatterning and attains a steady-state contraction force as the cell reaches the edges of the fibronectin-coated areas on the cantilever and substrate. To specifically test whether the magnitude of the steady-state tension is an internally regulated setpoint, we modulate the cell's displacement by moving the cantilever up or down. Interestingly, fibroblast cells can maintain the same magnitude of cellular tension when their height is either increased or decreased. This regulation is rate-dependent, breaking down for fast or step perturbations. These observations provide the first direct evidence for a widely cited process of tensional homeostasis, showing specific tension regulation at a single cell level. However, unlike a closed-loop feedback controller with a particular setpoint, cellular tensional homeostasis appears to operate through rate-dependent *tensional buffering*, whereby if the strain rate is faster than what the cell can buffer, a new tensional state will be regulated once the rate slows again. By measuring cellular elasticity throughout contraction and straining, we observe that elasticity is maintained during buffering, but changes with fast straining. These results suggest a process whereby cells will accommodate slow strains applied to a tissue, while they maintain a rigid state to stabilize the tissue to rapid loading.

INTRODUCTION

The interplay between microenvironmental forces and cell-generated forces is an increasingly important subject of study, as researchers seek to elucidate the myriad of ways in which physical signals affect biological processes, from differentiation (1) to metastasis (2). Adherent cells not only transduce applied forces into biochemical signals, but they also adjust their own mechanics in response (3). This can be manifested through structural changes within the cell to change attachments and to modulate cellular elasticity, or potentially a concomitant contractile response to applied forces.

One particular concept that has received significant attention when addressing the interplay between external and internal physical parameters of cells is *tensional homeostasis*. The disruption of tensional homeostasis has been implicated in numerous disease states, from cardio-vascular disease and developmental disorders, to cancer (5). In particular, a recent study looking at the disease floppy-eyelid syndrome, reported a significantly larger tensile setpoint for diseased fibroblast cells. Additionally, metastatic cancer is thought to be associated with a disruption of tensional homeostasis. Specifically, the increased invasiveness of breast cancer epithelial cells is thought to be in part a result of mis-regulation of tensional homeostasis (2).

Tension homeostasis can be broken down into two particular concepts. The first was described by Brown et al. to explain the tendency of millions of fibroblast cells embedded in a 3D collagen gel to counteract exogenous force application to move toward a previous force "setpoint" (4). The other definition was introduced by Paszek et al. where tensional homeostasis represented the tendency of cells to adjust endogenous forces to balance exogenous forces (2). We focus on the former concept, as first conceived by Brown et al., in order to definitively address the original hypothesis.

While tensional homeostasis is a pervasive concept within cellular mechanobiology (with over two dozen papers discussing it), there have been no studies that have shown direct evidence of the ability of cells to respond to external loading by maintaining a "homeostatic" level of tension. The only evidence consists of indirect measures of this behavior, either extrapolating the direction of force response to a step load (4, 6), or using cell stiffness as a proxy for contractile tension (7). We set out to look for direct evidence of tensional homeostasis in fibroblast cells building on the single cell contraction force microscopy system that we previously developed (8–10). As used in previous experiments investigating tensional homeostasis, fibroblasts present an excellent model cell system because of the importance of tension in their native connective tissue environment.

MATERIAL & METHODS

Cell culture and sample preparation

NIH 3T3 fibroblasts were cultured in DMEM (Mediatech, Manassas, VA) supplemented with 10% fetal bovine serum (Lonza, Walkersville, MD), and 1% Penicillin/Streptomycin (Sigma, St Louis, MO). Cells were collected by incubating in 0.25% trypsin for 3 minutes, followed by resuspension in trypsin neutralizing solution, centrifugation (300g for 5 min), and

resuspension in pre-heated CO_2-independent media (Invitrogen) supplemented with 10% FBS and 1% Pen/Strep. Cells were then given at least 15 minutes to recover from trypsinization before experiments began.

Experimental setup

Experiments were conducted using a BioScope Catalyst Atomic Force Microscope (Bruker AXS, Santa Barbara, CA) with a temperature-controlled stage mounted atop an inverted optical microscope (Zeiss Axio Observer Z1, Carl Zeiss, Thornwood, NY). Data acquisition and AFM control was done using a signal access module and custom-designed software (LabVIEW, National Instruments, Austin TX). Tipless, uncoated All-in-One silicon cantilevers from BudgetSensors (Sofia, Bulgaria) were used in all experiments with an average spring constant of 200 nN/mm as determined by fitting thermal fluctuations of each cantilever in air.

Constraining spreading

In order to prevent the cells from spreading unevenly between the substrate and cantilever surfaces, we pattern both surfaces with 200 - 250 μm^2 of an ECM ligand, blocking the remaining surface to prevent adhesion. Substrate patterning is done through micro-contact printing as described elsewhere (11). On the cantilever, a constrained pattern of ECM ligand was achieved using the dipping method, as previously described (12). Briefly, a micromanipulator was used to dip only the end of a cantilever in a 50 μg/ml fibronectin solution (Sigma, St Louis, MO). After a 20-minute incubation period, the cantilever was rinsed in ultra-pure water (UPW) and was incubated in a 10% BSA solution at 37°C for an hour to passivate the uncoated surface. The cantilever was then rinsed in UPW again and mounted directly onto the AFM. By adding 1% fluorescently labeled FN, we were then able to visualize the patterned areas and measure the size of available ligand on both surfaces.

Measuring contraction and spread area

We then add the fibroblast cells in suspension and establish simultaneous contact between the cell and both surfaces, as previously described (9). At this point, we measure the deflection of the cantilever as the cell spreads onto both surfaces. Cell spreading is monitored by expressing GFP-vinculin. After a cell has contracted and spread, we evaluate whether or not the cell has achieved a tensile steady state, which we define as the force remaining within 10% of its average value over the preceding 10 minute interval.

Testing tensional homeostasis

Once the cell has reached a steady-state force, we set out to test whether this force was a regulated value (tensional homeostasis). To this end, we use a closed-loop piezo-electric to control the separation of the base of the cantilever (or the cantilever chip) from the substrate to apply a 0.1 μm/min, 1 μm/min, or step input. By measuring how the cell force changes with these different perturbations, we can evaluate if the force is unregulated (leaves the steady-state condition) or is regulated (remains within the steady-state condition).

Micro-rheology

Rheology experiments were conducted using custom code written in LabVIEW to apply a 15 nm amplitude 2 Hz sinusoidal input to the cantilever holder piezo for a 30 sec period. A DSP lock-in amplifier (Ametek, Oak Ridge, TN) was used to read the magnitude and phase delay of the cantilever deflection, after correcting for magnitude and delay offsets by first running the measurement directly on the hard substrate. The following equation was used to calculate the storage (E') and loss (E'') moduli at 2 Hz:

$$E' = \frac{FH}{Ad}\cos\theta \quad (1)$$

$$E'' = \frac{FH}{Ad}\sin\theta \quad (2)$$

where F is the amplitude of the force of the cantilever deflection, H is the cell height, A is the cross-sectional area of cell between the surfaces, d is the amplitude of the piezo displacement, and θ is the phase lag of the cantilever deflection from the piezo displacement.

Statistical analysis

Unless otherwise noted, all tests for significance were conducted using the Student's t-test, with a two-tailed, $p \leq 0.05$ threshold for significance. Average values are presented ± SE unless otherwise noted.

RESULTS

Steady-state tension is achieved when spreading is constrained

In order to observe whether cells will actively maintain a given level of tension, we first considered the conditions necessary to allow a cell to reach a steady-state force. Using contraction force microscopy, as previously demonstrated in our group (8–10), we presented cells with two parallel surfaces coated with the extracellular matrix protein fibronectin. By micropatterning both surfaces to limit cell spreading to 200-250 μm^2 on each surface (Figure 1A), we observed that cells would pull the two surfaces together as they filled the patterns (Figure 1B). Contracting cells would form an extended columnar shape, spanning both the substrate and the cantilever, as seen by confocal microscopy (Figure 1C). By measuring the contraction force during this process, we observed that, when cell spreading was constrained on both surfaces, cells tended to remain attached to both surfaces and contraction leveled off to a steady-state tension (Figure 2A,B). If only one surface was patterned, cells tended to commit to the unpatterned surface (Figure S1). In the absence of any patterning, we observed that cells generally committed to either surface.

Cell spreading is necessary and precedes contraction in 3D

To better understand the nature of this contractile steady state, we quantified the relationship between spreading and force generation by imaging vinculin with TIRF microscopy (Figure 1B). Interestingly, we observed an initial period of spreading on both surfaces that did not generate any contractile force. This lasted about 5 minutes as the cell spread to about 40 μm^2. After this initial period of contraction-free spreading, the cell continued to spread, but now generated substantial contraction forces (Figure 2B). As the cell's lamellipodia reach the edges of the pattern, spread area stopped increasing. However, for a period of 5-10 minutes after total spread area stopped increasing, cellular contraction continued (Figure 2B). After this lagging period, contraction then followed spreading and leveled off to a plateau value, which remained unchanged for >25 min in the absence of any perturbations. We defined steady state as beginning when the contraction changed by less than 10% over the course of 10 minutes (grey box, Figure 2B).

To identify whether this relationship between spreading and contraction force was causative or merely correlative, we conducted an experiment to decouple spreading from contraction force generation. Specifically, by using a force clamp at zero force as soon as the cell makes contact with both surfaces, we are able to present with the cell with a zero stiffness environment, where it can freely adjust its height during spreading (9). Under these conditions, we observe that cell spreading continues in much the same way as when the cell is generating a contraction force >0 between the two surfaces (Figure 2C). By stopping the force clamp 5-10 minutes after spreading has reached a plateau, we then tested whether or not the cell will contract further, without being able to spread, in order to remain under some tension. Interestingly, we observe no increase in tension in the absence of spreading (Figure 2C), suggesting that spreading is necessary to drive traction generation.

Steady-state tension is maintained in a rate-dependent manner

Having demonstrated that single cells reach a steady-state contractile force, we set out to test whether the cell is capable of maintaining this force in the face of perturbations. Once a cell has remained at steady state for 10 minutes, we slowly increased or decreased cell height by 1 μm and quantified cell tension. Conceptually, tensional homeostasis predicts that cells will remain at the steady-state tension value in response to the perturbation in height. Consistent with this, the cell counteracted the changes in tensile force and maintained the steady-state tension during slow (0.1 μm/min) displacements, both for increasing and decreasing height (Figure 3A). In contrast, step displacements (>600 μm/min) of the same magnitude (1 μm) dramatically changed cellular tension, with the cell exhibiting classic viscoelastic relaxation (Figure S2). Of note, the cell does not return to the steady-state force after allowing for viscous equilibration, instead settling at a new intermediate tension. To isolate the role of viscosity, we applied a fast ramp that was still slow enough not to exhibit viscous relaxation after the ramp (1 μm/min). When applying this faster rate loading, over the same displacement as the slow or step perturbations, we saw a clear correlation between the applied displacement and the change in tensile force

(Figure 3B). These results suggest a clear rate dependence at which the cell can respond to perturbations to maintain a given tension.

Tensional homeostasis through tensional buffering

Our results indicated that cells do maintain their tension despite perturbations in height, but only under certain conditions. In order to better understand the nature of cellular tension regulation, we wanted to test if the cell had a given setpoint tension, or rather regulated tension by acting to prevent the current tension -- whatever it might be -- from changing. We assessed this question by observing the cell's response after we displaced the cell faster than it could counteract (fast ramp and step). The fact that after a step perturbation the force did not return to the steady-state value provided initial evidence against a setpoint mechanism. However, to avoid the issue of viscous relaxation we instead focused on the response after a fast ramp (1 μm/min). The fast rate was chosen so as to avoid viscous relaxation while being too fast for the regulation mechanism. After applying the fast ramp we observed that the cell remained at the new tension value (Figure 4A). Importantly, this new tension became the value that the cell tried to maintain. Immediately after applying a fast ramp, we applied a slow ramp and observed that the cell maintained this new tension when undergoing slow loading (Figure 4B). Rather than a feedback-type setpoint control, it appears that cellular tension regulation instead operates through a buffering-type mechanism.

Cellular elasticity measurements suggest rearrangement of cytoskeleton

Given the observation that the cell can buffer slow, but not fast deformations, we sought to identify the nature of the cells compensatory mechanism. The acto-myosin cytoskeleton has been previously implicated in tensile mechanosensation. Therefore, we set out to observe whether the cell's rheological properties changed during cellular tensional homeostasis. To that end, we used AFM micro-rheology to track the storage and loss moduli as the cell spread, contracted, and reached steady state. We observed that cellular elasticity increases as the cytoskeleton forms during contraction, peaking when the cell reaches steady state (Figure 5A). Notably, in the absence of an external perturbation, the cell remains at a steady-state force, spread area, and elasticity.

Upon step increases or decreases in cell height, significant changes in elasticity rapidly result, with elasticity increasing with cell height increases while decreasing with cell height decreases. Fast ramps (1 μm/min), which produce a new steady-state cellular tension, also change the elasticity of the cell to a new steady-state elasticity ($p \leq 0.001$, $N=8$), in the same direction as the step changes (Figure 5B). However, slow ramps (0.1 μm/min) that deform the cell by the same magnitude without a change in cell tension produce no distinguishable change in elasticity ($p > 0.1$, $N=5$, Figure 5B). Consequently, the tensional buffering process does not involve a change in cellular elasticity, while strain-rates beyond the cell's compensatory ability do change the cell's rigidity.

DISCUSSION

Controls of cellular tension

In this study, we observed that, when cells are sandwiched between two constrained surfaces, cell spreading drives contraction until adhesive area is filled. Tension then levels off to a steady-state value. Previous studies have observed the correlated nature of cell spreading and traction forces (13, 14). Our results extend this observation to out-of-adhesive-plane traction forces, and further clarify the force/area relationship. Area increases initially without generating much force, consistent with previous observations of the initial P0/P1 phases of cell spreading (13, 15). As area increases further, tension then starts to increase. However, as the available ligand becomes completely filled, area stops increasing, but force continues for a few minutes (5-10 min), suggesting some lag where force takes some time to reach equilibrium when presented with new area. Soon after spreading ceases, cellular traction force stops increasing and levels off to a steady state. We further demonstrated the necessity of spreading for driving contraction using a force clamp. The fact that after spreading in a zero stiffness environment, the cell would no longer contract to be under some degree of tension reinforces the results others have observed regarding the critical role of spreading in contraction (14, 16, 17).

Direct evidence for tensional homeostasis

The fact that cells established a tensile steady state in our system presented us with the perfect opportunity to test the widely asserted notion that cells maintain *tensional homeostasis* with their environment. Brown et al. first proposed this hypothesis in 1998: "We would define tensional homeostasis as the control mechanism by which fibroblasts establish a tension within their extracellular collagenous matrix and maintain its level against opposing influences of external loading." (4) Unfortunately, to date, no experiments have shown this ability of cells to maintain a tension when undergoing external loading. All three studies that have approached this question have only observed indirect evidence for tensional homeostasis in fibroblast cells (extrapolate a trend (4, 6); use stiffness as a proxy for tension (7)). To that end, in this study we show the first direct evidence of tensional homeostasis in fibroblast cells. Our study is the first to actually measure the tension produced by a single cell and observe the cell regulating its force to maintain a given tension when undergoing rather substantial straining (>10%).

Two features of this tensional homeostasis are particularly notable. First, the cell can only counteract external loading at a rate of ~100 nm/min or below, with loading at a rate of 1 μm/min or faster resulting in clear changes in tension. Second, loading the cell faster than it can adjust causes a change in steady-state cellular tension and elasticity. When loading ceases or slows down, the cell then maintains the new steady-state force. Taken together, these observations suggest a buffering regulation mechanism, as opposed to a mechanostat force setpoint feedback system. We propose that tensional homeostasis operates through strain-rate dependent tensional buffering.

Mechanism of tensional homeostasis

Our observations regarding tensional homeostasis suggest several key characteristics of the underlying mechanism responsible for this behavior. First, we observe a rate-dependent regulation of tension, with cells losing homeostasis between 0.1 μm/min and 1 μm/min. Second, we do not observe a tensile setpoint behavior; instead cells work to maintain whatever their current steady-state tension is once they are fully spread. Third, cellular elasticity does not change under loading when the cell remains in homeostasis, but dramatically changes when loading is faster than the cell's tensional buffering capacity.

Numerous models have been developed to explain tensional homeostasis, but the absence of direct and specific experimental evidence has limited the utility of these models. Several computational models have been developed to explore the dynamic nature of cellular spreading, contraction, and response to applied loads (16, 18, 19). Different length scales have also been explored from the single molecule, single adhesion or stress fiber level, to the whole cell or multi-cellular tissue scale. Previous studies suggest that there are two classes of potential mechanisms to explain tensional homeostasis: acto-myosin-based or focal adhesion-based models. Given our observation that focal adhesions did not change during the tensional homeostatic response to external loading, we focused on the acto-myosin class of models.

In order to better relate to potential acto-myosin models, we sought to characterize how the cytoskeleton responded during tensional homeostasis. Using AFM micro-rheology, we observed substantial stiffening of the cell as it contracted to steady state, achieving an elasticity on average of 4.5 (±1.7) kPa, consistent with previous observations of fibroblast elasticity (20). Slowly loading the cell did not change cell stiffness, while faster loading significantly changed the cell's elasticity.

There are a variety of ways in which the acto-myosin cytoskeleton could behave as a loading-rate mechanosensor. Recent evidence suggests a potential role of actin as a tension sensor (21) whereby actin binding protein affinity is affected by structural changes (22) or fluctuation changes (23) of the actin filament. These changes can either drive increased crosslinking with load (24, 25) or rather inhibition of depolymerization when the filament is under tension (26). Either way, if structural changes in the cell's cytoskeleton were taking place when the loading is faster than what the cell can buffer, we would expect to see a change in the cell's elasticity to reflect this rearrangement.

Two models proposed recently hold particular promise for explaining our observations. The first is the sarcomeric model of tensional homeostasis presented by Kaunas and colleagues (18). Starting by simplifying a stress fiber with a sarcomeric model, Kaunas et al. relate the tension and deformation of the stress fiber to the myosin cross-bridge cycling rate and the substrate loading rate. Using model parameters derived from experiments in the literature, they found a frequency dependence of the tension on stress fibers when undergoing sinusoidal loading. This model has since been expanded to irregular loading schemes (27), and notably it was found that the loading rate, and not the frequency, was the determinant of cellular tension. One result of this model is that for high strain rates, stress fibers behave elastically, with changes in length corresponding to a proportional

change in tension. However, for low strain rates, myosin activity counteracts substrate deformation and stress fiber tension does not change. Instead, acto-myosin filaments just slide past each other. This predicts both the tensional regulation that we observe and that cellular elasticity would not change during slow loading. However, the model does not yet capture our observation of tensional buffering of the new steady-state forces, which will need to be incorporated into the model in order to move it beyond only characterizing how the cell responds *during* loading to extend it to how it behaves *after* loading.

Another recent model by Abhilash and colleagues used discrete network modeling to observe rate-dependent elasticity in fibrous actin networks consisting of only actin, motors, and crosslinkers (19). Consistent with our observations, such a model predicts the network to have a very low stiffness (minimal force change for a given strain) for low strain rates, while for faster strain rates, the network would have an elevated stiffness (larger force change for the same given strain). This model has the added benefit of describing whole-cell scale responses based on underlying molecular modeling. However, it has not been extended to incorporate either the buffering response we observe, or the rheological observations we've made.

While no current model completely accounts for the behaviors we observe, numerous modeling efforts establish frameworks that hold the promise of being extendable to account for the tensional homeostasis through rate-dependent buffering that we observe. Indeed, given that acto-myosin based models have successfully predicted so much of what we observe, we think it likely that they point to the fundamental underlying mechanism driving tensional homeostasis.

Conclusions

By constraining spread area for fibroblast cells spreading between a substrate and an AFM cantilever, we observe that once cells stop spreading, they soon settle at a steady-state force. Then, by loading the cell at different rates, we discovered the first direct evidence for tensional homeostasis through a tensional buffering response, wherein cells can counteract loading up to some rate, above which results in tension changes. Notably, after rapid loading, the cell will maintain and buffer the new force, rather than return to some previous tensional setpoint. Measuring cellular elasticity throughout the contraction and loading conditions, we observe that the stiffness of the cell also changes in a loading-rate dependent manner.

These insights will prove useful to provide constraints for models trying to recapitulate the dynamic nature of cellular force regulation and elucidate the underlying molecular mechanism. Interestingly, tensional buffering may serve to help cells differentiate between slowly changing strains in tissue that the cell needs to accommodate, and rapid, transient strains applied to the tissue, in which case the cell behaves more rigidly to stabilize the tissue. Ultimately, this study highlights the need to consider the dynamics of a cell's microenvironment and not only equilibrium responses.

ACKNOWLEDGEMENTS

The authors would like to thank B Ricca, G Venugopalan, TD Li, as well as the rest of the Fletcher Lab for helpful feedback and technical consultation. This work was partially funded by the NSF Biomechanics & Mechanobiology program (Grant No. 1235569) and support from the NIH Bay Area Physical Sciences Oncology Center (PS-OC).

REFERENCES

1. Engler, A.J., S. Sen, H.L. Sweeney, and D.E. Discher. 2006. Matrix elasticity directs stem cell lineage specification. Cell. 126: 677–689.
2. Paszek, M.J., N. Zahir, K.R. Johnson, J.N. Lakins, G.I. Rozenberg, et al. 2005. Tensional homeostasis and the malignant phenotype. Cancer Cell. 8: 241–254.
3. Eyckmans, J., T. Boudou, X. Yu, and C.S. Chen. 2011. A Hitchhiker's Guide to Mechanobiology. Developmental Cell. 21: 35–47.
4. Brown, R.A., R. Prajapati, D.A. McGrouther, I.V. Yannas, and M. Eastwood. 1998. Tensional homeostasis in dermal fibroblasts: Mechanical responses to mechanical loading in three-dimensional substrates. Journal of Cellular Physiology. 175: 323–332.
5. DuFort, C.C., M.J. Paszek, and V.M. Weaver. 2011. Balancing forces: architectural control of mechanotransduction. Nature Reviews Molecular Cell Biology. 12: 308–319.
6. Ezra, D.G., J.S. Ellis, M. Beaconsfield, R. Collin, and M. Bailly. 2010. Changes in Fibroblast Mechanostat Set Point and Mechanosensitivity: An Adaptive Response to Mechanical Stress in Floppy Eyelid Syndrome. Invest Ophthalmol Vis Sci. 51: 3853–3863.
7. Mizutani, T., H. Haga, and K. Kawabata. 2004. Cellular stiffness response to external deformation: Tensional homeostasis in a single fibroblast. Cell Motility and the Cytoskeleton. 59: 242–248.
8. Lam, W.A., O. Chaudhuri, A. Crow, K.D. Webster, T.-D. Li, et al. 2011. Mechanics and contraction dynamics of single platelets and implications for clot stiffening. Nat Mater. 10: 61–66.
9. Webster, K.D., A. Crow, and D.A. Fletcher. 2011. An AFM-based stiffness clamp for dynamic control of rigidity. PLoS ONE. 6: e17807.
10. Crow, A., K.D. Webster, E. Hohlfeld, W.P. Ng, P. Geissler, et al. 2012. Contractile Equilibration of Single Cells to Step Changes in Extracellular Stiffness. Biophysical Journal. 102: 443–451.
11. Philipsborn, A.C. von, S. Lang, A. Bernard, J. Loeschinger, C. David, et al. 2006. Microcontact printing of axon guidance molecules for generation of graded patterns. Nature Protocols. 1: 1322–1328.
12. Parekh, S.H., O. Chaudhuri, J.A. Theriot, and D.A. Fletcher. 2005. Loading history determines the velocity of actin-network growth. Nature Cell Biology. 7: 1219–1223.
13. Dubin-Thaler, B.J., J.M. Hofman, Y. Cai, H. Xenias, I. Spielman, et al. 2008. Quantification of Cell Edge Velocities and Traction Forces Reveals Distinct Motility Modules during Cell Spreading. PLoS ONE. 3: e3735.
14. Califano, J.P., and C.A. Reinhart-King. 2010. Substrate Stiffness and Cell Area Predict Cellular Traction Stresses in Single Cells and Cells in Contact. Cell Mol Bioeng. 3: 68–75.
15. Cai, Y., O. Rossier, N.C. Gauthier, N. Biais, M.-A. Fardin, et al. 2010. Cytoskeletal coherence requires myosin-IIA contractility. J. Cell. Sci. 123: 413–423.
16. Lemmon, C.A., and L.H. Romer. 2010. A Predictive Model of Cell Traction Forces Based on Cell Geometry. Biophysical Journal. 99: L78–L80.

17. Han, S.J., K.S. Bielawski, L.H. Ting, M.L. Rodriguez, and N.J. Sniadecki. 2012. Decoupling Substrate Stiffness, Spread Area, and Micropost Density: A Close Spatial Relationship between Traction Forces and Focal Adhesions. Biophysical Journal. 103: 640–648.
18. Kaunas, R., Hsu, and Deguchi. 2011. Sarcomeric model of stretch-induced stress fiber reorganization. Cell Health and Cytoskeleton. 3: 13–22.
19. Abhilash, A.S., P.K. Purohit, and S.P. Joshi. 2012. Stochastic rate-dependent elasticity and failure of soft fibrous networks. Soft Matter. 8: 7004–7016.
20. Rotsch, C., K. Jacobson, and M. Radmacher. 1999. Dimensional and mechanical dynamics of active and stable edges in motile fibroblasts investigated by using atomic force microscopy. PNAS. 96: 921–926.
21. Schwarz, U.S., and M.L. Gardel. 2012. United we stand – integrating the actin cytoskeleton and cell–matrix adhesions in cellular mechanotransduction. J Cell Sci. 125: 1–10.
22. Galkin, V.E., A. Orlova, and E.H. Egelman. 2012. Actin filaments as tension sensors. Curr. Biol. 22: R96–101.
23. Risca, V.I., E.B. Wang, O. Chaudhuri, J.J. Chia, P.L. Geissler, et al. 2012. Actin filament curvature biases branching direction. Proc. Natl. Acad. Sci. U.S.A. 109: 2913–2918.
24. Uyeda, T.Q.P., Y. Iwadate, N. Umeki, A. Nagasaki, and S. Yumura. 2011. Stretching Actin Filaments within Cells Enhances their Affinity for the Myosin II Motor Domain. PLoS ONE. 6: e26200.
25. Luo, T., K. Mohan, V. Srivastava, Y. Ren, P.A. Iglesias, et al. 2012. Understanding the cooperative interaction between myosin II and actin cross-linkers mediated by actin filaments during mechanosensation. Biophys. J. 102: 238–247.
26. Hayakawa, K., H. Tatsumi, and M. Sokabe. 2011. Actin filaments function as a tension sensor by tension-dependent binding of cofilin to the filament. J Cell Biol. 195: 721–727.
27. Tondon, A., H.-J. Hsu, and R. Kaunas. 2012. Dependence of cyclic stretch-induced stress fiber reorientation on stretch waveform. J Biomech. 45: 728–735.

FIGURES

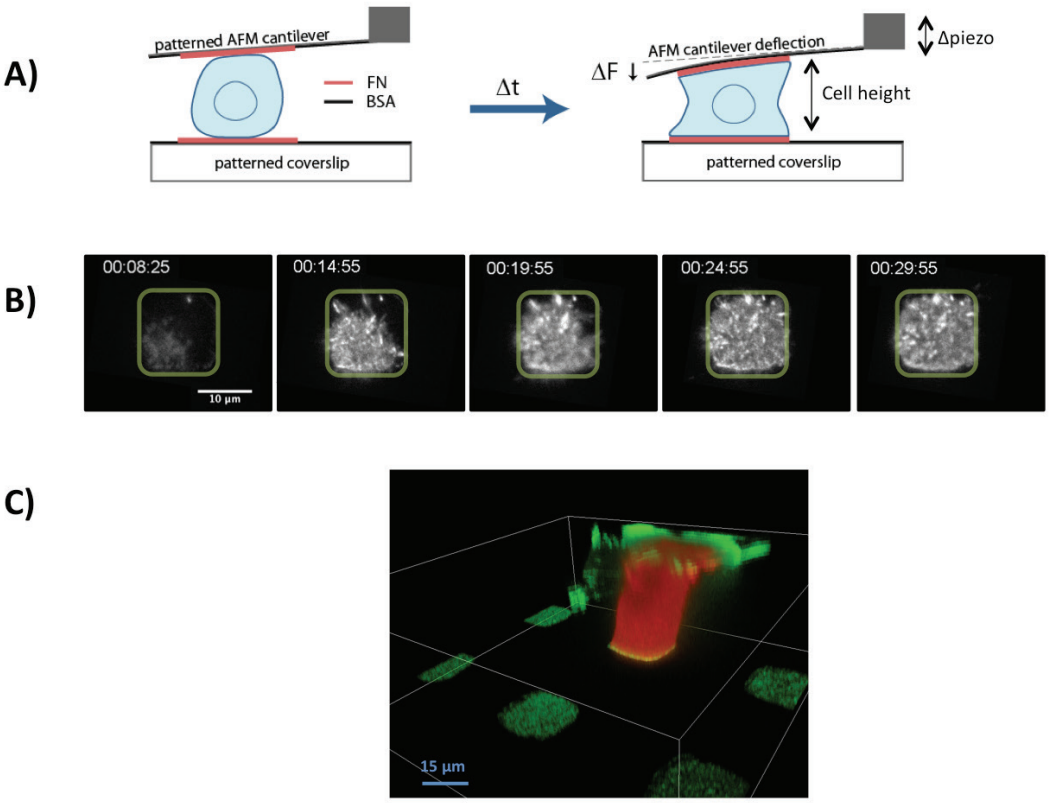

Figure 1. Cell contraction between dual patterned surfaces.

A) We use a combination of microcontact printing and dipping to pattern fibronectin on the substrate and AFM cantilever, respectively, with the remaining surface passivated using BSA. This presents a single cell with two constrained surfaces to spread between, deflecting the cantilever as it exerts force, which we can measure at the sub-nN, sub-second level. A piezo-electric element allows precise positioning of the cantilever to apply desired loading. B) A cell rapidly spreads to fill up the fibronectin pattern. In this case, we are observing a fibroblast cell expressing GFP-vinculin spreading between 15x15 μm^2 FN patterns over the course of 30 min. C) A custom-built confocal-AFM provides a 3D reconstruction of how a fibroblast cell expressing mCherry-LifeAct spreads between the patterned FN-GFP coated cantilever and substrate, after 30 min.

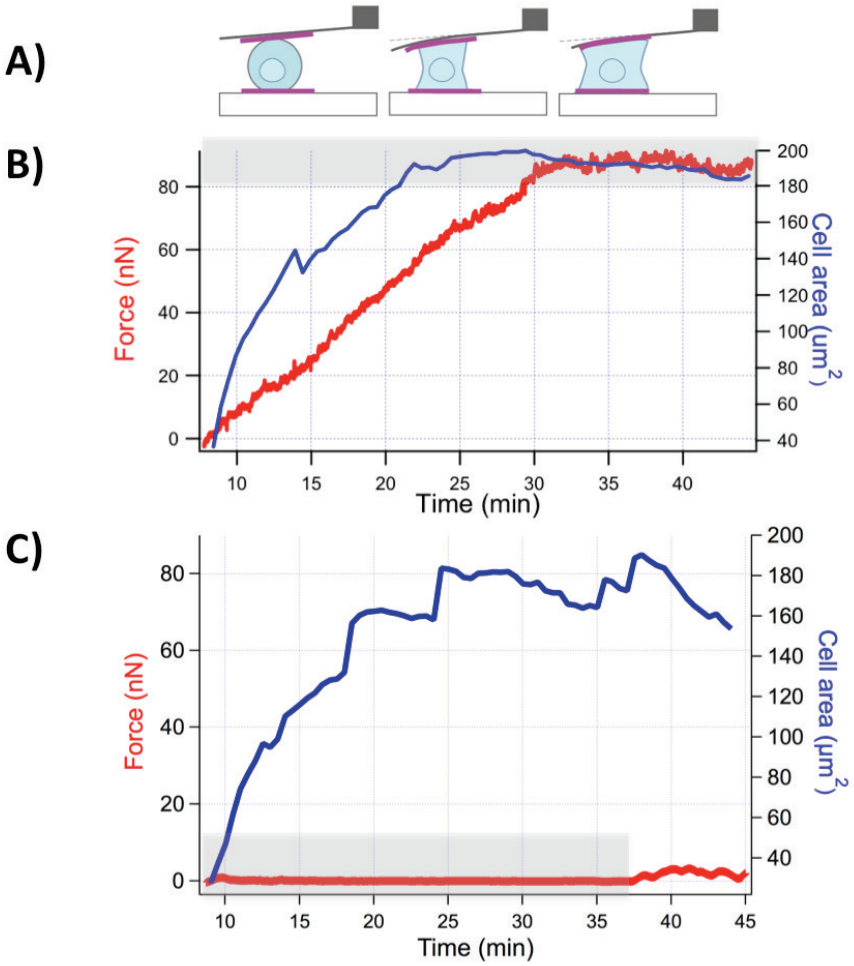

Figure 2. Limiting cell spreading results in a steady-state force.

A) Patterning both surfaces is required to repeatedly achieve a steady-state force, with the cell remaining attached to both surfaces. B) Cellular contraction increases tension until the force reaches a steady-state value, which we define as the force remaining within a 10% range (shaded area). By tracking cell area as well as contractile force, we observe that the tension continues for a short time (~5 min) after spreading ceases. Note Figure 1B shows a subset of the images from which the cell spread area data in this panel was calculated. C) Spreading is necessary to generate contractile force. If a force clamp maintains zero tension from first contact of the cell with both surfaces until spreading has stopped (shaded area), then when the force clamp is removed (after the shaded area), the cell does not contract further to generate any substantial tension.

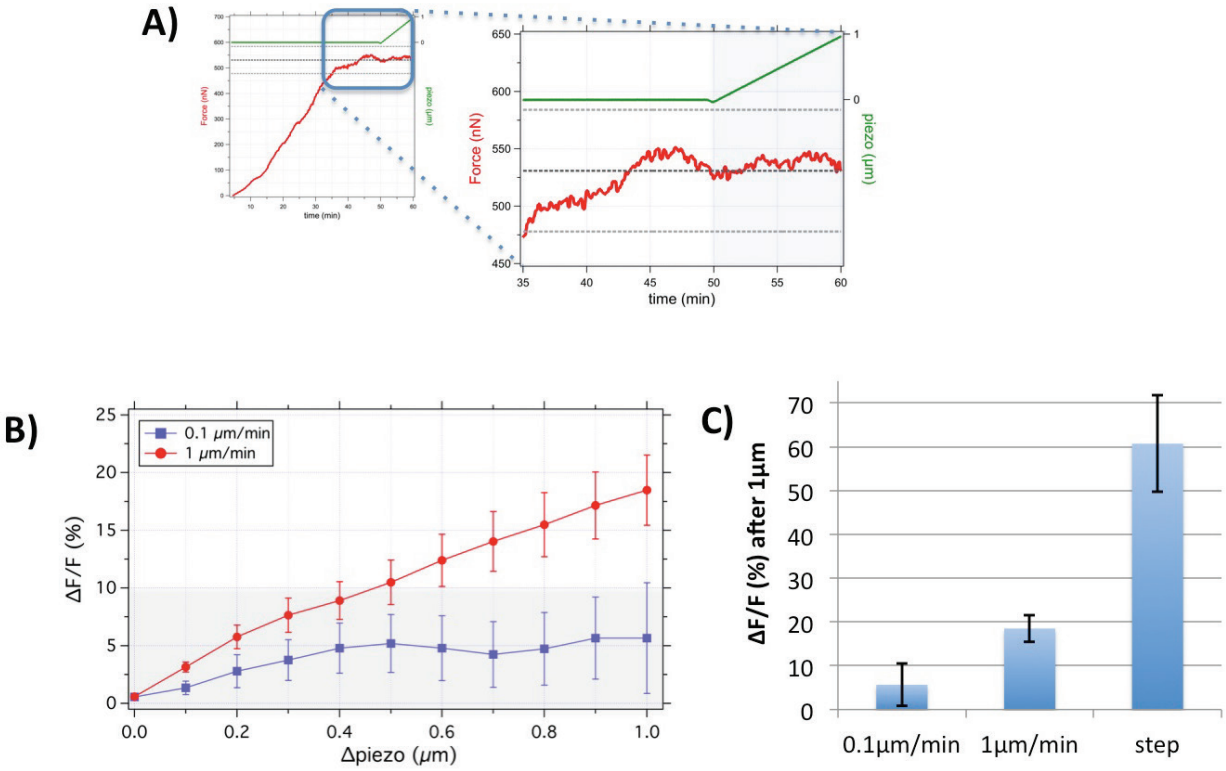

Figure 3. Cellular tension regulation is rate dependent.

A) Once a steady-state force is established, we stretch the cell by 1 µm at a rate of 0.1 µm/min. Notably, cellular tension is unchanged during this stretching. B) Averaging the response of all cells (normalizing by the steady-state force value), we can clearly observe that while the slow perturbations (0.1 µm/min, blue square) stay within the shaded, steady-state region (N=12), faster loading (1 µm/min, red circle) clearly changes the force beyond the shaded steady state (N=19). Error bars are ± SE. C) Displacements of 1 µm produce dramatically different force changes depending on the rate of loading. While slow loading produces a statistically indistinguishable change in force from the steady state, fast (N=19, $p<0.015$) and step loading (N=6, $p<0.01$) significantly change cell tension for the same strain.

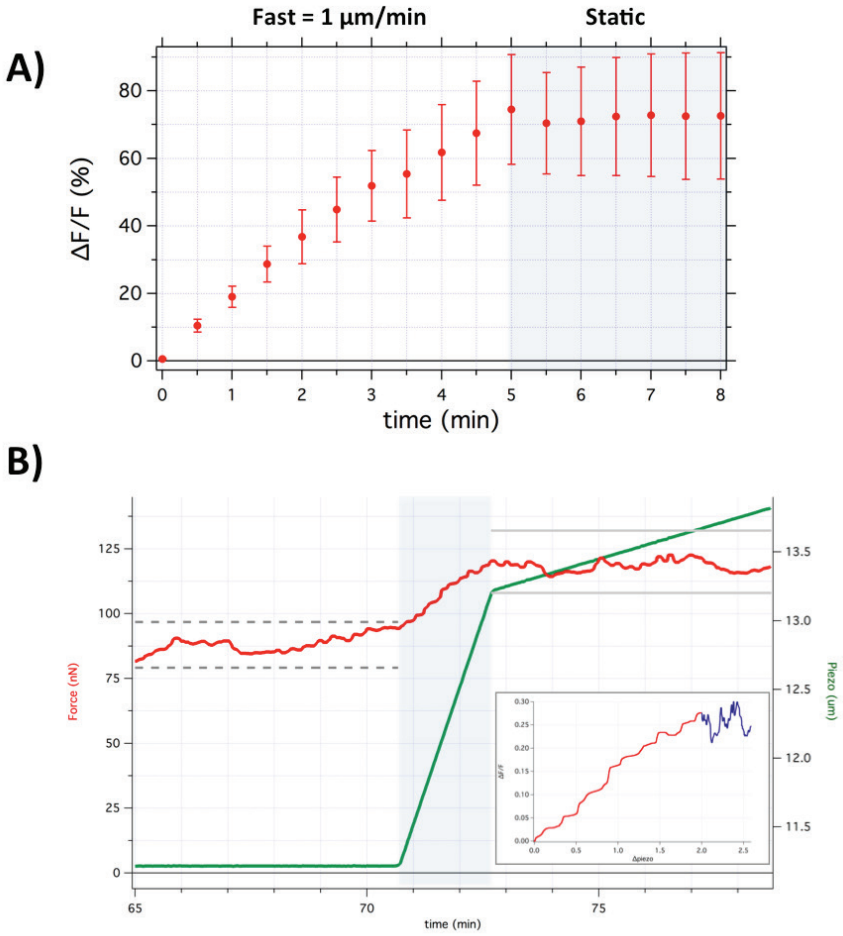

Figure 4. Tensional buffering rather than tensional setpoint.

A) Plotting the average response (N=8) of cells during and after a 5 µm fast displacement demonstrate that the cells remain at the new force value, instead of returning to the previous steady-state value. Error bars are ± SE. B) Switching directly from a fast ramp to a slow ramp shows that the cell starts maintaining the new force value immediately. (Inset) A clear transition from the fast (blue) to slow (red) ramp highlights the transition from an unregulated tension (blue) to regulated tension (red).

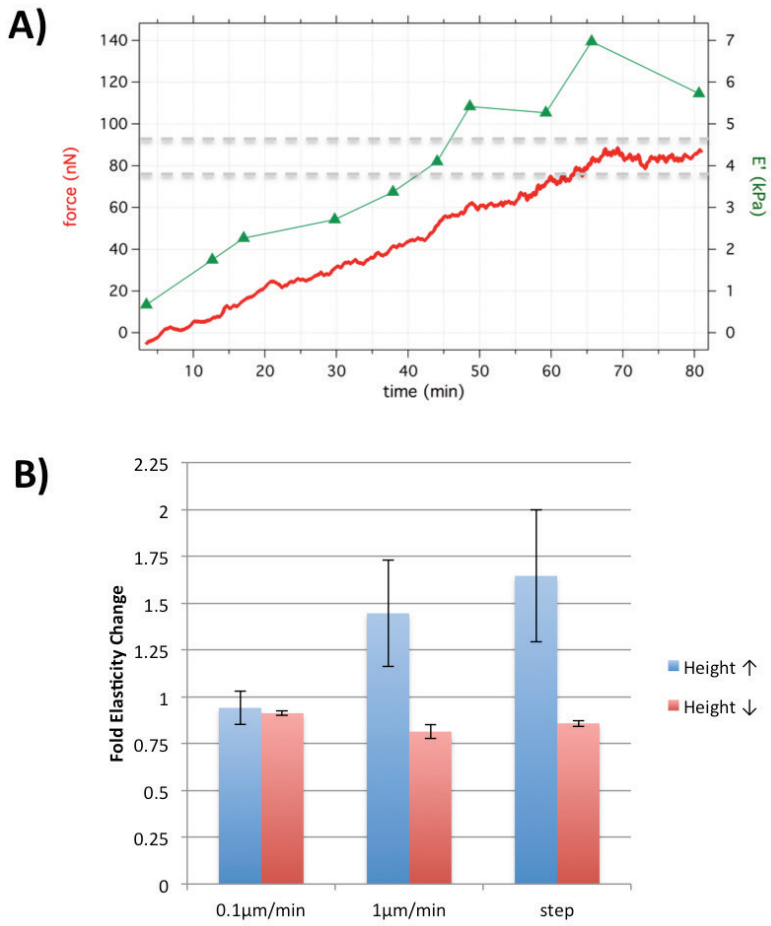

Figure 5. Cellular elasticity during contraction and dynamic loading.

A) Cellular elasticity increases as the cell spreads and contracts. Once the cell reaches a steady-state force, cellular elasticity also reaches a plateau. B) Slow loading (0.1 µm/min for 1 µm) does not change cellular elasticity from the steady-state value. However, rapidly increasing cell height (1 µm/min for 1 µm or a step change of 1 µm) dramatically increases cellular stiffness, while rapidly decreasing height significantly lower cellular elasticity ($n=15$, $p<0.005$).

SUPPORTING FIGURES

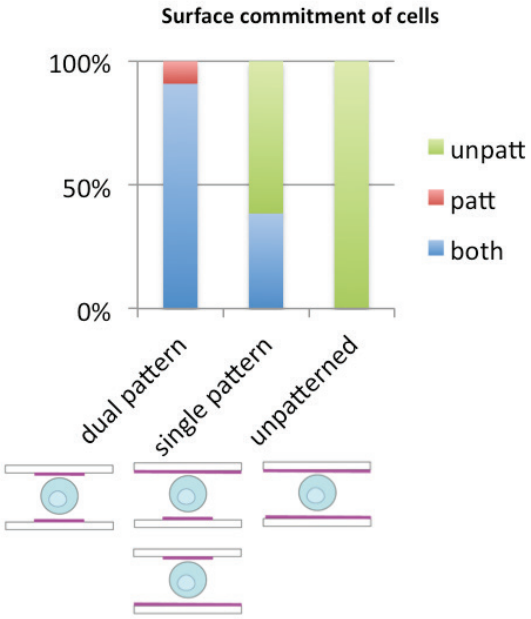

Figure S1. Micropatterning promotes stabile 3D attachment.

Constraining spread area on both surfaces dramatically increases the percentage of cells that achieve a steady state attached to both surfaces.

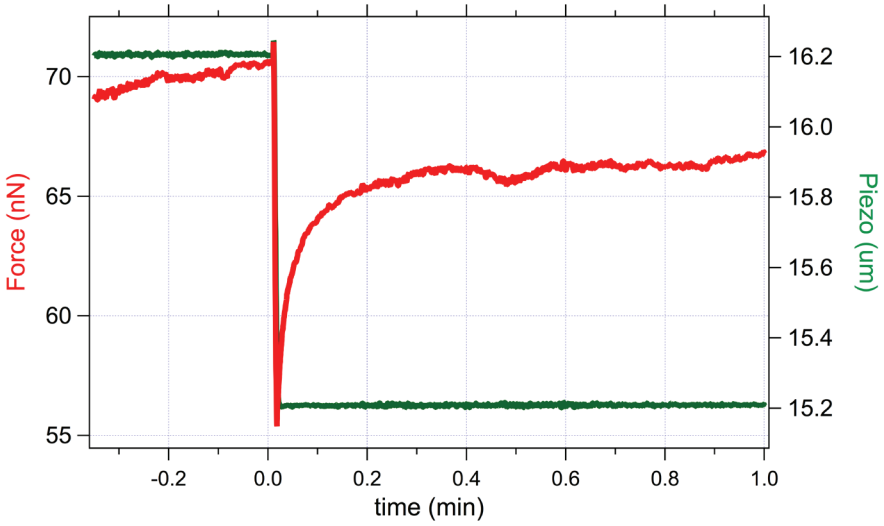

Figure S2. Viscoelastic response of cells to step strains.

When applying step strains to the cell, force changes rapidly and then viscoelastically relaxes towards the previous force. However, the cell does not return to the same tension, rather assuming a new steady state at some intermediate force.

Chapter 6.

Concluding remarks: Thoughts on the future of cellular mechanobiology

Summary

This dissertation is unified by the question: How do mechanics affect cellular behavior? In Chapter 1, I set the groundwork for this dissertation, giving an overview of the background literature necessary to understand my research. Then in Chapter 2, I report the development of a new technology, called a stiffness clamp, which when used in conjunction with contraction force microscopy, enables dynamic control of the microenvironmental stiffness experienced by single contractile cells. By instantly changing the apparent stiffness surrounding the cell, I observed an immediate change in cellular contraction rate in response. In Chapter 3, I look deeper into the cellular stiffness sensing response, observing a seconds-timescale equilibration in cellular contraction during stiffness changes. The timescale of this behavior was dependent on the viscoelastic properties of the cell's acto-myosin cytoskeleton. In fact, the response I observed was fully explained using a standard linear solid element in series with a constant velocity actuator. This observation provides a lower temporal bound on the cell's ability to sense stiffness signals perceived in its environment, where the cell must integrate its own viscoelasticity in combination with its environment.

Cancer tumors have long been known to have different mechanical properties from the surrounding tissue. In Chapter 4, I investigate the source of these mechanical changes in the context of invasive lobular breast carcinoma. Using atomic force microscopy (AFM) to apply creep tests to both single cell and mulit-cellular acinar structures, I observe a distinct stiffening of mature pre-malignant acini resulting from not mechanical changes on a single cell scale nor changes in cell-cell adhesion, but rather from the structural architecture of the acinus. I then show, using a custom developed 3D computational model, how the pre-malignant architecture itself affects the apparent microenvironmental stiffness experienced by a single epithelial cell within the acinus.

Finally, in Chapter 5 I tackle one of the most widely discussed hypotheses in mechanobiology: tensional homeostasis. For the first time since originally being proposed 15 years ago, I report conclusive, direct evidence for tensional homeostasis at a single cell level. However, unlike as had previously been hypothesized, homeostasis is not maintained through a "mechanostat", force setpoint behavior. Rather, tensional buffering enables the cell to maintain its steady-state force, up to some loading rate, at which point the cell tension will change to form a new homeostatic value. This strain-rate dependent homeostasis potentially enables the cell to behave in two different ways, depending on the nature of the mechanical load. One the one hand, for slow loading, the cell accommodates and deforms to absorb the load. One the other hand, when the tissue experiences rapid loading, the cell behaves more rigidly, thereby stabilizing the tissue.

One of the key takeaway points from my research is the importance of the dynamic behavior of cells with the mechanics of their environment. Ignored by most studies in the field, I have shown how important the element of time is in understanding cellular mechanosensation. Additionally, I have highlighted the role of other contributors to the mechanics of a cell's microenvironment, beyond the commonly considered extracellular matrix (ECM). In addition to the matrix, cells also sense the stiffness of the cells around them, as well as how those cells are geometrically arranged. All these factors combine to

form the mechanical tapestry with which adherent mammalian cells constantly interact. As we better understand how this interaction is important during healthy development, so too do we learn how disruptions in these interactions might be involved in disease.

Future challenges and opportunities

The field of cellular mechanobiology faces several key challenges, which simultaneously offer unique opportunities for moving forward. Addressing these issues will occupy researchers for years to come.

One of the prominent outstanding questions facing the field is identifying how mechanical signals become translated into changes in gene expression. Additionally, how does the mechanical history of the cell (or its lineage) affect its current mechanical perception? Understanding the transition from short-term sensing to a stable, long-term phenotype will require the development of new technologies to span the requisite timescales.

Another challenge facing the field is moving beyond model systems to better understand the mechanosensing behavior of primary cells within heterogeneous environments that more closely mirror in vivo tissue. One of the most important and limiting simplifications of most experimental platforms is the use of two-dimensional substrates. Moving to three-dimensional adhesive matrices, while presenting many technical challenges, provides an environment markedly more like the native tissue surrounding most cells. As we better understand simplified model systems, we will also begin to be able to identify how healthy responses of cells in vivo break down with various diseases.

Finally, another challenge facing the field is developing constitutive equations that characterize the cell's mechanical relationship with its environment. Tackling this would dramatically improve the utility of computational models that have sought to describe these behaviors, which to date have been limited by the absence of detailed, quantitative experimental data. Indeed, this will be of mutual benefit, as models will be able to make testable predictions to help guide experiments.

Ultimately, I believe the goal of the field of mechanobiology should be to become integrated into the rest of cellular biology, wherein mechanics are considered right alongside biochemical signaling when investigating questions of cell function. As the field initially formed, its task was to make the case that mechanics are important, that ever more cell types behave differently as a function of stiffness and force within their microenvironment. This evidence has mounted and now, any given cell type exhibiting mechanosensation is more of the rule than the exception. However, to be really useful, mechanobiology must demonstrate that incorporating its results are necessary for a deeper understanding of cell biology; that during development and disease, mechanics stands alongside biochemical signaling in regulating cell behavior. When this happens the field of mechanobiology will have fully matured.